2018

Cationic Metallocene-Containing Biomaterials For Antimicrobial Applications

Parasmani Pageni
University of South Carolina

CATIONIC METALLOCENE-CONTAINING BIOMATERIALS FOR ANTIMICROBIAL APPLICATIONS

by

Parasmani Pageni

Bachelor of Science
Milligan College, 2010

Master of Science
East Tennessee State University, 2013

Submitted in Partial Fulfillment of the Requirements

For the Degree of Doctor of Philosophy in

Chemistry

College of Arts and Sciences

University of South Carolina

2018

Accepted by:

Chuanbing Tang, Major Professor

John Lavigne, Committee Member

Maksymilian Chruszcz, Committee Member

Alan W Decho, Committee Member

Cheryl L. Addy, Vice Provost and Dean of the Graduate School

DEDICATION

To my parents, my wife, my son Ayven and all my family and friends, without their support and encouragement, none of my accomplishments would be possible.

ACKNOWLEDGEMENTS

First and foremost, I would like to show my gratitude to my advisor, Dr. Chuanbing Tang, who gave me the opportunity to work and learn in his research group, and offered endless support and guidance on my research projects. I feel very fortunate to be mentored by such an enthusiastic and knowledgeable person who has passion for polymer science. I am grateful for the foundation he has created for me and hope to learn more from him in the future.

I would also like to thank my research committee Dr. John Lavigne, Dr. Maksymilian Chruszcz, and Dr. Alan Decho for their advice, encouragement, and valuable suggestions on my research during graduate school. I want to thank Dr. Decho and his group members Dr. Yung Ping Chen and Tinom Shokfai for their collaborations with our group. Also, I want to thank Dr. Chruszcz and his group member Swanandi Pote for their collaborations with us. In addition, I want to mention Dr. Mitzi Nagarkatti and her group members Dr. Marpe Bam for a continued collaboration over the years.

I am very appreciative of the experiences shared and friendships formed with other graduate students and post-docs at USC. I want to specially mention the members in Tang Polymer Group. I thank Dr. Jiuyang Zhang and Dr. Yi Yan for being a great mentor during my early stages of graduate career. I also appreciate Dr. Peng Yang for closely working with me and it was a pleasant experience for me. Thanks a lot for Dr. Brian Benicewicz and Yucheng Huang for the collaborative work. Members of Tang group, Dr. Perry Wilbon, Dr. Yali Qiao, Dr. Alper Nese, Dr. Xiaodong Yin, Dr. Zhongkai Wang, Dr. Mitra

Ganewatta, Dr. Liang Yuan, Dr. Jifu Wang, Dr. Hui Li, Dr. Ye Sha, Dr. Shaobo Tan, Nathan Trenor, Pabel Kabir, Anisur Rahman, Tianyu Zhu, Meghan Lamm, Xinzhou Zhang, Yujin Cha, Ryan Miskin, Lin Fu, Moumita Sharmin Jui and Haijiao Kang. It was a great pleasure to work with all of you and learn from you.

Further, I want to give my sincerest gratitude to my parents, my wife and other family members for their unconditional love and support over the years. I thank all my friends for their encouragement and help. Finally, I acknowledge all the funding supports from University of South Carolina, SC EPSCoR, National Science Foundation (NSF) and National Institutes of Health (NIH).

ABSTRACT

Metal-containing polymers or metallopolymers, are one of the major classes of polymers which stand out independently because of a unique combination of organic and inorganic components in one macromolecular system. Among the variety of metallopolymers, metallocene-containing polymers have been widely utilized for applications ranging from electrochemical sensors to templates for advanced inorganic catalysts to battery materials, due to their unique physicochemical properties. This dissertation is focused on the synthesis, characterization, and application of cationic metallocene-containing polymeric materials. Cationic-cobaltocenium was grafted in various inorganic nanoparticles using polymerization techniques such as reversible addition-fragmentation chain transfer polymerization.

In Chapter 1, the overall background of metallopolymers, antimicrobial polymers and modification of nanoparticle polymerization methods is included. Chapter 2 focuses on the study of electrostatic charge on the relative affinity and comparison of the relative binding strength of a cobaltocenium-containing polyelectrolyte. The nature and relative strength of intermolecular interaction between cationic polyelectrolytes and anionic probes were investigated. Chapter 3-4 reports the preparation of inorganic silica and iron oxide nanoparticles grafted with charged cobaltocenium-containing metallopolymers by surface-initiated reversible addition-fragmentation chain transfer (RAFT) polymerization. In Chapter 5, cobaltocenium-containing polymers were coated on gold nanoparticles by a

grafting-to mechanism. β-lactam antibiotic like penicillin-G were then conjugated with all the nanoparticles by ion-pairing between the cationic cobaltocenium moiety in the nanoparticles and carboxylate anions of antibiotics. Such bio-conjugated nanoparticles not only reduced the activity of β-lactamase but effectively lysed both Gram-positive and Gram-negative bacterial cells. All these nanoparticles were characterized and subjected for antimicrobial evaluation against a range of bacteria and biocompatibility with mammalian cells.

TABLE OF CONTENTS

DEDICATION iii

ACKNOWLEDGMENTS iv

ABSTRACT vi

LIST OF TABLES xi

LIST OF FIGURES xii

LIST OF ABBREVIATIONS xvi

CHAPTER 1 GENERAL INTRODUCTION 1

1.1 METALLOCENE-CONTAINING POLYMERS 2

1.2 ANTIMICROBIAL POLYMERS 5

1.3 NANOPARTICLES 6

1.4 POLYMERIZATION TECHNIQUES 8

1.5 DISSERTATION OUTLINE 9

1.6 REFERENCES 11

CHAPTER 2 BINDING OF COBALTOCENIUM-CONTAINING POLYELECTROLYTES WITH ANIONIC PROBES 15

2.1 ABSTRACT 16

2.2 INTRODUCTION 16

2.3 EXPERIMENTAL SECTION 19

2.4 Results and discussion 24

2.5 Conclusions 34

2.6 References 34

Chapter 3 Charged metallopolymer-grafted silica nanoparticles for antimicrobial applications 37

3.1 Abstract 38

3.2 Introduction 38

3.3 Experimental Section 41

3.4 Results and Discussion 48

3.5 Conclusions 59

3.6 References 59

Chapter 4 recyclable magnetic nanoparticles grafted with antimicrobial metallopolymer-antibiotic bioconjugates 64

4.1 Abstract 65

4.2 Introduction 65

4.3 Experimental Section 68

4.4 Results and Discussion 76

4.5 Conclusion 89

4.6 References 89

Chapter 5 gold nanoparticles with cobaltocenium-antibiotic conjugates toward broad spectrum antimicrobial efficacy 97

5.1 Abstract 98

5.2 Introduction 98

5.3 Experimental Section 100

5.4 Results and Discussion 105

5.5 Conclusions 115
5.6 References 115
Chapter 6 Summary and Outlook 122
6.1 Dissertation Summary 123
6.2 future Work 124
Appendix A – Permission to Reprint 126

LIST OF TABLES

Table 2.1 Anionic probes used to investigate the binding interaction with a cobaltocenium polymer.....25

Table 3.1 Cobaltocenium-containing silica nanoparticles and their characterization. 50

Table 3.2 Minimum inhibitory concentrations (MICs) of different agents against five strains of bacteria 55

Table 4.1 Minimum inhibitory concentrations (MICs) of different agents against five strains of bacteria. 82

Table 5.1 The Minimum Inhibitory Concentrations of different antimicrobial agents against Gram-positive and Gram-negative strains.....112

LIST OF FIGURES

Figure 1.1 Two strategies to modify nanoparticles surface with polymers 7

Figure 1.2 Overall mechanism of RAFT polymerization 8

Figure 1.3 Grubbs' catalysts for ROMP 10

Figure 2.1 ^{1}H NMR spectrum of poly (dimethylamino methacrylate) 20

Figure 2.2 ^{1}H NMR spectrum of cobaltocenium monomer in CD_3COCD_3 21

Figure 2.3 Fluorescence intensity and absorbance isotherms from titration of a PCFn complex with different displacer (DP). [CF] = 1.0×10^{-6} M, [Co^{+}] = 4.0×10^{-6} M in buffered solution (50 mM Tris at pH 7.40), λexc = 494 nm. 27

Figure 2.4 Fluorescence and absorbance isotherms from titration of a P-CFn complex with trianionic displacers with different shape. [CF] = 1.0×10^{-6} M, [Co^{+}] = 4.0×10^{-6} M in buffered solution (50 mM Tris at pH 7.4), λexc = 494nm**.** 28

Figure 2.5 Fluorescence intensity and absorbance isotherms from titration of a P-CFn complex with trianionic aliphatic and aromatic guests. [CF] = 1.0×10^{-6} M, [Co^{+}] = 4.0×10^{-6} M in buffered solution (50 mM Tris at pH 7.40), λexc = 494nm. 28

Figure 2.6 Proposed C-H-π interaction between cobaltocenium-containing polymer and trimesate anion. 29

Figure 2.7 The transmittance of various polyelectrolyte solutions: A) 1.0 mL 0.10 mM PDMAEMA solution with addition of different volumes of 0.01 mM PSSNa; B) 1.0 mL 0.10 mM PCoCl solution with addition of different volumes of 0.01 mM PSSNa; C) 1.0 mL 0.20 mM PDMAEMA solution with addition of different volumes of 0.01 mM PSSNa D) 1.0 mL 0.20 mM PCoCl solution with addition of different volumes of 0.01 mM PSSNa; E) Transmittance ratio (T_t/T_o) as a function of volumes of PSSNa (mL) added with each concentration of PCoCl and PDMAEMA solutions at 0.10 mM; F) Transmittance ratio (T_t/T_o) as a function of volumes of PSSNa (mL) added with each concentration of PCoCl and PDMAEMA solutions at 0.20 mM. 31

Figure 2.8 The transmittance of various polyelectrolyte solutions: A) 1.0 mL 0.10 mM PCoCl solution with different concentration of 1.0 mL PSSNa; B) 1.0 mL 0.10 mM PDMAEMA solution with various concentrations of 1.0 mL PSSNa; C) Transmittance ratio (T_t/T_o) as a function of concentrations of PSSNa. 32

Figure 2.9 Size distribution of PCoCl-PSSNa and PDMAEMA-PSSNa complexes using DLS 33

Figure 3.1 EDX elemental analysis of homopolymer and nanoparticles 43

Figure 3.2 FT-IR spectrum of nanoparticles.....44

Figure 3.3 ^{1}H NMR spectrum of cobaltocenium-containing nanoparticle-penicillin conjugate CsNP in D_2O 44

Figure 3.4 (a) Optical view of nitrocefin solution with different amounts of CsNP after adding β-lactamase for 1 h; and (b) UV−vis absorption.....47

Figure 3.5 Hemolysis test results for CsNP-penicillin conjugate 48

Figure 3.6 a) Dynamic Light Scattering measurements showing sizes of nanoparticles; and b) Thermogravimetric analysis of cobaltocenium-containing silica nanoparticles. 51

Figure 3.7 TEM images of nanoparticles: a) CsNP 1; b) CsNP 2; c) CsNP 3. 52

Figure 3.8 Inhibition zones of CsNP-Peni conjugates against various strains of bacteria at 6 μg penicillin-G/disk using disk-diffusion assays: a) *S. aureus*; b) *E. coli;* c) *P. vulgaris;* d) *K. pneumonia*; e) *P. aeruginosa*. 54

Figure 3.9 Confocal scanning laser microscopy images of control, penicillin and CsNP-penicillin conjugates with a concentration of penicillin 6 μg/mL (using BacLight live/dead stain, green indicates live cells, red indicates dead cells) against *E. coli* and *S. aureus.* The bacterial solution without CsNPs was used as the control.....56

Figure 3.10 Scanning electron microscopy (SEM) images of control and CsNP-penicillin conjugates with a concentration of penicillin at 6 μg/mL against *E. coli* and *S. aureus*. Bacterial solutions without CsNPs were used as the control.....57

Figure 3.11 Drug resistance study of nanoparticle conjugates against various bacteria ...58

Figure 4.1 EDX elemental analysis of cobaltocenium-containing iron oxide nanoparticles and cobaltocenium-containing homopolymer.....71

Figure 4.2 Images of cobaltocenium-containing iron oxide nanoparticles incubating and recycling against various bacteria.....74

Figure 4.3 Hemolysis test results for FeNP nanoparticles.....76

Figure 4.4 a) TEM image of FeNP-Cl nanoparticles; and b) Dynamic Light Scattering (DLS) measurements showing sizes of nanoparticles. 79

Figure 4.5 Inhibition zones of different agents against various strains of bacteria at an equivalent of 7 μg penicillin-G/disk using disk-diffusion assays: a) *S. aureus*; b) *B. cereus* C) *E. coli;* d) *K. pneumoniae*; e) *P. vulgaris.* 81

Figure 4.6 Confocal scanning laser microscopy (CSLM) images of controls and FeNP-penicillin conjugates exposed to a concentration equivalent of penicillin 7 μg/mL. Cells *S. aureus, B. cereus, E. coli, K. pneumonia* and *P. vulgaris* were stained using BacLight Live/Dead stain, where green indicates live cells, and red indicates dead cells). The bacterial solution without FeNP was used as the control. 83

Figure 4.7 Scanning electron microscopy (SEM) images of control and FeNP-penicillin conjugates with a concentration of penicillin at 7 μg/mL against various Gram-positive and Gram-negative bacteria. Bacterial solutions without FeNP were used as the control. All scale bars are 2.0 μm.....84

Figure 4.8 Inhibition activities of recyclable magnetic cobaltocenium-containing FeNP conjugates against *S. aureus* and *E. coli*. 86

Figure 4.9 Time-kill curves of FeNP-conjugates against *S. aureus* and *E. coli*. Bactericidal activities were monitored for first 12 hours. The concentrations used were MIC, 4×MIC, and 8×MIC, respectively.....87

Figure 4.10 Drug resistance study of FeNP-penicillin conjugates against *S. aureus* and *E. coli*.....87

Figure 4.11 TEM images of *S. aureus* after incubating with (A) Control; and (B) FeNP-conjugates, with the concentration of penicillin at 7 μg/mL 88

Figure 5.1 TEM images of a) Au NPs b) Au@PCo-6K, c) Au@PCo-15K, and d) Au@PCo-30K.....107

Figure 5.2 a) Size distribution of different gold nanoparticles analyzed by DLS. b) UV-vis absorption spectra of various samples c) TGA data of Au NPs, PCo homopolymers and Au@PCo NPs with different cobaltocenium polymer molecular weights. d) TGA data of Au@PCo-15K NPs, penicillin-G and Au@PCo-Peni. 108

Figure 5.3 a) Disk-diffusion assays against (i) *S. aureus* (i)*E. coli*, (i) *K. pneumonia*, and (iv) *P. vulgaris* by penicillin-G, PCo-Peni and Au@PCo -Peni NPs. b) OD_{600} values and c) inhibitory percentage of four bacteria incubated with penicillin-G, PCo-Peni and Au@PCo-Peni NPs, respectively. The bacterial TSB solution without antimicrobial agents was used as the control. 111

Figure 5.4 a) CLSM and b) SEM images of the control and Au@PCo-Peni NPs (18.5 μg/mL, with the concentration of penicillin-G at 5 μg/mL) against various strains of bacteria. CLSM using BacLight live/dead stain, green indicates live cells, red indicates

dead cells. Bacteria concentration were 1.0×10^6 CFU/mL. All scale bars in SEM images are 2 μm 113

Figure 5.5 TEM images of the control and Au@PCo-Peni NPs (18.5 μg/mL, with the concentration of penicillin-G at 5 μg/mL) against *S.aureus* and *E.coli*. Bacteria concentration were 1.0×10^6 CFU/mL. All scale bars are 1 μm.....114

Figure 5.6 Hemolysis test results for Au@PCo nanoaprticles. 115

Figure A.1 Copyright release for Chapter 2.....127

Figure A.2 Copyright release for Chapter 3.....128

Figure A.3 Copyright release for Chapter 4.....129

LIST OF ABBREVIATIONS

AFM ..... Atomic Force Microscopy

AIBN ..... Azobisisobutyronitrile

AMP ..... Antimicrobial Peptide

ATRP ..... Atom Transfer Radical Polymerization

CDC ..... Centers for Disease Control

CFU ..... Colony Forming Unit

CLSM ..... Confocal Laser Scanning Microscopy

$CoAEMAPF_6$ ..... 2-Cobaltoceniumamidoethyl Methacrylate Hexafluorophosphate

CPDB ..... 4-Cyanopentanoic Acid Dithiobenzoate

DCM ..... Dichloromethane

DLS ..... Dynamic Light Scattering

DMF ..... *N*,*N*-Dimethylformamide

DMSO ..... Dimethyl Sulfoxide

DSC ..... Differential Scanning Calorimetry

EDC-HCl ..... N-(3-dimethylaminopropyl)-N'- ethylcarbodiimide hydrochloride

EDX ..... Energy-dispersive X-ray Spectrometry

FeNP ..... Iron-oxide Nanoparticles

FE-SEM ..... Field-emission Scanning Electron Microscopy

FTIR ..... Fourier Transform Infrared Spectrometry

GPC ..... Gel Permeation Chromatography

HC ..... Hemolytic Concentration

MeOH ..... Methanol

MDR..... Multi-Drug Resistance

MW.....Molecular Weight

MIC ..... Minimum Inhibitory Concentration

MRSA.....Methicillin-resistant *Staphylococcus aureus*

NMR.....Nuclear Magnetic Resonance

PBS..... Phosphate-buffered Saline

PEC.....Polyelectrolyte Complex

PDMAEMA.....Poly (2-dimethylamino) ethyl methacrylate

PSSNA.....Poly (sodium styrene sulfonate)

RAFT.....Reversible Addition-Fragmentation Chain Transfer

RBC..... Red Blood Cells

SI-RAFT..... Surface-initiated Reversible Addition-Fragmentation Chain Transfer

TBACl .....Tetrabutyl Ammonium Chloride

TEM .....Transmission Electron Microscopy

TGA.....Thermogravimetric Analysis

THF .....Tetrahydrofuran

TMS.....Tetramethylsilane

TSB.....Tryptic Soy Broth

CHAPTER 1

GENERAL INTRODUCTION

1.1 Metallocene-containing Polymers

Metal-containing polymers or metallopolymers are a new class of materials which show interesting properties and use as they have processing advantages of polymers and functionalities provided by metal centers. During the past several decades, metallopolymers have been widely studied due to their diverse applications as optic, electronic, and magnetic materials, catalysts, and ceramic precursors.[1, 2] Metallocene-based polymers represent classical metallopolymers by incorporating functional sandwich-structured metallocenes into polymer materials.[3-5] The first member of the metallocene family, ferrocene, was introduced by Geoffrey Wilkinson and Ernst Otto Fischer in early 1950s.[6] Ferrocene is the most widely studied metallocene which has received a lot of attention. Tremendous progress has been made in the last two decades in the field of ferrocene-containing polymers.[7-10] Generally, there are two major states of a metallocene: the neutral metallocene and the cationic metallocenium. Neutral metallocenes, predominantly 18 electron ferrocene and ruthenocene, have been widely explored. In comparison to ferrocene, cobaltocene and cobaltocene containing polymers have received far less attention and have been much less explored. One of the main reasons behind the limited research is due to the difficulty in synthesizing substituted derivatives of cobaltocene. Ferrocene has 18 valence electrons and can easily undergo electrophilic aromatic substitution reactions. Cobaltocene has 19 valence electrons and readily oxidizes to cobaltocenium, which is incapable of undergoing electrophilic aromatic substitution reactions due to its great stability and inertness. Due to the high chemical stability of cobaltocenium, it is challenging to make cobaltocenium-containing derivatives by direct substitution on cyclopentadiene ring.

Different from neutral ferrocene-containing polymers, cobaltocenium-containing polymers are quite unique due to their charged state and highly stable chemical property.[11-13] The charged state poses a considerable challenge to synthesize mono-substituted cobaltocenium, which is the initial step to prepare side-chain cobaltocenium-containing polymers. The pioneer work on cobaltocenium-containing polymers was done by Sheats *et. al.* that focused on the synthesis of main-chain cobaltocenium-containing oligomers with poor solubility.[14, 15] Manners *et. al.* did notable work using ring-opening polymerization (ROP) techniques to prepare well defined main-chain cobaltocenium polymers such as ring-tilted dicarba[2]cobaltococenophane in an effort to overcome the problem. However, anionic ROP gave oligomers with degree of polymerization less than 9.[16] The two important aspects that plays a crucial role in synthesizing cobaltocenium-containing polymers are: (i) synthesis of mono-substituted cobaltocenium, which can be further converted to polymerizable monomers; (ii) control over the polymer structure. Controlled polymerization techniques such as atom transfer radical polymerization (ATRP), RAFT and ring-opening metathesis polymerization (ROMP) could offer a good control on molecular weight, architecture and functionality as well as low dispersity. Mono-substituted cobaltocenium has been synthesized by using a statistical reaction between methyl cyclopentadiene, cyclopentadiene and cobalt bromide, followed by further oxidation and exhausted separation to give cobaltocenium monoacid, which can be further converted into vinyl monomers (method 1 in Scheme 1). Due to the nature of the statistical reaction, the synthetic methodology is very tedious with a low yield (less than 10%). Another method developed independently around the same time by Blidstein[17] and Tang[18] uses a reaction between un-substituted cobaltocenium and a nucleophile based on

organolithium reagents, followed by hydride abstraction to give mono-substituted cobaltocenium (method 2 in Scheme 1).

Scheme 1.1 Different methods to synthesize mono-substituted cobaltocenium with various functional groups

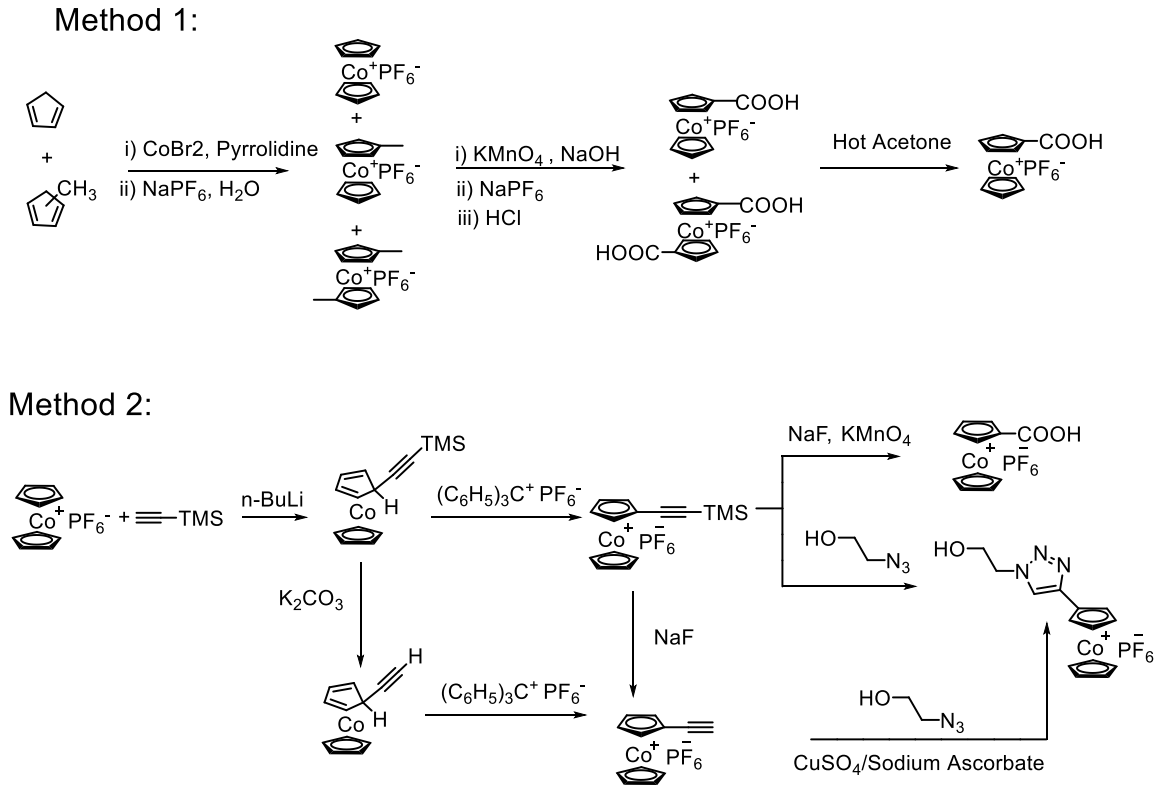

This method not only improves the yield but also results in ethynylcobaltocenium, which can react with different azides through a copper-catalyzed azide-alkyne cycloaddition (CuAAC) to give mono-substituted cobaltocenium with different functional groups. Different from the main-chain polymers, Tang group established a synthetic platform to prepare side-chain cobaltocenium-containing polymers with high molecular weight and low dispersity.[19-22] They used a direct synthesis route to prepare monomers by obtaining monosubstituted cobaltocenium-containing compounds instead of using electrophilic substitution reactions. The obtained mono-functionalized cobaltocenium

carboxylic acid was then modified into various polymerizable groups to result in a variety of polymers.[22-25]

1.2 Antimicrobial Polymers

Antimicrobial peptides (AMPs) are natural cationic amphiphilic peptides which act as the first line of defense to prevent organisms from various microbial infections. Even though there has been a prolonged discussion over bactericidal mechanism of AMPs, it is commonly acceptable that AMPs could adopt amphipathic structures to associate with bacterial membranes. The cationic part is believed to interact with negatively charged bacteria to disrupt the membrane.[26] However, the toxicity and the ability of AMPs to lyse eukaryotic cells is a major hurdle to overcome before their use. Also, the peptides themselves are vulnerable to proteolysis and hence degrade too rapidly once in the body, and are often immunogenic *in vivo*. In addition, many AMPs are very expensive, limiting their use in large scale. Inspired by the AMPs, synthetic macromolecules have been introduced as antimicrobial agents. Rather than targeting proteins as most β-lactam antibiotics do, cationic polymers[27-33] can disrupt membranes, and have shown efficacy against bacteria. Synthesis of cationic polymers is not labor-intensive, so the production in a large scale is quite feasible. For example, poly(vinyl alcohol)s[34], polyacrylates[35], polyimines[36], polystyrenes[37], polysiloxanes[38], and polyurethanes[35] have been functionalized with various cationic moieties to be used as an antibacterial agents. In Gram-positive bacteria, teichoic acids are linked to either the peptidoglycan cell wall or to the underlying cell membrane to impart net negative charges because of the presence of phosphate moieties in their structure. While an additional outer membrane bearing

phospholipids and lipopolysaccharides is present in Gram-negative bacteria, the strongly negative charges to cell surface is imparted by lipopolysaccharides.

Currently the majority of synthetic antimicrobial agents are compounds or polymers having cationic functional groups, which promote rapid adsorption onto the negatively-charged bacterial cell surfaces. The surface of eukaryotic cell membranes is composed of zwitterionic phospholipids such as phosphatidylcholine, cholesterol and sphingomyelin, so only interacts weakly with cationic species. The cationic polymers interact with bacterial membrane initially by electrostatic interaction and then the hydrophobic side chains insert into the membranes via hydrophobic interactions with the fatty tails of membrane phospholipids, causing the membrane to depolarize and the cell death. However, most of these strategies have been restricted by their limitations, such as the high toxicity of cationic polymers and peptides, poor release of antibiotics, and low targeting efficiency toward bacteria.[39, 40]

1.3 Nanoparticles

Nanoparticles are objects ranging in size from 1-100 nm. Nanoparticles usually have novel physical and chemical properties when compared to their larger-sized (bulk) counterparts, such as greater chemical reactivity and useful optical features (e.g., strong visible fluorescence).[41] Such properties are being executed for various applications, from medical treatments, using in various branches of industry production such as solar and oxide fuel batteries for energy storage, to diverse materials of everyday use such as cosmetics or clothes.[39, 42] The nanoparticles have large surface area/volume ratio and tend to agglomerate into large clusters losing the specific properties associated with their nanometer dimensions. Therefore, appropriate surface modification and particle

stabilization plays a crucial role in extending the utility of nanoparticles into bioapplications. Nanoparticles are often coated with polymers to prevent from aggregation or degradation. Traditionally polymers are usually coated on nanoparticles by physisorption to provide a passivation layer in colloidal chemistry. Another method employs polyelectrolytes as the coating materials using coulombic attraction between charged nanoparticles and the oppositely charged polyelectrolyte polymer. The thickness of the coating is controlled by depositing additional layers of opposite charged polyelectrolytes. However, not all polymers are available in polyelectrolyte form so this approach is quite limited. More pragmatic attachment of polymers to nanoparticle surfaces is through covalent linkages by two common approaches: grafting onto[43-46] and grafting-from[47-50]. The grafting to method involves the synthesis of a polymer with a reactive end group that is attached to the surface of the nanoparticle. By this approach polymers are end-functionalized and can react with surface functionalities on the nanoparticles. This method allows explicit control of the molecular weight (Mn) and polydispersity index (PDI). Alternatively, grafting from involves in situ polymerization of monomers directly from the nanoparticles. While the grafting from approach promises high grafting ratios, it typically requires the attachment of an initiating group prior to polymerization.

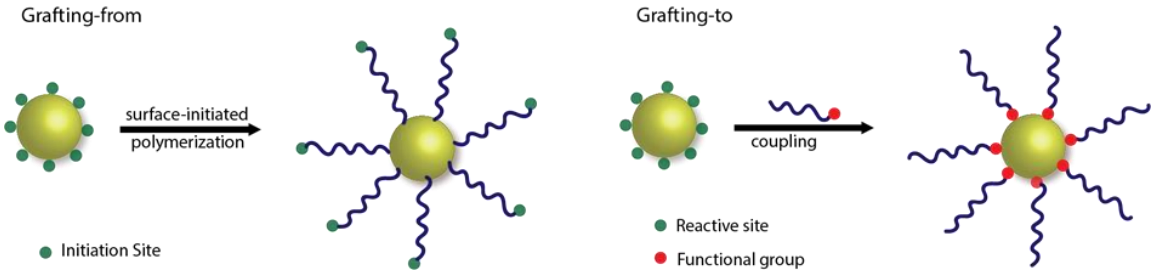

Figure 1.1 Two strategies to modify nanoparticles surface with polymers

1.4 Polymerization Techniques

Reversible Addition Fragmentation Chain Transfer Polymerization (RAFT). RAFT polymerization is a common controlled radical polymerization technique that was developed in late 1990s at CSIRO. It can obtain predetermined molecular weight, and narrow molecular weight distributions.[51-53] The RAFT process consists of traditional free radical polymerization of a monomer in the presence of a chain transfer agent, also known as RAFT agent or chain transfer agent. The chemical structure of a RAFT agent typically has a dithioester group (S=C-S) with substituents R and Z that impact the polymerization kinetics. The Z groups are chosen in such a way that to stabilize propagating radicals while the R group plays a vital role to the initiation of the radical intermediate and its ability to fragment. Phenyl group is most often encountered as the Z group in RAFT agent. The best R groups are those that have steric hindrance and contain an electron withdrawing group. The most widely used R groups are cumyl and cyanoisopropyl groups.

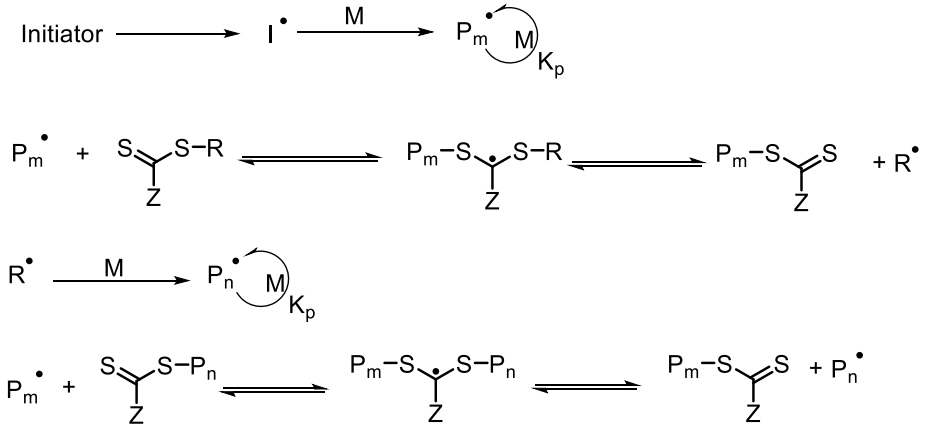

Figure 1.2 Overall mechanism of RAFT polymerization

Currently dithiobenzoates are the most commonly used RAFT agents because of their ability to show control over various monomers and radical initiators. RAFT

polymerization has been used to prepared polymers of complex architectures, including block copolymers, brush polymers and dendrimers.

Ring-Opening Metathesis Polymerization (ROMP). ROMP is a recently-developed polymerization method which is an attractive technique to prepare new polymers with controlled molecular architectures. It is robust, high efficient, and easy to operate.[54] ROMP is an olefin metathesis chain-growth polymerization and the overall mechanism of ROMP is metal-mediated carbon-carbon double bond exchange with release of the ring strain energy as the driving force.[55] Polymers prepared by ROMP contain unsaturated double bonds in each repeating unit. The catalysts used in ROMP includes a variety of metals and the most well-known, high efficient catalysts are ruthenium based Grubbs' catalysts. Figure 1.7 shows the three different generations of Grubbs catalysts.

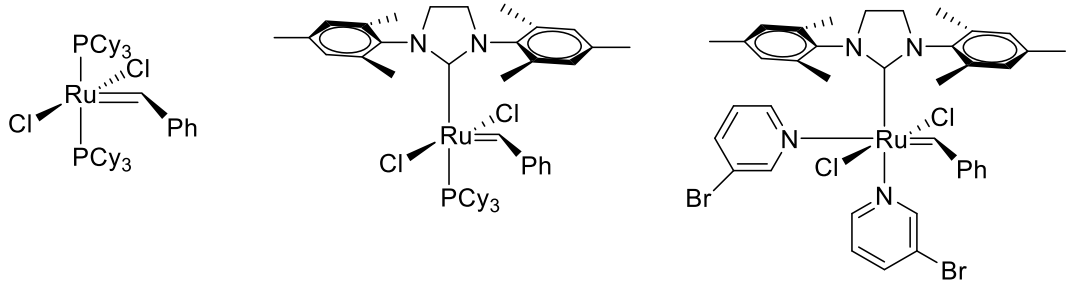

Grubbs' I catalyst Grubbs' II catalyst Grubbs' III catalyst

Figure 1.3 Grubbs catalysts for ROMP

1.5 Dissertation Outline

Inspired by the advance of metal-containing small molecular drugs and promoted by the great progress in polymer chemistry, metal-containing polymers have gained momentum during recent decades. In addition, the emergence of drug-resistant bacteria necessitates the development of new antimicrobial agents. The objectives of this dissertation are blended on those two areas of research. The goal of this dissertation is to

investigate cationic cobaltocenium polyelectrolytes and also prepare novel cobaltocenium-containing materials for antimicrobial application.

Chapter 2 describes study of binding of cobaltocenium-containing polyelectrolytes with various anion probes using optical spectroscopy methods. The effect of various factors like electrostatic charge, conformation, size of anionic probes was investigated. Also, the polyelectrolyte complexes between a cationic cobaltocenium polymer and an anionic polymer were prepared to compare with a cationic quaternary ammonium polymer along with the study of comparative binding strength.

Chapter 3 focuses on the synthesis of a nontraditional strategy of resurrecting the traditional antibiotics by complexing with charged metallopolymer-grafted silica nanoparticles. This method not only saves the time but also ensures improved activity against both Gram-positive and Gram-negative bacteria.

Chapter 4 focuses on design and synthesis of highly efficient charged metallopolymer-grafted magnetic nanoparticles via surface-initiated RAFT polymerization. These nanoparticles displayed a response to external magnetic fields and were easily recycled after antibacterial tests. The recycled nanoparticle conjugates retained aqueous dispersibility and high antibacterial efficacy.

In Chapter 5, a strategy to prepare ultra-small cobaltocenium-containing nanoparticles using grafting-to mechanism is presented. The thiol end-capped cobaltocenium polymers were coated on gold nanoparticle surface and complexed with anionic penicillin-G to be used against notorious pathogens.

Finally, a summary is given in Chapter 6. In addition, some suggestions about continued and future research of cobaltocenium-containing polymers are provided.

1.6 References

1. Whittell, G. R.; Hager, M. D.; Schubert, U. S.; Manners, I., Functional soft materials from metallopolymers and metallosupramolecular polymers. *Nat. Mat.* **2011,** 10, 176.
2. Eloi, J.-C.; Chabanne, L.; Whittell, G. R.; Manners, I., Metallopolymers with emerging applications. *Mater. Today* **2008,** 11, (4), 28-36.
3. Hardy, C. G.; Zhang, J.; Yan, Y.; Ren, L.; Tang, C., Metallopolymers with transition metals in the side-chain by living and controlled polymerization techniques. *Prog. Polym. Sci* **2014,** 39, (10), 1742-1796.
4. Cui, C.; Heilmann-Brohl, J.; Sánchez Perucha, A.; Thomson, M. D.; Roskos, H. G.; Wagner, M.; Jäkle, F., Redox-Active Ferrocenylboronium Polyelectrolytes with Main Chain Charge-Transfer Structure. *Macromolecules* **2010,** 43, (12), 5256-5261.
5. Abd-El-Aziz, A. S.; Strohm, E. A., Transition metal-containing macromolecules: En route to new functional materials. *Polymer* **2012,** 53, (22), 4879-4921.
6. Wilkinson, G.; Rosenblum, M.; Whiting, M. C.; Woodward, R. B., THE STRUCTURE OF IRON BIS-CYCLOPENTADIENYL. *J. Am. Chem. Soc* **1952,** 74, (8), 2125-2126.
7. Neuse, E. W., Ferrocene-containing Polymers : Polycondensation of Ferrocene with Aldehydes. *Nature* **1964,** 204, 179.
8. Hudson, R. D. A., Ferrocene polymers: current architectures, syntheses and utility. *J. Organomet. Chem* **2001,** 637-639, 47-69.
9. R., W. G.; I., M., Metallopolymers: New Multifunctional Materials. *Adv. Mat.* **2007,** 19, (21), 3439-3468.
10. Astruc, D., Why is ferrocene so exceptional? *Eur. J. Inorg. Chem* **2017,** 2017, (1), 6-29.
11. Hardy, C. G.; Ren, L.; Tamboue, T. C.; Tang, C., Side-chain ferrocene-containing (meth) acrylate polymers: Synthesis and properties. *J. Polym. Sci. A: Polymer Chemistry* **2011,** 49, (6), 1409-1420.
12. Qiu, H.; Gilroy, J. B.; Manners, I., DNA-induced chirality in water-soluble poly (cobaltoceniumethylene). *Chem. Comm.* **2013,** 49, (1), 42-44.
13. Gilroy, J. B.; Patra, S. K.; Mitchels, J. M.; Winnik, M. A.; Manners, I., Main-Chain Heterobimetallic Block Copolymers: Synthesis and Self-Assembly of Polyferrocenylsilane-b-Poly (cobaltoceniumethylene). *Angew. Chem. Int. Ed* **2011,** 50, (26), 5851-5855.
14. Sheats, J. E.; Rausch, M. D., Synthesis and properties of cobalticinium salts. I. Synthesis of monosubstituted cobalticinium salts. *J. Org. Chem.* **1970,** 35, (10), 3245-3249.
15. U., P. C.; E., A. O.; B., S.; P., M. S.; E., S. J., Organometallic polymers, 28 Condensation polymerization of cobalticinium salts. *Die Makromolekulare Chemie* **1974,** 175, (5), 1427-1437.

16. Mayer, U. F. J.; Gilroy, J. B.; O'Hare, D.; Manners, I., Ring-Opening Polymerization of 19-Electron [2]Cobaltocenophanes: A Route to High-Molecular-Weight, Water-Soluble Polycobaltocenium Polyelectrolytes. *J. Am. Chem. Soc.* **2009,** 131, (30), 10382-10383.
17. Vanicek, S.; Kopacka, H.; Wurst, K.; Müller, T.; Schottenberger, H.; Bildstein, B., Chemoselective, Practical Synthesis of Cobaltocenium Carboxylic Acid Hexafluorophosphate. *Organometallics* **2014,** 33, (5), 1152-1156.
18. Yan, Y.; Zhang, J.; Qiao, Y.; Tang, C., Facile Preparation of Cobaltocenium-Containing Polyelectrolyte via Click Chemistry and RAFT Polymerization. *Macromol. Rapid Comm.* **2014,** 35, (2), 254-259.
19. Ren, L.; Hardy, C. G.; Tang, C., Synthesis and Solution Self-Assembly of Side-Chain Cobaltocenium-Containing Block Copolymers. *J. Am. Chem. Soc.* **2010,** 132, (26), 8874-8875.
20. Ren, L.; Hardy, C. G.; Tang, S.; Doxie, D. B.; Hamidi, N.; Tang, C., Preparation of Side-Chain 18-e Cobaltocenium-Containing Acrylate Monomers and Polymers. *Macromolecules* **2010,** 43, (22), 9304-9310.
21. Ren, L.; Zhang, J.; Bai, X.; Hardy, C. G.; Shimizu, K. D.; Tang, C., Preparation of cationic cobaltocenium polymers and block copolymers by "living" ring-opening metathesis polymerization. *Chem. Sci.* **2012,** 3, (2), 580-583.
22. Yi, Y.; Jiuyang, Z.; Yali, Q.; Chuanbing, T., Facile Preparation of Cobaltocenium-Containing Polyelectrolyte via Click Chemistry and RAFT Polymerization. *Macromol. Rapid Comm.* **2014,** 35, (2), 254-259.
23. Zhang, J.; Ren, L.; Hardy, C. G.; Tang, C., Cobaltocenium-Containing Methacrylate Homopolymers, Block Copolymers, and Heterobimetallic Polymers via RAFT Polymerization. *Macromolecules* **2012,** 45, (17), 6857-6863.
24. Yi, Y.; Jiuyang, Z.; Perry, W.; Yali, Q.; Chuanbing, T., Ring-Opening Metathesis Polymerization of 18-e Cobalt(I)-Containing Norbornene and Application as Heterogeneous Macromolecular Catalyst in Atom Transfer Radical Polymerization. *Macromol. Rapid Comm.* **2014,** 35, (21), 1840-1845.
25. Yang, P.; Pageni, P.; Kabir, M. P.; Zhu, T.; Tang, C., Metallocene-Containing Homopolymers and Heterobimetallic Block Copolymers via Photoinduced RAFT Polymerization. *ACS Macro Letters* **2016,** 5, (11), 1293-1300.
26. Matsuzaki, K., Control of cell selectivity of antimicrobial peptides. *Biochimica et Biophysica Acta (BBA)-Biomembranes* **2009,** 1788, (8), 1687-1692.
27. Chen, Y.; Wilbon, P. A.; Chen, Y. P.; Zhou, J. H.; Nagarkatti, M.; Wang, C. P.; Chu, F. X.; Decho, A. W.; Tang, C. B., Amphipathic antibacterial agents using cationic methacrylic polymers with natural rosin as pendant group. *Rsc Advances* **2012,** 2, (27), 10275-10282.
28. Wang, J.; Chen, Y. P.; Yao, K.; Wilbon, P. A.; Zhang, W.; Ren, L.; Zhou, J.; Nagarkatti, M.; Wang, C.; Chu, F.; He, X.; Decho, A. W.; Tang, C., Robust Antimicrobial Compounds and Polymers Derived from Natural Resin Acids. *Chem. Comm.* **2012,** 48, 916-918.
29. Lienkamp, K.; Madkour, A. E.; Kumar, K. N.; Nüsslein, K.; Tew, G. N., Antimicrobial Polymers Prepared by Ring-Opening Metathesis Polymerization: Manipulating Antimicrobial Properties by Organic Counterion and Charge Density Variation. *Chemistry – A European Journal* **2009,** 15, (43), 11715-11722.

30. Lienkamp, K.; Madkour, A. E.; Musante, A.; Nelson, C. F.; N., K.; Tew, G. N., Antimicrobial Polymers Prepared by ROMP with Unprecedented Selectivity: A Molecular Construction Kit Approach. *J. Am. Chem. Soc.* **2008,** 130, (30), 9836-9843.
31. Li, P.; Poon, Y.; Li, W. F.; Zhu, H.; Yeap, S. H.; Cao, Y.; Qi, X. B.; Zhou, C.; Lamrani, M.; Beuerman, R. W.; Kang, E. T.; Mu, Y.; Li, C.; Chang, M.; Jan Leong, S. S.; Chan-Park, M. B., A polycationic antimicrobial and biocompatible hydrogel with microbe membrane suctioning ability. *Nat. Mat.* **2011,** 10, (2), 149-156.
32. Nederberg, F.; Zhang, Y.; Tan, J. P. K.; Xu, K.; Wang, H.; Yang, C.; Gao, S.; Guo, X.; Fukushima, K.; Li, L.; Hedrick, J. L.; Yang, Y., Biodegradable nanostructures with selective lysis of microbial membranes. *Nat. Chem.* **2011,** 3, 409-414.
33. Ganewatta, M. S.; Chen, Y. P.; Wang, J.; Zhou, J.; Ebalunode, J.; Nagarkatti, M.; Decho, A. W.; C., T., Bio-inspired Resin Acid-Derived Materials as Anti-Bacterial Resistance Agents with Unexpected Activities. *Chem. Sci.* **2014,** 5, 2011-2016.
34. Baudrion, F.; Perichaud, A.; Coen, S., Chemical modification of hydroxyl functions: Introduction of hydrolyzable ester function and bactericidal quaternary ammonium groups. *J. Appl. Polym. Sci.* **1998,** 70, (13), 2657-2666.
35. Palermo, E. F.; Kuroda, K., Chemical Structure of Cationic Groups in Amphiphilic Polymethacrylates Modulates the Antimicrobial and Hemolytic Activities. *Biomacromolecules* **2009,** 10, (6), 1416-1428.
36. Chen, C. Z.; Beck-Tan, N. C.; Dhurjati, P.; van Dyk, T. K.; LaRossa, R. A.; Cooper, S. L., Quaternary Ammonium Functionalized Poly(propylene imine) Dendrimers as Effective Antimicrobials: Structure−Activity Studies. *Biomacromolecules* **2000,** 1, (3), 473-480.
37. Tashiro, T., Antibacterial and Bacterium Adsorbing Macromolecules. *Macromol. Mater. Eng.* **2001,** 286, (2), 63-87.
38. Rózga-Wijas, K.; Mizerska, U.; Fortuniak, W.; Chojnowski, J.; Hałasa, R.; Werel, W., Quaternary Ammonium Salts (QAS) Modified Polysiloxane Biocide Supported on Silica Materials. *J. Inorg. Organomet. Polym. Mat.* **2007,** 17, (4), 605-613.
39. Nederberg, F.; Zhang, Y.; Tan, J. P.; Xu, K.; Wang, H.; Yang, C.; Gao, S.; Guo, X. D.; Fukushima, K.; Li, L., Biodegradable nanostructures with selective lysis of microbial membranes. *Nat. Chem.* **2011,** 3, (5), 409.
40. Yavuz, M. S.; Cheng, Y.; Chen, J.; Cobley, C. M.; Zhang, Q.; Rycenga, M.; Xie, J.; Kim, C.; Song, K. H.; Schwartz, A. G., Gold nanocages covered by smart polymers for controlled release with near-infrared light. *Nat. Mat.* **2009,** 8, (12), 935.
41. Aruguete, D. M.; Kim, B.; Hochella, M. F.; Ma, Y.; Cheng, Y.; Hoegh, A.; Liu, J.; Pruden, A., Antimicrobial nanotechnology: its potential for the effective management of microbial drug resistance and implications for research needs in microbial nanotoxicology. *Environmental Science: Processes & Impacts* **2013,** 15, (1), 93-102.
42. Petros, R. A.; DeSimone, J. M., Strategies in the design of nanoparticles for therapeutic applications. *Nat. Rev. Drug Discov.* **2010,** 9, (8), 615.
43. Zhao, B.; Brittain, W. J., Polymer brushes: surface-immobilized macromolecules. *Prog. Polym. Sci* **2000,** 25, (5), 677-710.
44. Saleh, N.; Phenrat, T.; Sirk, K.; Dufour, B.; Ok, J.; Sarbu, T.; Matyjaszewski, K.; Tilton, R. D.; Lowry, G. V., Adsorbed triblock copolymers deliver reactive iron nanoparticles to the oil/water interface. *Nano letters* **2005,** 5, (12), 2489-2494.

45. Pyun, J.; Kowalewski, T.; Matyjaszewski, K., Synthesis of polymer brushes using atom transfer radical polymerization. *Macromol. Rapid Comm.* **2003,** 24, (18), 1043-1059.
46. Huang, J.; Koepsel, R. R.; Murata, H.; Wu, W.; Lee, S. B.; Kowalewski, T.; Russell, A. J.; Matyjaszewski, K., Nonleaching antibacterial glass surfaces via "grafting onto": the effect of the number of quaternary ammonium groups on biocidal activity. *Langmuir* **2008,** 24, (13), 6785-6795.
47. Matyjaszewski, K.; Miller, P. J.; Shukla, N.; Immaraporn, B.; Gelman, A.; Luokala, B. B.; Siclovan, T. M.; Kickelbick, G.; Vallant, T.; Hoffmann, H., Polymers at interfaces: using atom transfer radical polymerization in the controlled growth of homopolymers and block copolymers from silicon surfaces in the absence of untethered sacrificial initiator. *Macromolecules* **1999,** 32, (26), 8716-8724.
48. Murata, H.; Koepsel, R. R.; Matyjaszewski, K.; Russell, A. J., Permanent, non-leaching antibacterial surfaces—2: How high density cationic surfaces kill bacterial cells. *Biomaterials* **2007,** 28, (32), 4870-4879.
49. Matyjaszewski, K.; Dong, H.; Jakubowski, W.; Pietrasik, J.; Kusumo, A., Grafting from surfaces for "everyone": ARGET ATRP in the presence of air. *Langmuir* **2007,** 23, (8), 4528-4531.
50. Tsujii, Y.; Ohno, K.; Yamamoto, S.; Goto, A.; Fukuda, T., Structure and properties of high-density polymer brushes prepared by surface-initiated living radical polymerization. In *Surface-initiated polymerization I*, Springer: 2006; pp 1-45.
51. Li, C.; Han, J.; Ryu, C. Y.; Benicewicz, B. C., A Versatile Method To Prepare RAFT Agent Anchored Substrates and the Preparation of PMMA Grafted Nanoparticles. *Macromolecules* **2006,** 39, (9), 3175-3183.
52. Chiefari, J.; Chong, Y. K.; Ercole, F.; Krstina, J.; Jeffery, J.; Le, T. P. T.; Mayadunne, R. T. A.; Meijs, G. F.; Moad, C. L.; Moad, G.; Rizzardo, E.; Thang, S. H., Living Free-Radical Polymerization by Reversible Addition−Fragmentation Chain Transfer: The RAFT Process. *Macromolecules* **1998,** 31, (16), 5559-5562.
53. Moad, G.; Rizzardo, E.; Thang, S. H., Radical addition–fragmentation chemistry in polymer synthesis. *Polymer* **2008,** 49, (5), 1079-1131.
54. Bielawski, C. W.; Grubbs, R. H., Living ring-opening metathesis polymerization. *Prog. Polym. Sci* **2007,** 32, (1), 1-29.
55. Hejl, A.; Scherman, O. A.; Grubbs, R. H., Ring-opening metathesis polymerization of functionalized low-strain monomers with ruthenium-based catalysts. *Macromolecules* **2005,** 38, (17), 7214-7218.

CHAPTER 2

BINDING OF COBALTOCENIUM-CONTAINING POLYELECTROLYTES WITH ANIONIC PROBES[1]

[1] Pageni, P.; Kabir, M.P.; Yang, P.; Tang, C. Binding of Cobaltocenium-Containing Polyelectrolytes with Anionic Probes. *J. Inorg. Organomet. Polym.*, **2017**, 27, 1100-1109. Reprinted here with permission of publisher.

2.1 Abstract

Cationic cobaltocenium-containing polyelectrolytes have a unique ability to form ionic complex with various anionic species. However, the relative binding strength is under explored. We carried out two sets of model study to compare the relative binding strength of a cobaltocenium-containing polyelectrolyte. Firstly, the nature and relative strength of intermolecular interaction between cobaltocenium-containing polyelectrolytes and different anionic probes were investigated by spectroscopic methods. A dye-displacement method was used to monitor absorbance and fluorescence emissions. Secondly, the binding strength of this cobaltocenium-containing polyelectrolyte was compared with a classical quaternary ammonium polymer. Formation of polyelectrolyte complex between the cobaltocenium-containing polyelectrolyte and a common anionic polyelectrolyte at various concentrations was examined by optical absorption and light scattering.

2.2 Introduction

A polyelectrolyte refers to a macromolecule with ionically charged motifs either on their side chain or on the backbone. It is often termed as a polymeric-electrolyte with dual characteristics of a polymer and an electrolyte. The most significant property of polyelectrolytes turns out to be the water solubility, which opens the door for various applications in food industry,[1, 2] ultrafiltration,[3, 4] waste water treatment,[5, 6] fuel cells,[7-10] biomaterials[11-14] and nanotechnology.[15-18] Cationic polyelectrolytes have basic groups such as phosphonium, sulfonium, ammonium, imidazolium or pyridinium in their structure, while anionic polyelectrolytes have acidic groups like sulfonate, phosphate, carboxylate, phosphonate and arsenate.[19-21] Some of the commonly used polyelectrolytes are polystyrene sulfonate, polyacrylic and polymethacrylic acid along with their salts, DNA

and other polybases and polyacids.[22] There have been notable advancements made in designing structures with respect to the nature of ionic moieties. Cationic metallocene such as cobaltocenium is particularly interesting as it possesses intrinsic cationic metal center coupled with counterions and is a good candidate to be used as an ionic center in polyelectrolytes. However, synthetic challenges posed by the high chemical stability of cobaltocenium limits the synthesis of cobaltocenium-containing polymers.[23, 24]

Most of metallocene-containing electrolytes have been exclusively based on ferrocene and widely utilized for applications ranging from electrochemical sensors to templates for advanced materials to biomedicines.[25-34] Compared with ferrocene, it is difficult to prepare derivatives from cobaltocene or cobaltocenium by electrophilic substitution due to the ease in oxidation of cobaltocene and the inertness of cobaltocenium salts.[35] Thus, the incorporation of cobaltocene/cobaltocenium into polymers has been far less explored than ferrocene. Most of the initial work on cobaltocenium-containing polymers started off with synthesis of short main-chain polymers via condensation polymerization.[36-38] It was partly because of the straightforward synthesis of disubstituted cobaltocenium. Manners and coworkers were able to employ ring-opening polymerization (ROP) to prepare high molecular weight water soluble main-chain cobaltocenium-containing polymers.[39, 40] In addition, significant amount of efforts was directed to synthesize cobaltocenium-containing dendrimers.[41-44] Solid phase peptide synthesis was utilized by Metzler-Nolte and co-workers to make series of cobaltocenium bioconjugates using cobaltocenium acid.[45, 46] The development of practical synthesis of the monosubstituted cobaltocenium achieved by our group[47] and others[48] paved the way for the efficient and scalable synthesis of side-chain cobaltocenium-containing

polyelectrolytes. A major thrust for creating novel cobaltocenium polyelectrolytes is fueled by the progress in controlled free radical polymerization (CFRP) techniques.[49] Recently, we reported the synthesis of side-chain cobaltocenium-containing polyelectrolytes and their applications as advanced materials.[50-53] In addition, side-chain cobaltocenium-containing polyelectrolytes were utilized as novel antimicrobial materials to kill bacteria.[54] These cobaltocenium-containing polyelectrolytes were able to rejuvenate the traditional β-lactam antibiotics by forming an ionic interaction between carboxylic anions and cationic cobaltocenium moieties to inhibit the degradation of drugs. However, the effects of different parameters of small anionic probes such as electrostatic charge, size, conformation and π-electron system on the interactions of these useful polyelectrolytes have not been investigated. Also, the relative binding strength of these polymers in comparison to other cationic polymers is still a mystery.

To explore those pristine fields, we designed two separate experiments. First, a qualitative study was carried out with a fluorescence dye to make a complex with polymers followed by the addition of small anionic probes to displace the dye. The released amount of dye was measured using optical absorption, which gives the relative binding affinity of anionic probes to polymers. The second aspect of this study was to conduct the comparative study of binding strength of cobaltocenium-containing polyelectrolyte with anionic polyelectrolyte. Formation of polyelectrolyte complex (PEC) in various concentrations was examined, and the optical transmittance was measured.

2.3 Experimental Section

Characterization

^{1}H NMR spectra (400 MHz) were recorded on a Varian Mercury 400 NMR spectrometer with tetramethylsilane (TMS) as an internal reference. Mass spectrometry was conducted on a Waters Micromass Q-TOF mass spectrometer, and the ionization source was positive ion electrospray. UV-vis was carried out on a Shimadzu UV-2450 spectrophotometer with a 10.00 mm quartz cuvette and monochromatic light of various wavelengths over a range of 190-900 nm. Dynamic light scattering (DLS) was operated on a Nano-ZS instrument, model ZEN 3600 (Malvern Instruments. Fluorescence emission intensity was measured by using Cary Eclipse Fluorescence Spectrophotometer).

Materials and Methods

2-Cobaltocenium amidoethyl methacrylate hexafluorophosphate ($CoAEMAPF_6$) was synthesized according to our earlier report.[51] 2-Aminoethyl methacrylate hydrochloride (90%), *N*-(3-dimethylaminopropyl)-*N′*-ethylcarbodiimide hydrochloride (EDC-HCl, 98%), 4-(dimethylamino) pyridine and tetrabutylammonium chloride (TBACl) were purchased from Aldrich and used as received. Tris buffer solution was prepared from tris(hydroxymethyl)aminomethane (Tris base) (Sigma-Aldrich) and concentrated hydrochloric acid (Sigma-Aldrich). Poly(sodium styrene sulfonate) (M_n = 70,000 g/mol) was purchased from Sigma as an anionic polyelectrolyte. The fluorescent probe 5(6)-carboxyfluorescein (as a mixture of isomers) was purchased from Sigma-Aldrich. Displacer anion solutions were prepared from succinic acid (Sigma), tricarballylic acid and 1,4-cyclohexanedicarboxylic acid (Acros), 1,2,3,4-butanetetracarboxylic acid and pimelic acid (Alfa Aesar), trimesic acid and 1,3,5- cyclohexanetricarboxylic acid (TCI America).

Water was from Thermo Scientific with ion conductivity at 18.20 MΩ. All other chemicals were from commercial sources and used as received.

Synthesis of Cationic (2-dimethylamino)ethyl methacrylate (DMAEMA)

Neutral DMAEMA (5.00 g, 31.90 mmol) was dissolved in 30 mL of dry DCM and chilled to 0 °C. Iodomethane (9.00 g, 63.80 mmol) was then added dropwise to the solution under stirring and reacted for 30 min at room temperature. After precipitation in ether, a white powder was obtained with a yield of 87%.

Synthesis of Cationic Poly((2-dimethylamino)ethyl methacrylate) (PDMAEMA)

Throughout this experiment cationic PDMAEMA will be used and will be referred as simply PDMAEMA. Cationic DMAEMA (0.50 g, 2.42 mmol), RAFT agent (6.75×10^{-3} g, 24.20×10^{-3} mmol) and AIBN (1.20×10^{-3} g, 7.31×10^{-4} mmol) were dissolved in 1.5 mL of dry MeOH in a 10 mL Schlenk flask and degassed by three cycles of freeze-pump-thaw. The reaction was heated under 70 °C until the desired conversion was reached and quenched by opening to air and cooled with ice water. The reaction was precipitated in acetone three times and vacuum-dried to afford a pink powder.

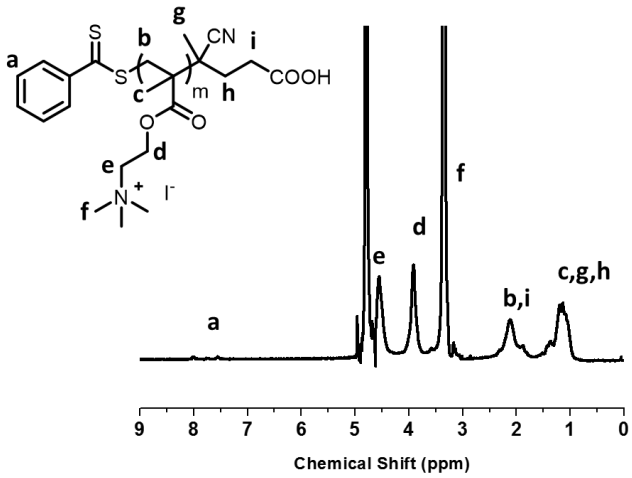

Figure 2.1 ^{1}H NMR spectrum of poly (dimethylamino methacrylate)

Synthesis of 2-Cobaltoceniumamidoethyl Methacrylate Hexafluorophosphate (MAEACoPF$_6$)

An amidation reaction was employed to synthesize MAEACoPF$_6$. Cobaltocenium carboxylic acid hexafluorophosphate (2.00 g, 5.29 mmol), 2-aminoethyl methacrylate hydrochloride (0.94 g, 5.68 mmol), and 4-(dimethylamino) pyridine (0.13 g, 1.06 mmol) were dissolved in 20 mL dry acetonitrile and the solution was cooled to 0 ^{o}C. Solution of EDC-HCl (1.10 g, 5.74 mmol) was then slowly added into previously cooled solution. Then, dry triethylamine (1.60 g, 15.80 mmol) was added into the reaction. The reaction was stirred for 4 hours. Solution was then extracted by saturated sodium hexafluorophosphate aqueous solution three times to remove unreacted starting materials. The organic phase was collected, condensed and precipitated into diethyl ether. Yellow solid was collected and dried under vacuum overnight. Yield: 1.60 g, 58%. ^{1}H NMR (CD_3COCD_3, δ, ppm): 8.30 (broad, *NH*CH2, 1H), 6.42 (t, Cp, 2H), 6.22 (m, *CH2*C, 1H), 6.10 (t, Cp, 2H), 5.92 (s, Cp, 5H), 5.62 (m, *CH2*C, 1H), 4.42 (m, O*CH2*CH2NH, 2H), 3.66 (m, OCH2*CH2*NH, 2H), 1.94 (m, *CH3*CCO, 3H).

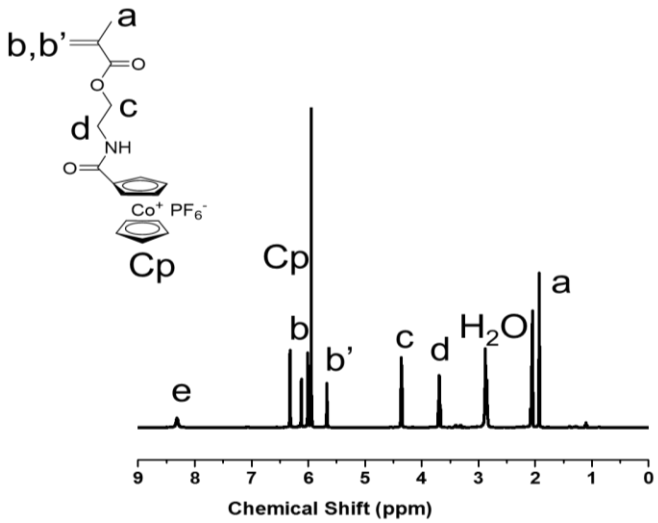

Figure 2.2. ^{1}H NMR spectrum of cobaltocenium monomer CoAEMAPF$_6$ in CD_3COCD_3

Synthesis of Poly(2-(methacrylolyamide) ethyl cobaltoceniumcarboxylate hexafluorophosphate) via RAFT polymerization ($PCoPF_6$)

$MAECoPF_6$ (0.30 g, 0.61 mmol), cumyl dithiobenzoate (CDB) (1.67×10^{-3} g, 6.10×10^{-3} mmol) and AIBN (0.20×10^{-3} g, 1.23×10^{-3} mmol) were dissolved by 0.40 mL DMF in a 10mL Schlenk flask and then were purged with N_2 for 30 min. The polymerization was started by heating the mixture at 90°C. Samples were taken out periodically to monitor the monomer conversion. Once the desired conversion was reached, polymerization reaction was quenched by exposure to air. The reaction mixture was then precipitated in cold DCM three times and vacuum dried overnight. Yield: 150×10^{-3} g, 80%. ^{1}H NMR (CD_3CN, δ): 7.4 (broad N*H*CH2), 6.2, 5.9, 5.8 (m, m, s, *Cp*), 4.2(broad, C*H*2OO) 3.6 (broad, NH*CH*2), 1.8 (broad, *CH2*C), 0.6-1.0 (broad, CC*H3*).

Titration conditions

All experiments were carried out in aqueous solutions buffered to pH 7.4 with Tris buffer solution at a temperature of 25 °C. The pH of the working solutions was adjusted prior to use by addition of NaOH or HCl solution and checked during a titration to make sure that it stayed at the desired value of 7.4. The concentration of polyelectrolytes in all experiments was maintained at 1.00×10^{-6} M.

Binding Isotherm

Stock solutions of dye, polymer, and displacer anions in a buffered solution were used as starting points for all experiments. All solutions used in this study were made by dilution of aliquots of these stock solutions. Binding isotherm experiment was conducted using constant polyelectrolytes (1.00×10^{-6} M) and different fluorophore concentration.

Absorbance and fluorescence emission readings were blanked by subtracting the corresponding reading for the buffer. The resulting data were plotted as a function of the [polyelectrolytes]/[fluorophore] ratio to produce binding isotherms.

General Displacement Titration Protocol

Displacement experiments were carried out using two separate working solutions: a "titrant" and a "cuvette" solution. Titrant and cuvette solutions were made fresh for each experiment. A cuvette solution contained both the dye ([CF] = 2.00×10^{-6} M) and the polyelectrolyte ([P] = 1.00×10^{-6} M) at an appropriate ratio to form the desired bound dye complex (P-CFn). The titrant solution contained a displacer anion at an appropriate concentration to carry out the titration. Titrations on benchtop instruments were carried out by addition of different aliquots of titrant solution to a constant volume of cuvette solution. The total volume of mixture was kept constant by addition of buffer solution. Using this method, the concentration of dye and polyelectrolyte remained constant but the concentration of displacer anion varied throughout the titration. The resulting data from fluorescence and UV-vis spectroscopy were plotted as a function of the [displacer anion]/[fluorophore] ratio to produce fluorescence intensity and absorbance isotherms.

Measurement of Transmittance

A typical experiment is described as an example. 1.00 mL of 0.10 mM PCoCl and PDMAEMA was placed in two different glass cuvettes followed by the measurement of transmittance. Different volumes of PSSNa (concentration= 0.10 mM) from 0.10 mL to 1.00 mL was added to both cuvettes. The addition of PSSNa was increased each time by 0.10 mL and subsequent transmittance of the resulting PEC solution was measured.

2.4 Results and Discussion

2.4.1 Binding of small anions with cobaltocenium-containing polymer.

In this model study, we synthesized a cobaltocenium-containing polymer, poly (cobaltocenium methacrylate) (PCoCl)with molecular weight of M_n = 19,000 g/mol via RAFT polymerization (Scheme 2.1). The disappearance of vinyl protons from methacrylate monomers around 5.0- 6.2 ppm and appearance of broad peaks around 0.5-2.0 ppm in ^{1}H NMR spectrum suggested the successful polymerization.

Scheme 2.1. Synthesis of poly (cobaltocenium methacrylate) by RAFT polymerization.

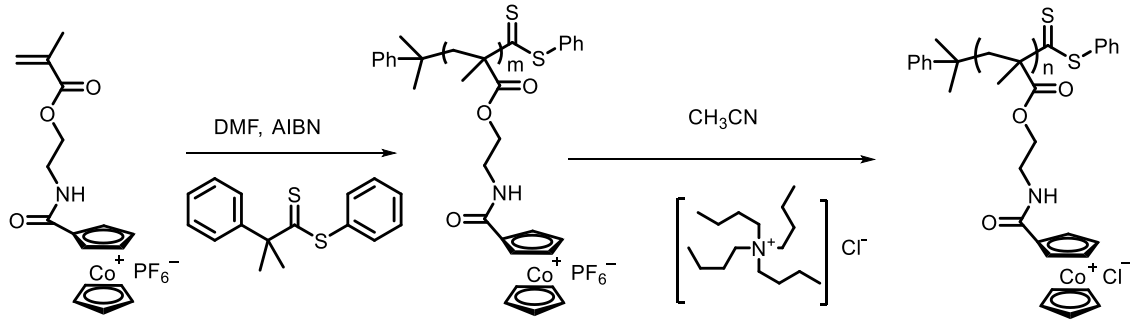

A number of small organic probes were selected to systematically investigate the relative binding affinity between polyelectrolytes and anionic probes. As shown in Table 2.1, the anionic probes in the same category differ by one key property, so that comparison of the relative affinities provides the important structural features for intermolecular interactions. The common techniques to investigate such intermolecular interactions like nuclear magnetic resonance (NMR) and mass spectrometry (MS) are not desirable in this situation. For effective NMR, higher concentration of samples is required but those concentrations of polymer-dye complex would result in a viscous solution with slow diffusion. Therefore, an optical spectroscopy method would be ideal as it is fast and efficient even at low concentrations.[55, 56] However, neither the polyelectrolytes nor the

organic probes have any significant chromophore or fluorophore to monitor their binding ability. Thus, the introduction of a reporting agent in the system is necessary.

Table 2.1 Anionic probes used to investigate the binding interaction with a cobaltocenium polymer

Properties under study	**Anionic Probes**
Electrostatic Interactions	$succinate^{2-}$ vs $tricarballylate^{3-}$ vs $butanetetracarboxylate^{4-}$
Guest Size	succinate (short) vs pimelate (long)
Guest Shape	tricarballylate (flexible) vs cyclohexanetricarboxylate (rigid)
Charge –π interactions	cyclohexanetricarboxylate (aliphatic) vs trimesate (aromatic)

In this approach, a trianion dye, 5(6)-carboxyfluorescein (CF), was used as a fluorescent indicator because the binding affinity of monoanion and dianion towards polyelectrolytes would be too low at a lower concentration. All experiments were conducted in a 50 mM aqueous Tris buffer solution with pH = 7.4 at 25°C. The polymer-dye complex (P-CFn) was firstly made as shown in Scheme 2.2, and then the nonfluorescent displacer probe was introduced to displace the dye from its polymer-dye complex to form a polymer-probe complex ($P\text{-}D_m$).

Scheme 2.2 Dye displacement assay used to detect binding of spectroscopically silent anionic guests (D) to the polymer (P) by using tri-anionic fluorescent dye 5(6)-carboxyfluorescein (CF).

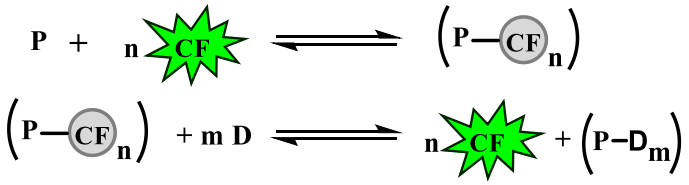

The polymer-probe complex can be monitored through the change in spectroscopic signature of the dye from its bound state to free state by UV-visible and fluorescence

emission spectroscopy. The spectroscopic signature is represented by the free dye anion. The ratio of the concentration of polymer to the concentration of dye is critical in the displacement experiment. When the polymer is used in excess, the dye would not fully bind to the polymer. This would result in unoccupied space in the polymer and resist any signal change. On the other hand, if the polymer is not enough, the excess dye would add to the displaced dye signature, which would result in the wrong estimation. We found the polymer could bind at least 85% dye. The fluorescence intensity and absorbance isotherms profiles were obtained by the titrations of displacer probes into a buffered solution of the polymer−dye complex. By comparing isotherm profiles for different displacer anions, the important structural properties for the binding to these polymers can be estimated.

i) Electrostatic charge

The effect of the electrostatic charge on the relative affinity for cobaltocenium polyelectrolytes was carried out by using a series of model carboxylate anions succinate, propane-1,2,3-tricarboxylate, and 1,2,3,4-butanetetracarboxylate, which respectively represents dianionic, trianionic, and tetraanionic species. The results showed that with the increase in charge in a guest anion, the binding affinity increased significantly (Figure 2.3). On average, the increase of one negative charge in the probe could increase the relative binding affinity by one order of magnitude,[57] highlighting the importance of electrostatic interactions.

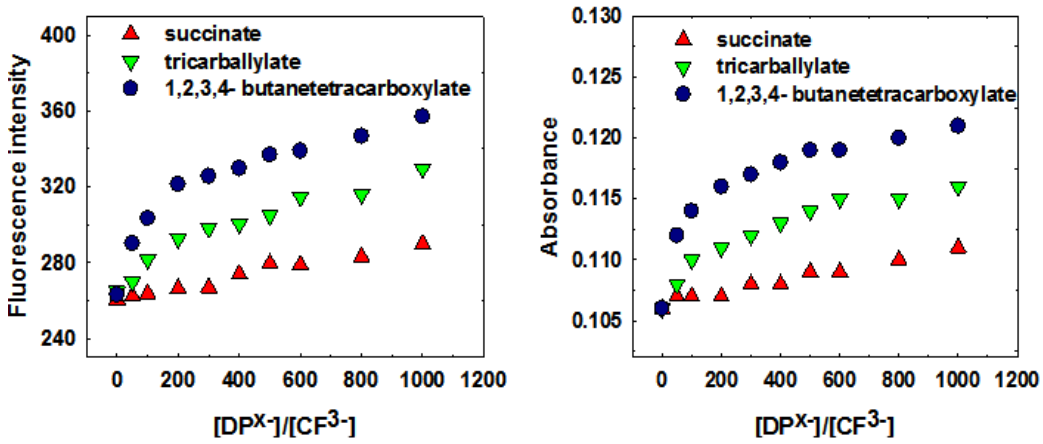

Figure 2.3 Fluorescence intensity and absorbance isotherms from titration of a PCFn complex with different displacer (DP). [CF] = 1.0 × 10^{-6} M, [Co^{+}] = 4.0× 10^{-6} M in buffered solution (50 mM Tris at pH 7.40), λexc = 494 nm.

ii) Guest Conformation

The effect of conformation of a guest anion on the relative affinity with the polymer was investigated by using cyclohexanetricarboxylate and tricarballylate. Both anions have three negative charges, but cyclohexanetricarboxylate is much more rigid due to its chair conformation whereas tricarballylate has less conformational restrictions because of linear backbone. As shown in the isotherms in Figure 2.4, the two anions showed similar binding affinity.

In order to explore the effect of guest size on the relative binding affinity, succinate and pimelate anions were studied. Both anions have two negative charges but differ in carbon chain length. The electrostatic contribution in their binding to the polymer would be equal. The result showed no difference in the binding behavior between two linear anions with different chain length. Thus, the size and conformation of the guest molecules

do not have significant influence on binding affinity for the cobaltocenium polymer.

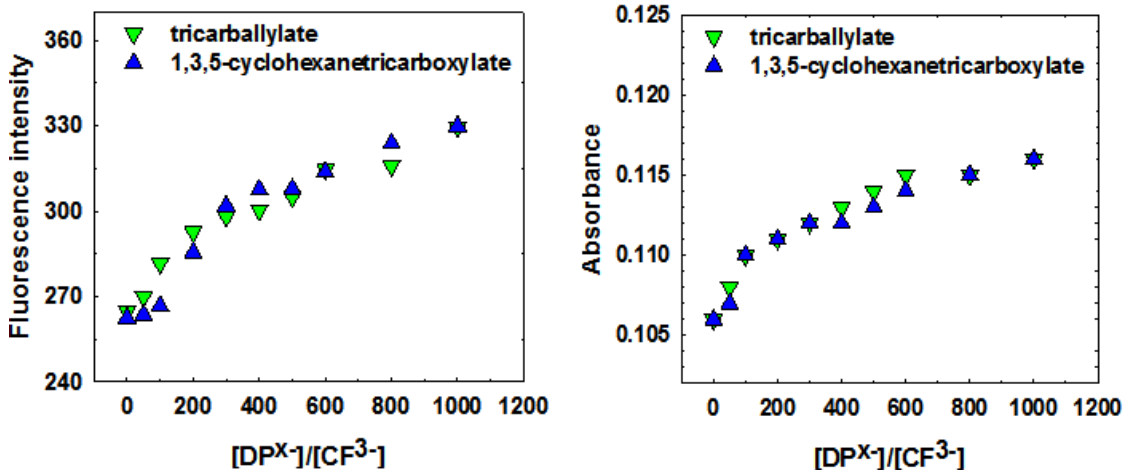

Figure 2.4 Fluorescence and absorbance isotherms from titration of a P-CFn complex with trianionic displacers with different shape. [CF] = 1.0×10^{-6} M, [Co^{+}] = 4.0×10^{-6} M in buffered solution (50 mM Tris at pH 7.4), λexc = 494nm**.**

iii) π-system

Finally, the effect of aromaticity of the displacer probe on the relative affinity was examined. For this purpose, Benzene- 1,3,5-tricarboxylate (trimesate) and 1,3,5-cyclohexanetricarboxylate anions were used. Both are trianions with similar size and conformation but have different π- electron system.

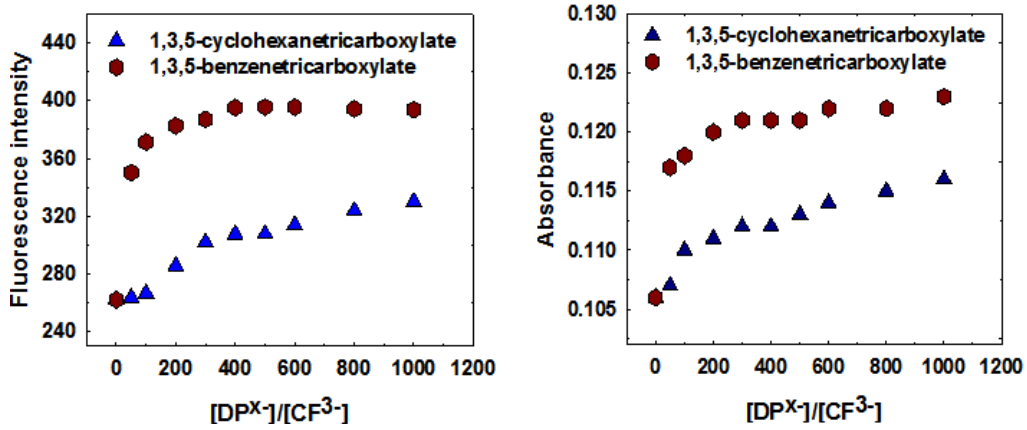

Figure 2.5 Fluorescence intensity and absorbance isotherms from titration of a P-CFn complex with trianionic aliphatic and aromatic guests. [CF] = 1.0×10^{-6} M, [Co^{+}] = 4.0×10^{-6} M in buffered solution (50 mM Tris at pH 7.40), λexc = 494nm.

As shown in Figure 2.5, the presence of π-system on guest anion (benzene- 1,3,5-tricarboxylate) increases the affinity for cationic cobaltocenium significantly. The difference on the relative affinity is due to an interaction mediated by the aromatic core of the trimesate anion. The positive charge in the cobaltocenium cation induces significant polarization of the C-H bonds in the cyclopentadiene. One of these C-H bonds in cyclopentadiene ring interacts with the π-electron cloud of the guest species. The overall process of interaction is promoted by the electrostatic charge on cobaltocenium in the polymer (Figure 2.6).

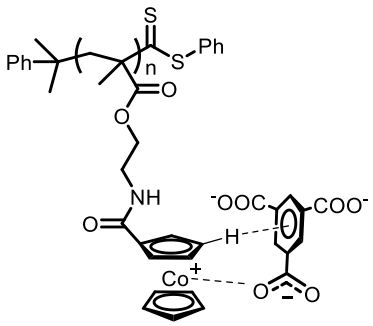

Figure 2.6 Proposed C-H-π interaction between cobaltocenium-containing polymer and trimesate anion.

2.4.2 Comparative study of binding strength of cobaltocenium-containing polymer.

The primary goal of this part of experiment was to compare the relative binding strength of cobaltocenium containing polymer with quaternary ammonium-containing polymer. For this purpose, PEC was formed between the cationic polymers under study and an anionic polymer, poly (sodium styrene sulfonate) (PSSNa), through strong Coulomb interactions. PEC has been used for various applications ranging from industrial applications for coatings, binders to biomedical and biotechnological applications.[58]

Poly((2-dimethylamino)ethyl methacrylate) (PDMAEMA) is one of the widely used cationic polymers that have found applications in various fields as a polyelectrolyte.[59-62] Cationic PDMAEMA (referred simply as PDMAEMA hereafter) with a similar structure to PCoCl was synthesized using RAFT polymerization (Scheme 2.3).

Scheme 2.3 Synthesis of poly((2-dimethylamino)ethyl methacrylate) by RAFT polymerization.

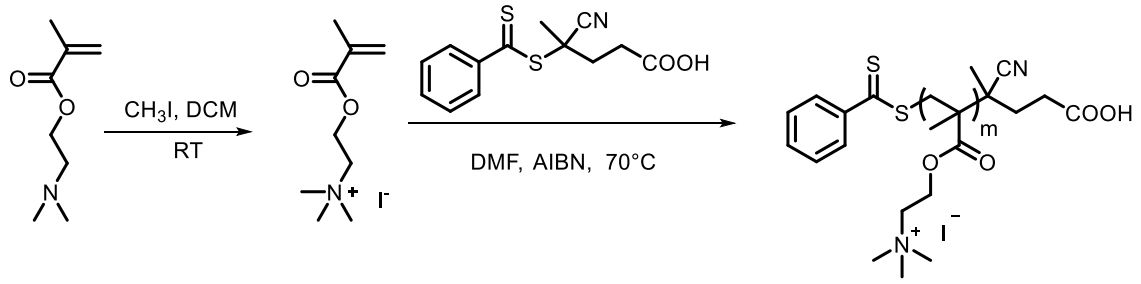

The degree of polymerization of both cationic polymers was controlled at 50 by tracking the monomer conversion during the polymerization process using ^{1}H NMR. The molecular weight of PCoCl and PDMAEMA was 19,000 g/mol and 15,000 g/mol, respectively. Throughout the experiment, equivalent moles of PCoCl and PDMAEMA were used against the same volume of PSSNa to measure the optical transmittance. To get the quantitative results, the formation of PEC between a cationic polymer and PSSNa at various concentrations were examined by a UV-vis spectrophotometer at room temperature.

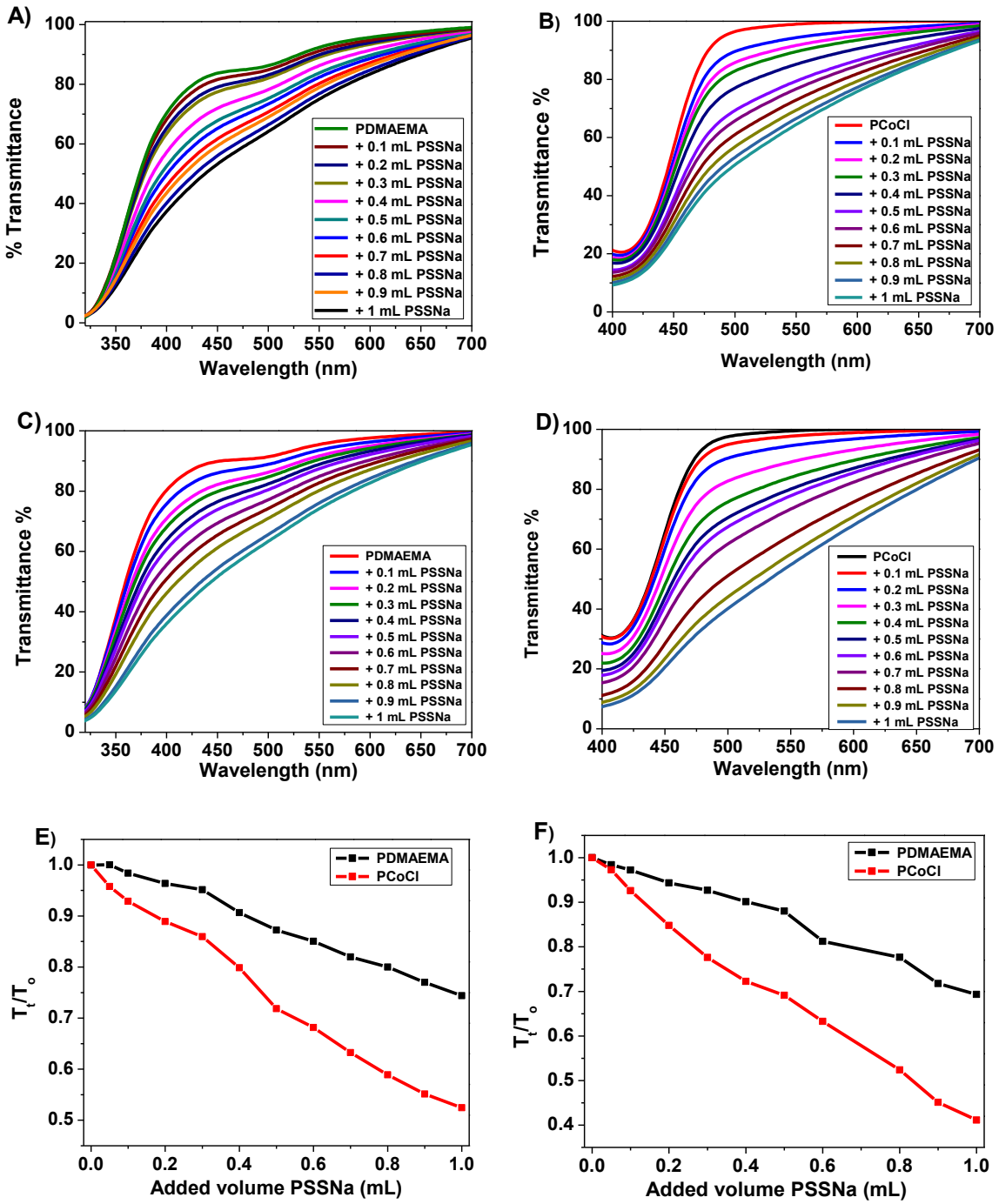

Figure 2.7 The transmittance of various polyelectrolyte solutions: A) 1.0 mL 0.10 mM PDMAEMA solution with addition of different volumes of 0.01 mM PSSNa; B) 1.0 mL 0.10 mM PCoCl solution with addition of different volumes of 0.01 mM PSSNa; C) 1.0 mL 0.20 mM PDMAEMA solution with addition of different volumes of 0.01 mM PSSNa D) 1.0 mL 0.20 mM PCoCl solution with addition of different volumes of 0.01 mM PSSNa; E) Transmittance ratio (T_t/T_o) as a function of volumes of PSSNa (mL) added with each concentration of PCoCl and PDMAEMA solutions at 0.10 mM; F) Transmittance ratio (T_t

/T_o) as a function of volumes of PSSNa (mL) added with each concentration of PCoCl and PDMAEMA solutions at 0.20 mM.

As shown in Figure 2.7, the transmittance of polyelectrolyte solutions (T_t) was compared with that of deionized water (T_o) as described by the ratio of T_t/T_o as a function of volume of PSSNa added. The difference observed in the transmittance of PEC solution could provide information about the relative binding strength between cationic polyelectrolytes and the anionic polyelectrolyte. Initially, 1.0 mL of 0.10 mM solutions of PCoCl and PDMAEMA was placed in two different cuvettes, and the transmittance was measured separately for both polymer solutions. Then, 0.10 mL PSSNa solution (0.01 mM) was added to both cuvettes. The transmittance of the resulting PEC solution was measured accordingly. The volume of PSSNa was increased each time by 0.10 mL until it reached 1.0 mL. The initial solutions of both cationic polymers were transparent. With the increase amount of PSSNa, the solutions gradually turned milky and turbid, formed opaque suspension, and then finally precipitated.

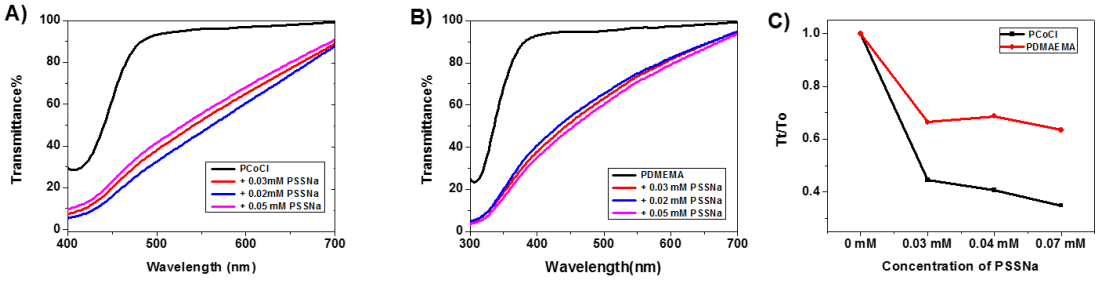

Figure 2.8 The transmittance of various polyelectrolyte solutions: A) 1.0 mL 0.10 mM PCoCl solution with different concentration of 1.0 mL PSSNa; B) 1.0 mL 0.10 mM PDMAEMA solution with various concentrations of 1.0 mL PSSNa; C) Transmittance ratio (T_t/T_o) as a function of concentrations of PSSNa.

The transmittance ratio clearly showed a higher decrease for PCoCl than PDMAEMA. When the concentration of each cationic polymer solution was 0.10 mM, the final transmittance caused by PCoCl was decreased to 52% as opposed to 74% by

PDMAEMA. The decrease in %T was even more prominent when 0.20 mM cationic polymer solutions were used. The final %T with PCoCl was about 41% while it was close to 69% for PDMAEMA.

A separate experiment was carried out by increasing the concentration of PSSNa to 0.02 mM, 0.03 mM and 0.07 mM. Accordingly, 1.0 mL of higher concentration PSSNa was added to 1.0 mL 0.01 mM cationic polymer solutions. With the addition of 1.0 mL 0.03 mM PSSNa, the reduction in transmittance was quite noteworthy for PCoCl. It decreased to 45% as compared to 66% for PDMAEMA as shown in Figure 2.8. Higher concentrations of PSSNa provided negatively charged motifs in excess so that cationic polymers can bind instantly, leading to a sudden decrease in transmittance. The effect of higher concentration was prominent when 0.07 mM PSSNa was used. The transmittance of PDMAEMA decreased to 65%, while the final transmittance of PCoCl reached down to 35%. It can be inferred that more PECs were formed in case of PSSNa-PCoCl than PSSNa-PDMAEMA as a result of stronger binding between PSSNa and PCoCl. Any concentrations higher than 0.07 mM PSSNa resulted in instant precipitation.

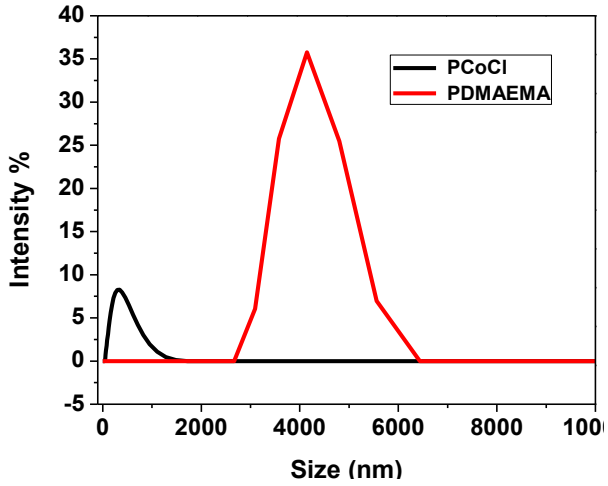

Figure 2.9 Size distribution of PCoCl-PSSNa and PDMAEMA-PSSNa complexes using DLS.

We further studied the size of PEC particles resulted from the mixing of cationic and anionic polymers by dynamic light scattering (DLS). As shown in Figure 2.9, the average diameter of PDMAEMA-PSSNa particles was about 4 μm, much larger than the average size of 300 nm for PCoCl-PSSNa particles. Based on these findings a more compact structure for PCoCl-PSSNa can be speculated in comparison to PDMAEMA-PSSNa.

2.5 Conclusions

In summary, we carried out two model studies to investigate the nature and relative strength of intermolecular interactions between cobaltocenium-containing polyelectrolytes and anionic probes using optical spectroscopy methods. We found that the electrostatic charge and the interaction with a π-electron moiety in the small molecular probes are the most influential factors in determining the binding affinity. However, the conformation and size of anionic probes do not significantly influence the binding affinity with the cationic polyelectrolyte. Furthermore, the polyelectrolyte complexes between a cationic cobaltocenium polymer and an anionic polymer were prepared to compare with a cationic quaternary ammonium polymer. The results demonstrated the cobaltocenium-containing polymer showed significantly higher binding with the anionic polymer than the quaternary ammonium counterpart. This work facilitated a better understanding on the fundamental interactions between cobaltocenium-containing polyelectrolytes and anionic probes.

2.6 References

1. J. Weiss, P. Takhistov and D. J. McClements, J. Food Sci. **71**, R107 (2006)
2. D. Guzey and D. J. McClements, Adv. Colloid Interface Sci. **128**, 227 (2006)
3. I. Korus and K. Loska, Desalination **247**, 390 (2009)
4. C.-W. Li, C.-H. Cheng, K.-H. Choo and W.-S. Yen, Chemosphere **72**, 630 (2008)
5. B. Bolto and J. Gregory, Water Res. **41**, 2301 (2007)

6. L. A. Chen, R. G. Carbonell and G. A. Serad, Water Res. **34**, 510 (2000)
7. B. R. Einsla, Y. S. Kim, M. A. Hickner, Y.-T. Hong, M. L. Hill, B. S. Pivovar and J. E. McGrath, J. Membr. Sci. **255**, 141 (2005)
8. S. P. Jiang, Z. Liu and Z. Q. Tian, Adv. Mater. **18**, 1068 (2006)
9. B. Smitha, S. Sridhar and A. A. Khan, Macromolecules **37**, 2233 (2004)
10. Y. Wan, B. Peppley, K. A. M. Creber, V. T. Bui and E. Halliop, J. Power Sources **185**, 183 (2008)
11. C. Boura, P. Menu, E. Payan, C. Picart, J. C. Voegel, S. Muller and J. F. Stoltz, Biomaterials **24**, 3521 (2003)
12. P.-H. Chua, K.-G. Neoh, E.-T. Kang and W. Wang, Biomaterials **29**, 1412 (2008)
13. G. Kumar, Y. C. Wang, C. Co and C.-C. Ho, Langmuir **19**, 10550 (2003)
14. C. Vodouhê, E. L. Guen, J. M. Garza, G. Francius, C. Déjugnat, J. Ogier, P. Schaaf, J.-C. Voegel and P. Lavalle, Biomaterials **27**, 4149 (2006)
15. J. García-Serrano, U. Pal, A. M. Herrera, P. Salas and C. Ángeles-Chávez, Chem. Mater. **20**, 5146 (2008)
16. T. K. Sau and C. J. Murphy, J. Am. Chem. Soc. **126**, 8648 (2004)
17. T. K. Sau and A. L. Rogach, Adv. Mater. **22**, 1781 (2010)
18. A. Rabiee, Journal of Vinyl and Additive Technology **16**, 111 (2010)
19. A. M. Herrera González, M. Caldera Villalobos, J. García-Serrano and A. A. Peláez Cid, Designed Monomers and Polymers **19**, 330 (2016)
20. A. Laschewsky, Curr. Opin. Colloid Interface Sci. **17**, 56 (2012)
21. F. Zhang, Y. Zhou, Y. Chen, Z. Shi, Y. Tang and T. Lu, J. Colloid Interface Sci. **351**, 421 (2010)
22. A. V. Dobrynin and M. Rubinstein, Prog. Polym. Sci. **30**, 1049 (2005)
23. L. Ren, C. G. Hardy and C. Tang, J. Am. Chem. Soc. **132**, 8874 (2010)
24. Y. Yan, P. Pageni, M. P. Kabir and C. Tang, Synlett **27**, 984 (2016)
25. C. G. Hardy, L. Ren, T. C. Tamboue and C. Tang, J. Polym. Sci., Part A: Polym. Chem. **49**, 1409 (2011)
26. W. Kaminsky, J. Polym. Sci., Part A: Polym. Chem. **42**, 3911 (2004)
27. A. S. Abd-El-Aziz and I. Manners, *Frontiers in Transition Metal-Containing Polymers*, Wiley, 2007.
28. G. R. Whittell, M. D. Hager, U. S. Schubert and I. Manners, Nat Mater **10**, 176 (2011)
29. D. Astruc, Eur. J. Inorg. Chem. **2017**, 6 (2017)
30. D. A. Foucher, B. Z. Tang and I. Manners, J. Am. Chem. Soc. **114**, 6246 (1992)
31. D. Astruc, Nat. Chem. **4**, 255 (2012)
32. E. W. Neuse, Journal of Inorganic and Organometallic Polymers and Materials **15**, 3 (2005)
33. A. I. Mufula, B. Aderibigbe, E. W. Neuse and H. E. Mukaya, Journal of Inorganic and Organometallic Polymers and Materials **22**, 423 (2012)
34. E. W. Neuse, M. G. Meirim, D. D. N" Da and G. Caldwell, J. Inorg. Organomet. Polym. **9**, 221 (1999)
35. J. E. Sheats and M. D. Rausch, The Journal of Organic Chemistry **35**, 3245 (1970)
36. C. Pittman Jr, O. Ayers, S. McManus, J. Sheats and C. Whitten, Macromolecules **4**, 360 (1971)

37. C. E. Carraher, G. F. Peterson, J. E. Sheats and T. Kirsch, Macromol. Chem. Phys. **175**, 3089 (1974)
38. C. Pittman, O. Ayers, B. Suryanarayanan, S. McManus and J. Sheats, Die Makromolekulare Chemie **175**, 1427 (1974)
39. U. F. Mayer, J. B. Gilroy, D. O'Hare and I. Manners, J. Am. Chem. Soc. **131**, 10382 (2009)
40. J. B. Gilroy, S. K. Patra, J. M. Mitchels, M. A. Winnik and I. Manners, Angew. Chem. Int. Ed. **50**, 5851 (2011)
41. D. Astruc, C. Ornelas and J. Ruiz, Acc. Chem. Res. **41**, 841 (2008)
42. C. M. Casado, B. González, I. Cuadrado, B. Alonso, M. Morán and J. Losada, Angew. Chem. **112**, 2219 (2000)
43. C. Ornelas, J. Ruiz and D. Astruc, Organometallics **28**, 2716 (2009)
44. K. Takada, D. J. Díaz, H. D. Abruña, I. Cuadrado, B. González, C. M. Casado, B. Alonso, M. Morán and J. Losada, Chemistry–A European Journal **7**, 1109 (2001)
45. A. Maurer, H. B. Kraatz and N. Metzler-Nolte, Eur. J. Inorg. Chem. **2005**, 3207 (2005)
46. A. Gross, D. Habig and N. Metzler-Nolte, ChemBioChem **14**, 2472 (2013)
47. Y. Yan, J. Zhang, Y. Qiao and C. Tang, Macromol. Rapid Commun. **35**, 254 (2014)
48. S. Vanicek, H. Kopacka, K. Wurst, T. Müller, H. Schottenberger and B. Bildstein, Organometallics **33**, 1152 (2014)
49. K. Matyjaszewski and J. Spanswick, Mater. Today **8**, 26 (2005)
50. J. Zhang, L. Ren, C. G. Hardy and C. Tang, Macromolecules **45**, 6857 (2012)
51. J. Zhang, J. Yan, P. Pageni, Y. Yan, A. Wirth, Y.-P. Chen, Y. Qiao, Q. Wang, A. W. Decho and C. Tang, Sci. Rep. **5**, 11914 (2015)
52. J. Zhang, Y. Yan, M. W. Chance, J. Chen, J. Hayat, S. Ma and C. Tang, Angew. Chem. Int. Ed. **52**, 13387 (2013)
53. J. Zhang, Y. Yan, J. Chen, W. M. Chance, J. Hayat, Z. Gai and C. Tang, Chem. Mater. **26**, 3185 (2014)
54. J. Zhang, Y. P. Chen, K. P. Miller, M. S. Ganewatta, M. Bam, Y. Yan, M. Nagarkatti, A. W. Decho and C. Tang, J. Am. Chem. Soc. **136**, 4873 (2014)
55. A. M. Jolly and M. Bonizzoni, Supramol. Chem. **27**, 151 (2015)
56. A. M. Mallet, A. B. Davis, D. R. Davis, J. Panella, K. J. Wallace and M. Bonizzoni, Chem. Commun. **51**, 16948 (2015)
57. A. M. Jolly and M. Bonizzoni, Macromolecules **47**, 6281 (2014)
58. S. Chen, M. Liu, S. Jin and Y. Chen, Polym. Int. **56**, 1305 (2007)
59. S. Agarwal, Y. Zhang, S. Maji and A. Greiner, Mater. Today **15**, 388 (2012)
60. J. Niskanen, C. Wu, M. Ostrowski, G. G. Fuller, S. Hietala and H. Tenhu, Macromolecules **46**, 2331 (2013)
61. M. Thomas, M. Gajda, C. Amiri Naini, S. Franzka, M. Ulbricht and N. Hartmann, Langmuir **31**, 13426 (2015)
62. W. Xu, I. Choi, F. A. Plamper, C. V. Synatschke, A. H. E. Müller, Y. B. Melnichenko and V. V. Tsukruk, Macromolecules **47**, 2112 (2014)

CHAPTER 3

CHARGED METALLOPOLYMER-GRAFTED SILICA NANOPARTICLES FOR ANTIMICROBIAL APPLICATIONS[2]

[2] Pageni, P.; Yang, P.; Chen, Y.;Huang, Y.; Bam, M.; Zhu, T.; Nagarkatti, M.;Benicewicz, B.; Decho A; Tang, C. Charged Metallopolymer-Grafted Silica Nanoparticles for Antimicrobial Applications *Biomacromolecules*, **2018**, 19, 417-425. Reprinted here with permission of publisher.

3.1 Abstract

Inappropriate and frequent use of antibiotics has led to the development of antibiotic-resistant bacteria, which cause infectious diseases that are difficult to treat. With the rising threat of antibiotic resistance, a need to develop effective new antimicrobial agents is prominent. We report antimicrobial metallopolymer nanoparticles, which were prepared by surface-initiated reversible addition−fragmentation chain transfer (RAFT) polymerization of cobaltocenium-containing methacrylate monomer from silica nanoparticles. These particles are capable of forming a complex with β-lactam antibiotics, such as penicillin, rejuvenating the bactericidal activity of antibiotic. Disk diffusion assays showed significantly increased antibacterial activities against both Gram-positive and Gram-negative bacteria. The improved efficiencies were attributed to the inhibition of hydrolysis of the β-lactam antibiotics, and enhancement of local antibiotics concentration on a nanoparticle surface. In addition, hemolysis evaluations demonstrated minimal toxicity to red blood cells.

3.2 Introduction

The widespread and excessive use of antimicrobial drugs has increased the endurance of microbes, making them more tolerant towards conventional antibiotics. Antimicrobial resistance has been highlighted as “one of the greatest threats to human health worldwide” by the Infectious Diseases Society of America, and the White House announced the National Strategy for Combating Antibiotic-Resistant Bacteria (CARB).[1] According to U.S. Centers for Disease Control and Prevention, at least 2 million people are affected annually by drug resistant bacteria in the U.S. alone, and 23,000 of them lose their lives.[2] The burden created by these infections on the economy is also substantial, and

estimated to result in $20 billion in additional health care costs and $35 billion in lost productivity annually.[3] As a result of antibiotic resistance, it is hard to treat major diseases because the drugs used are becoming progressively less effective. A variety of antibiotics are now being labelled ineffective, and the proliferation of bacteria is surging. The growing need to develop powerful antibacterial agents is fueled by the increasing daily incidence of bacterial infections. Therefore, it is urgent to direct efforts towards the development of novel antibiotics and more-effective therapeutics strategies to tackle this escalating health crisis.

The predominant synthetic microbial agents are compounds or polymers having cationic groups like quaternary ammonium or phosphonium, which promote rapid adsorption onto the negatively-charged bacterial cell surfaces.[4-8] Due to the physical nature of membrane disruption, the possibility of developing new resistant strains reduces significantly. However, many of these antimicrobial agents, while effective against certain types of bacterial strains, are notoriously toxic toward mammalian cells, thus limiting their roles in battling infections.[9-13] The use of nanotechnology has often been considered in developing alternative antimicrobial therapies. Nanoparticles have been widely used in pharmaceuticals, biomedicine and microbiology.[14,15] Nanoparticles could be a powerful tool to combat bacterial infections.[16] Antimicrobial agents have been constructed by both organic and inorganic nanoparticles such as silver,[17-19] gold,[20-22] zinc oxide,[23, 24] titanium dioxide,[25, 26] silica,[27, 28] copper oxide,[29] magnesium oxide[30], carbon based nanoparticles such as carbon nanotubes,[31-33] fullerenes,[34] graphene oxide[35]. In particular, silica nanoparticles have a high chemical, thermal and colloidal stability, and have been found to be useful in biomedical applications due to their biocompatibility, low toxicity, low

density, capacity for encapsulation and easy synthesis.[36, 37] In addition, they have larger surface areas, which can be functionalized using organo-silane chemistry to introduce desirable functional groups to regulate drug loading. The bactericidal effect of silica nanostructures could be fine-tuned by adjusting various parameters like particle size, shape, porosity and surface functionalization.[38] Kim *et al.* synthesized dual mode silica nanoparticles for specific binding to his-tagged proteins for purification and labeling of proteins.[39] Bharali *et al.* used amino-surface functionalized plasmid DNA-bounded silica nanoparticles for *in vivo* gene delivery.[40] Lui *et al.* broadened dimensions of silica nanoparticles to enhance image contrast and reported a detectable ultrasound behavior after administering 100 nm solid silica nanoparticles into mice.[41 42] A new class of nanoparticles, polymeric nanoparticle has been touted for various biomedical applications due to the versatility in modification to incorporate different functionalities.[15, 43-45] Nederberg *et al.* synthesized polymeric nanoparticles consisting of cationic amphiphilic triblock polycarbonates which selectively lysed microbial membranes.[46] They were not only biodegradable but also *in vivo* applicable and highly effective against drug resistant bacteria.

We recently demonstrated that low cytotoxic cationic cobaltocenium metallopolymers have antimicrobial efficacy against various bacterial strains including multidrug resistant bacteria by disarming activities of β-lactamase.[47] These charged metallopolymers were capable of protecting conjugated antibiotics via ion-pairing with cobaltocenium. We showed that these metallopolymers can inhibit the detrimental effects of the β-lactamase enzyme that is responsible for the hydrolysis of β-lactam antibiotics.

In an effort to further enhance the efficacy of cobaltocenium polymers, herein we

report surface-grafted cobaltocenium-containing silica nanoparticles. We carried out surface-initiated reversible addition−fragmentation chain transfer (RAFT) polymerization of cobaltocenium-containing methacrylate monomer from silica nanoparticles coated with 4-cyanopentanoic acid dithiobenzoate (CPDB). We then conjugated the antibiotic penicillin-G with the nanoparticles by ion-pairing between the cationic cobaltocenium moiety in the nanoparticles and carboxylate anions of antibiotics. Such bio-conjugated nanoparticles not only reduced the activity of β-lactamase but effectively lysed both Gram-positive and Gram-negative bacterial cells.

3.3 Experimental

Characterization

^{1}H (400 MHz), ^{13}C (100 MHz), and ^{19}F (376 MHz) NMR spectra were recorded on a Varian Mercury 400 NMR spectrometer with tetramethylsilane (TMS) as an internal reference. Mass spectrometry was conducted on a Waters Micromass Q-TOF mass spectrometer, and the ionization source was positive ion electrospray. UV−vis absorbance was carried out on a Shimadzu UV-2450 spectrophotometer with a 10.00 mm quartz cuvette and monochromatic light of various wavelengths over a range of 190−900 nm. A Hitachi 8000 transmission electron microscope (TEM) was used to acquire images at an operating voltage of 150 kV. TEM samples were prepared by dropping a solution of nanoparticles on carbon-supported copper grids and then dried before observation. Dynamic light scattering (DLS) was operated on a Nano-ZS instrument, Model ZEN 3600 (Malvern Instruments). Field-Emission Scanning Electron Microscopy (FE-SEM, Zeiss UltraPlus) was used for imaging of bacterial cells after overnight incubations with test

drugs. The samples were first coated for 45 s with gold using a Denton Dest II Sputter Coater, then observed by SEM.

Materials and Methods

2-Cobaltoceniumamidoethyl methacrylate hexafluorophosphate ($CoAEMAPF_6$) was synthesized according to our earlier report.[48] 2-Aminoethyl methacrylate hydrochloride (90%), *N*-(3-dimethylaminopropyl)-*N′*-ethylcarbodiimide hydrochloride (EDC-HCl, 98%), 4-(dimethylamino) pyridine and tetrabutylammonium chloride (TBACl) were purchased from Aldrich and used as received. Water was from Thermo Scientific Nanopure with ion conductivity at 18.2 MΩ. The following bacterial strains were purchased from ATCC: *Staphylococcus aureus* (ATCC-33591), *Escherichia coli* (ATCC-11775), *Klebsiella pneumoniae* (ATCC-35596), *Proteus vulgaris* (*P. vulgaris*, ATCC-33420), and *Pseudomonas aeruginosa* (ATCC-10145). Nitrocefin was purchased from TOKU-E and used as received. The sodium salt of penicillin-G was purchased from VWR and used as received. 4-Cyanopentanoic acid dithiobenzoate (CPDB) was obtained from Strem Chemical Inc. Azobisisobutyronitrile (AIBN) was recrystallized from methanol before use. CPDB immobilized silica nanoparticles were synthesized according to the literature.[49] All other chemicals were from commercial sources and used as received.

Synthesis of cobaltocenium-containing silica nanoparticles

$CoAEMAPF_6$ (200 mg, 0.41 mmol) CPDB-coated silica nanoparticles (69.5 mg, 59 μmol/g, 1 mmol) and 0.4 mL dry dimethyformamide (DMF) were added to a 10 mL schlenk tube. To ensure adequate dispersion of silica nanoparticles, the solution was sonicated for 5 minutes, and AIBN (0.2 mg, 1.23 μmol) was added. The resulting solution was degassed by purging nitrogen for 30 minutes and then placed in an oil bath of 90°C

until the desired conversion was met. The polymerization was quenched by opening to air and cooling with ice water. The reaction mixture was precipitated in cold dichloromethane three times and vacuum-dried. Ion-exchange to Cl^- was performed according to a previous report using tetrabutylammonium chloride salt (TBACl)[50]. A typical procedure was as follows:1 mL PF_6^- paired CsNP (30 mg/mL in acetonitrile) was slowly dropped into 5 mL TBACl solution (in acetonitrile) under vigorous stirring. After stirring for 5 minutes, the precipitated Cl^- paired CsNP was collected and washed by acetonitrile three times to remove PF_6^- anions and excess TBACl. The solid yellow CsNP-Cl was then vacuum-dried and collected. The polymer chains were cleaved using HF, and NMR was done on the cleaved polymer chains.

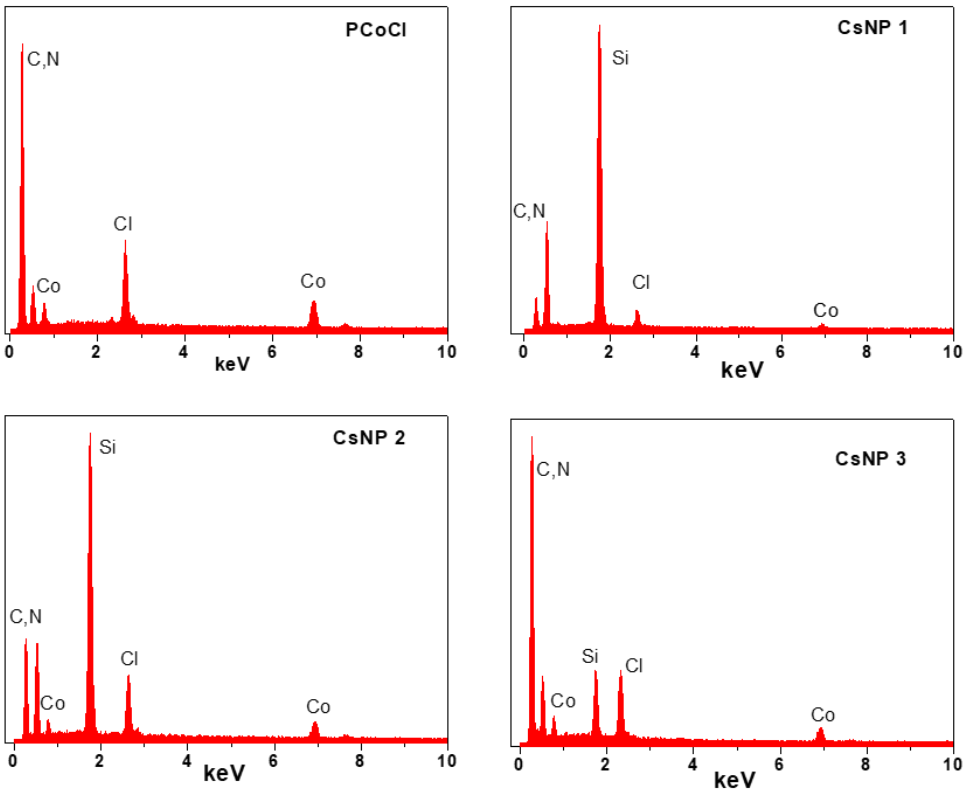

Figure 3.1 EDX elemental analysis of homopolymer and nanoparticles

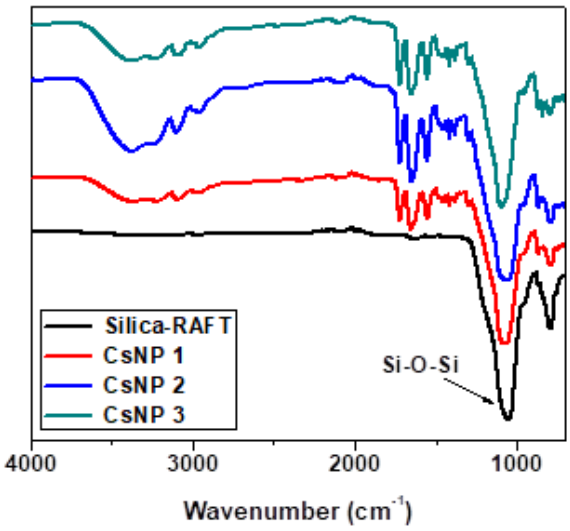

Figure 3.2 FT-IR spectrum of nanoparticles

Synthesis of CsNP-Penicillin bioconjugates

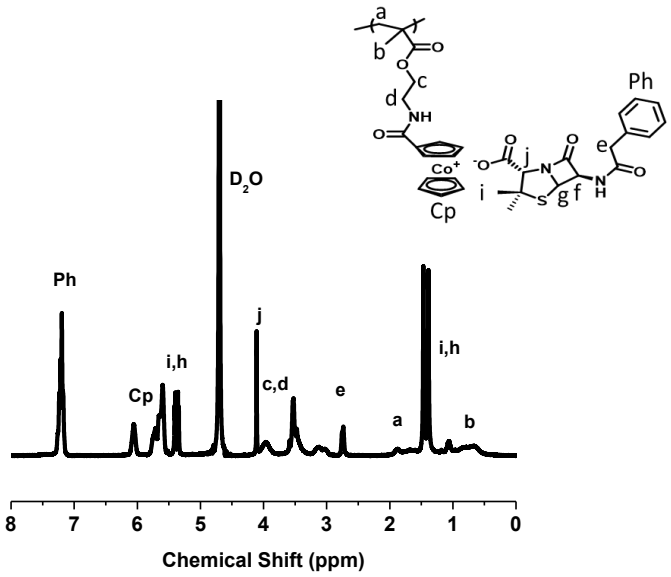

Figure 3.3. ^{1}H NMR spectrum of cobaltocenium-containing nanoparticle-penicillin conjugate CsNP in D_2O.

Cobaltocenium-containing silica nanoparticles with Cl^- and penicillin-G sodium salt were initially dissolved in deionized water (1 mL) with molar ratios (penicillin salt to cobaltocenium moieties) in the range of 1.15 to 1.0. The solution was stirred for 2 h and

then dialyzed against 3L deionized water for 9 hours. The solution in a dialysis bag was collected and freeze-dried. The CsNP-Peni conjugates were obtained as a yellow powder.

Growth of bacteria

The antibacterial activity of cobaltocenium-containing silica nanoparticles was evaluated using standard disk-diffusion assays (ASTM: the Kirby Bauer diffusion test). Firstly, actively-growing cultures of each bacterial strain, previously grown on Mannitol salt agar (MSA), were inoculated on Tryptic Soy Broth (TSB) agar plates. A subsample (10 μL) of each bacterial culture (cell concentrations were 1.0×10^6 CFU/mL) was diluted to 1 mL in TSB, and 100 μL of cell culture was spread on TSB agar plates to form a bacterial lawn covering the plate surface. Then a 6 mm filter disc was laid on the agar surface, to which the nanoparticle solution was added at the desired concentration. All plates were incubated overnight at 37ºC. The development of a clear zone around the disk was indicative of the ability of antimicrobial drugs to kill bacteria. By quantifying the area (knowing its diameter and the depth of the agar) of inhibition, a minimum inhibitory concentration (MIC) was calculated for each material/bacterial combination using established protocols[51].

Bacterial morphology by FE-SEM.

Field-emission scanning electron microscopy (FE-SEM) was used to examine changes in the morphology of bacterial cells after incubations with test drugs. In summary, 20 μL of bacterial cell solutions were grown on glass slides in a six-well plate containing 2 mL TSB medium at 37 ºC overnight. Cell suspensions were diluted to OD_{600} = 1.0. After adding predetermined amounts of test drugs to the 1 mL cell stock solution, they were incubated overnight at 37 ºC. A cell suspension without any chemicals was used as the

control. The samples were then fixed in cacodylate buffer with 2.5% glutaraldehyde solution (pH = 7.2) for 2–3 h at 4 ^{o}C, and post-fixed with 1% osmium tetraoxide at 4 ^{o}C for 1 h. Samples were dehydrated under critical point, then coated with gold using a Denton Dest II Sputter Coater for 120s and observed by FE-SEM.

LIVE/DEAD bacterial viability assays

The five bacterial strains were inoculated and prepared by a similar procedure as mentioned above. One mL of active bacterial stock solution was introduced to 5 μg penicillin solutions. An untreated cell suspension was used as the control. Following overnight incubation at 37 ^{o}C, 1 μL LIVE/DEAD BacLight (Bacterial Viability Kit; Invitrogen Inc.) was added to the incubation solution. After incubation for 15 minutes, cells were imaged using a Leica TCS SP5 Laser Scanning Confocal Microscope with 63X oil immersion lens. When excited at 488 nm with Argon and Helium/Neon lasers, bacteria with intact membranes display green fluorescence (Emission = 500 nm) and bacteria with disrupted membranes fluoresced red (Emission = 635 nm).

Drug Resistance Study

At first 50 μL aqueous solution of CsNP-penicillin conjugates with 0.5 x the MIC concentration were added to 96-well plates. Then, 150 μL bacterial TSB solution (OD_{600} = 1.00) were added to the wells. The bacterial TSB solution without conjugates was used as the control. The assay plate was incubated at 37^{o}C until the bacteria were grown to an optical density of about 1.00 (OD_{600} = ~ 1.00) in control samples. All assays were carried out in duplicate in the same assay plate. The experiment was repeated for 15 passages.

Effects of CsNP copolymers on β-lactamase activity

50 µL nitrocefin (DMSO solution 1.0 µg/mL) and CsNP with different concentrations (100, 200 and 400 µg) were added into 1 mL H_2O and stirred for 12 h. Then, 1 µL β-lactamase PBS buffer solution (0.1 µg/mL, determined by Bio-rad Protein Assay) was added to the above solution. A solution without nanoparticles was used as a control. After 1 h, the β-lactamase activity was measured by UV-vis absorbance at 480 nm.

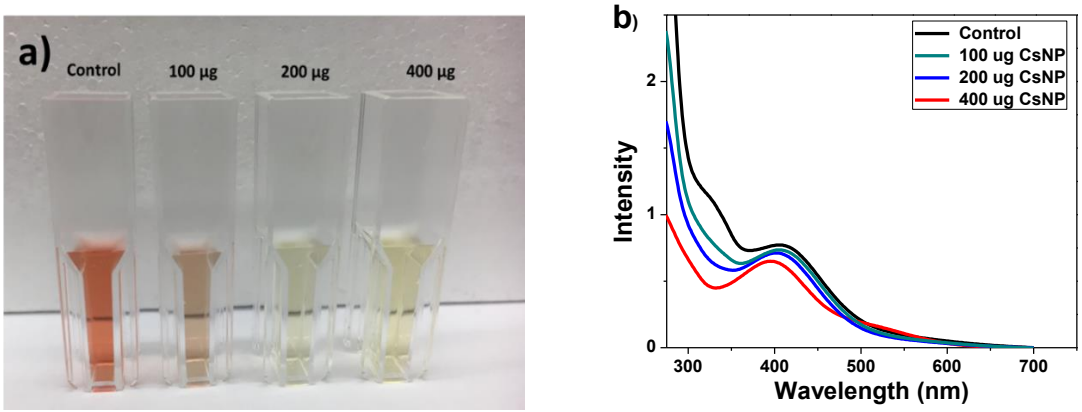

Figure 3.4**.** (a) Optical view of nitrocefin solution with different amounts of CsNP after adding β-lactamase for 1 h; and (b) UV−vis absorption.

Hemolysis evaluation for cytotoxicity determination

Blood was collected from mice in heparinized tubes and diluted by mixing 800 µL blood with 1000 µL PBS. Nanoparticle samples were prepared in PBS at concentrations 10, 50, 100 and 500 µg/mL and added 60 µL of the diluted blood samples to 3 mL of the nanoparticle conjugates, PBS or 0.1% Triton-X100 in PBS. The samples were incubated for 1 h at 37°C followed by centrifugation for 10 minutes at 1500 rpm. Supernatants were collected and OD was measured at 545 nm to calculate Hemolysis rate by using the formulae, HR=(AS-AN)/(AP-AN) where AS, AN and AP are OD values of the supernatants from test samples, negative control (PBS) and positive control (0.1% Triton-X100) respectively.

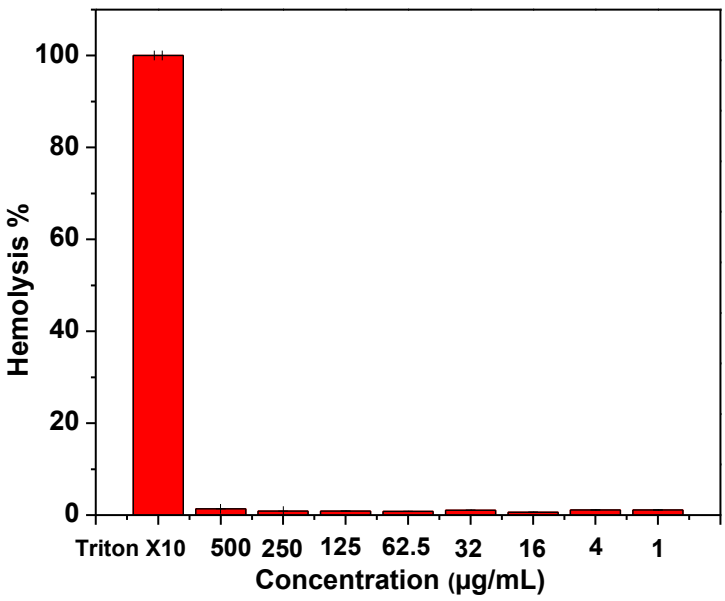

Figure 3.5**.** Hemolysis test results for CsNP-penicillin conjugate.

3.4 Results and Discussion

Synthesis of Cobaltocenium-Containing Silica Nanoparticles

The cobaltocenium-containing silica nanoparticles (CsNP) were prepared via RAFT polymerization using 2-cobaltocenium amidoethyl methacrylate hexafluorophosphate ($CoAEMAPF_6$) as a monomer, AIBN as an initiator, mediated by CPDB-coated silica nanoparticles in DMF at 90 °C (Scheme 3.1). We previously synthesized a cobaltocenium methacrylate monomer with ester and amide linkers for various applications and studies.[52-54,27] A similar procedure was followed to synthesize $CoAEMAPF_6$ by reacting cobaltocenium monoacid with 2-aminoethyl methacrylate hydrochloride in the presence of a coupling agent *N*-(3-di-methylaminopropyl)-*N'*-ethylcarbodiimide (EDC).

Scheme 3.1 Synthesis of cobaltocenium-containing silica nanoparticles by surface-initiated RAFT polymerization.

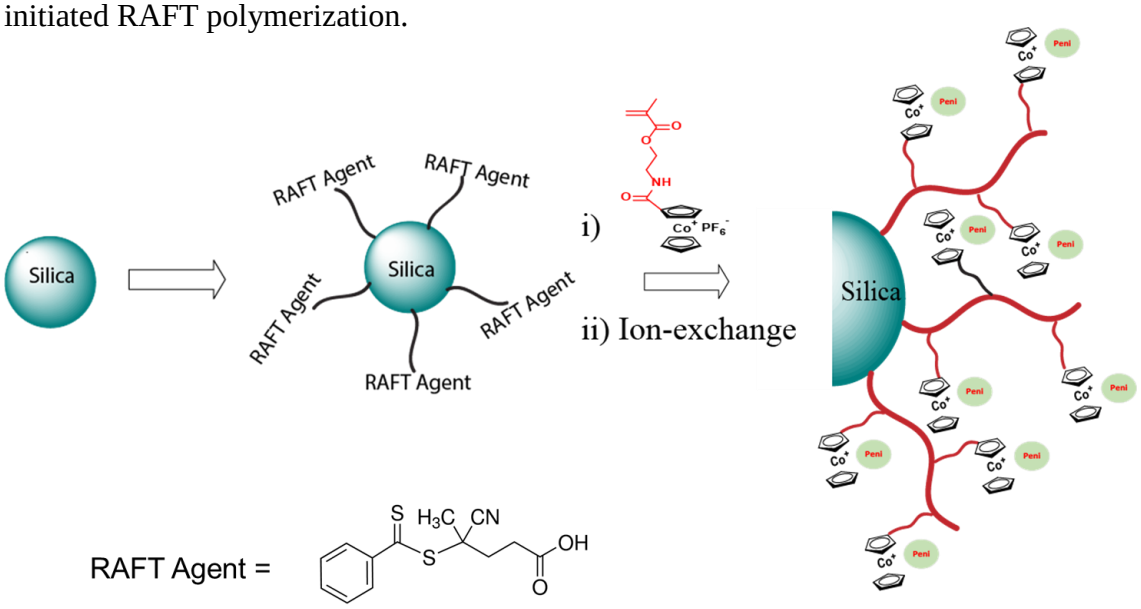

RAFT polymerization has been demonstrated to provide quantitative and precise control over the molecular weight.[55-57] We carried out RAFT polymerization by exploiting a "grafting from" technique.[49, 58-60] The silane surface chemistry was used to treat the colloidal silica nanoparticles with 3-aminopropyldimethylethoxysilane followed by the n amidation reaction between amino groups and CPDB RAFT agent. The amount of RAFT agent anchored onto the modified silica nanoparticles was determined quantitatively by comparing the absorption at about 303 nm for the CPDP anchored silica nanoparticles to a standard absorption curve made from known amounts of the free CPDB. Three different types of silica nanoparticles were synthesized by differing various grafting densities from 0.084 chain/nm^2 to 0.481 chain/nm^2 (20 µmol/g, 59 µmol/g and 114 µmol/g CPDB). These grafting densities were all significantly under the maximum grafting density of CPDB (~0.7 chain/nm^2). The disappearance of the vinyl protons from methacrylate around 6.2 and 5.6 ppm and appearance of broad peaks around 0.5-2.0 ppm in the ^{1}H NMR spectrum suggested the successful polymerization (Figure 3.3). The molecular weight was controlled

by tracking the conversion during the polymerization process using NMR. The polymers were obtained with the degree of polymerization in the range of 26-28. The targeted molecular weight was in the range of 12,000-15,000 g/mol, which displayed strong antibacterial properties based on our previous studies (Table 3.1).[47] The nanoparticles were further characterized by FTIR and EDX elemental analysis to confirm the presence of major bonds and elements in the nanoparticles respectively (Figure 3.1 and Figure 3.2).

Table 3.1 Cobaltocenium-containing silica nanoparticles and their characterization.

Entry	Total surface density[a] (μmol/g)	Total surface density (chain/nm^2)	M_n [b] (g/mol)	Diameter [c] (nm)	Zeta potential [d] (mV)
CsNP 1	20	0.084	12,700	48	40.4
CsNP 2	59	0.249	13,700	50	55.1
CsNP 3	114	0.481	13,200	51	62.6

[a] Equivalent of CPDB**;** [b] M_n calculated by conversion of $CoAEMAPF_6$ via NMR; [c] Diameter calculated via DLS; [d] Zeta potential calculated via DLS

A facile phase-transfer ion-exchange method has been established to prepare hydrophilic cationic cobaltocenium-containing polyelectrolytes with diverse counterions using tetra-butylammonium chloride (TBACl) salts.[50] Thus nanoparticles with PF_6^- anions were subjected to anion exchange with TBACl to result in hydrophilic chloride-based particles. The complete conversion from PF_6^- to Cl^- was confirmed by running ^{19}F NMR of resultant nanoparticles. The switch of anions to chloride significantly increased the hydrophilicity of the nanoparticles and facilitated the use of these particles for biomedical applications. The strong electrostatic interaction between the cationic cobaltocenium moieties and stationary phase of microstyragel columns made it impossible to observe use gel permeation chromatography (GPC). The nanoparticles were further conjugated with penicillin based on the ionic interaction between anionic penicillin sodium salt and cationic

cobaltocenium moiety, resulting in penicillin-conjugated cobaltocenium-containing silica nanoparticles (CsNP). The excess penicillin salt, which was not complexed with nanoparticles, was removed by dialysis. For the convenience, the nanoparticle conjugates were referred to as CsNP 1(20 µmol/g), CsNP 2 (59 µmol/g) and CsNP 3 (114 µmol/g) hereafter.

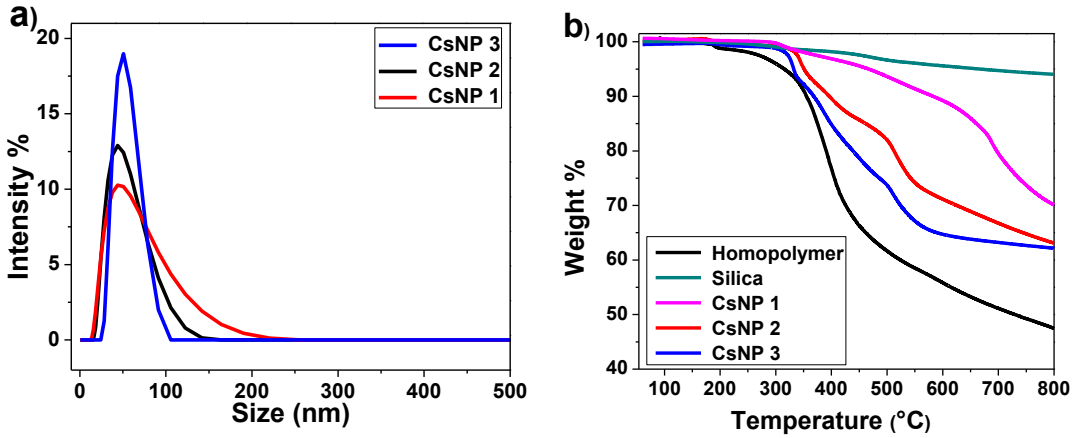

Figure 3.6. a) Dynamic Light Scattering measurements showing sizes of nanoparticles; and b) Thermogravimetric analysis of cobaltocenium-containing silica nanoparticles.

The mean diameter of cobaltocenium-containing nanoparticles was found to in the range of 40-50 nm, as measured by dynamic light scattering (Figure 3.5a). The diameter of bare silica nanoparticles was around 20-25 nm, and after polymerization the mean diameter increased as expected. The diameter of individual cobaltocenium-containing nanoparticles from TEM images (Figure 3.7) were consistent with DLS results. Thermogravimetric analyses (TGA) showed accurate weight loss of nanoparticles with different grafting densities (Figure 3.6b). To determine the weight percentage of the cobaltocenium, TGA of homopolymers and bare silica nanoparticles were compared with that of cobaltocenium-grafted nanoparticles. Based on the TGA measurements, the total weight percentage of cobaltocenium in the nanoparticle in CsNP ranged from 56 wt% to 65 wt%. This information together with ^{1}H NMR allowed us to calculate the weight percentage of

penicillin in the nanoparticles, which was in the range of 28-35 wt%. The equimolar pairing of penicillin with cobaltocenium was confirmed by ^{1}H NMR by calculating the integration ratio of aromatic peaks ~7.2 ppm from penicillin to the cyclopentadienyl peaks of polymers ~ 5.5-6.1 ppm (Figure 3.3).

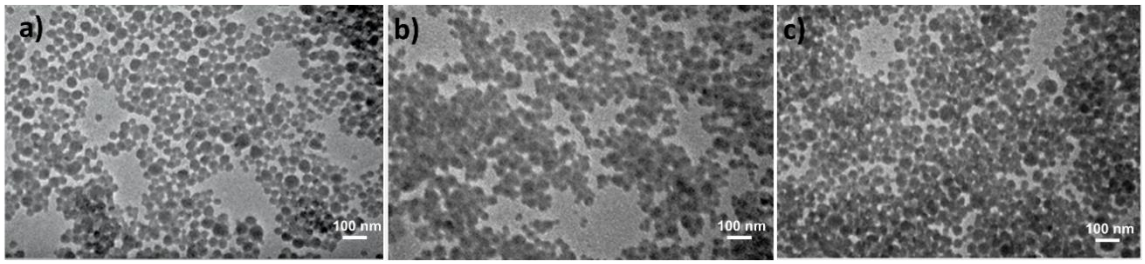

Figure 3.7 TEM images of nanoparticles: a) CsNP 1; b) CsNP 2; c) CsNP 3.

Antimicrobial Activity of Cobaltocenium-Containing Silica Nanoparticles

Antimicrobial susceptibility was determined by the conventional agar disk-diffusion assay following a protocol of Kirby Bauer diffusion test.[61] *Staphylococcus aureus* and *Escherichia coli* were chosen as representative Gram-positive and Gram-negative bacteria, respectively. To find the effective optimal concentration, three different amounts of penicillin (4µg, 6µg and 8 µg) were tested against the two bacterial strains. While carrying out the disk diffusion assays, concentrations of penicillin were kept constant in both nanoparticle treatments and controls. The optimal activity was obtained with 6 µg penicillin and used throughout the tests. The ability of the complex to kill the bacteria was represented by the development of a clear zone around the disk, also known as the inhibition zone. Higher inhibition zones were seen in case of the Gram-positive *S. aureus* in comparison to the Gram-negative *E. coli*. The additional outer polysaccharide layer in the Gram-negative bacteria might have acted as an extra layer of shielding for the test drugs to penetrate, resulting in the smaller inhibition zone.[61]

For further investigations of Gram-negative bacteria, tests were extended to the following bacteria using the above-mentioned protocol: *Pseudomonas aeruginosa, Proteus vulgaris,* and *Klebsiella pneumonia.* Among them, *P. aeruginosa*, *K. pneumonia* and *S. aureus* are among the six pathogens in a class "ESKAPE" termed by CDC, which can evade the influence of antibiotics and develop resistance.[62] As shown in Figure 3.8, penicillin-G alone showed minimal antibacterial efficacy at a given concentration, when compared to the CsNP bioconjugates. In case of *S. aureus*, the inhibition zone caused by penicillin was 9 mm while the zones created by CsNP-penicillin conjugates were much larger: approx. 19 mm. The amount of cobaltocenium in the control CsNP-Cl was probably too low for observing the onset of any antimicrobial activity. The inhibition zone caused by homopolymer conjugate (PCo-Peni) was 12 mm, which was larger than the penicillin alone, but still smaller than those observed for nanoparticle-penicillin conjugates. All three CsNP-penicillin conjugates resulted in bigger inhibition zones than penicillin, CsNP-Cl nanoparticles and the homopolymer-penicillin conjugate.

The results demonstrated the synergistic effects of the cobaltocenium-penicillin complex in protecting the antibiotics leading to increased lysis of bacterial cells. This led us to believe that CsNP-penicillin conjugates could be an upgraded ammunition from the currently known homopolymer-penicillin conjugate in combating bacterial infections.

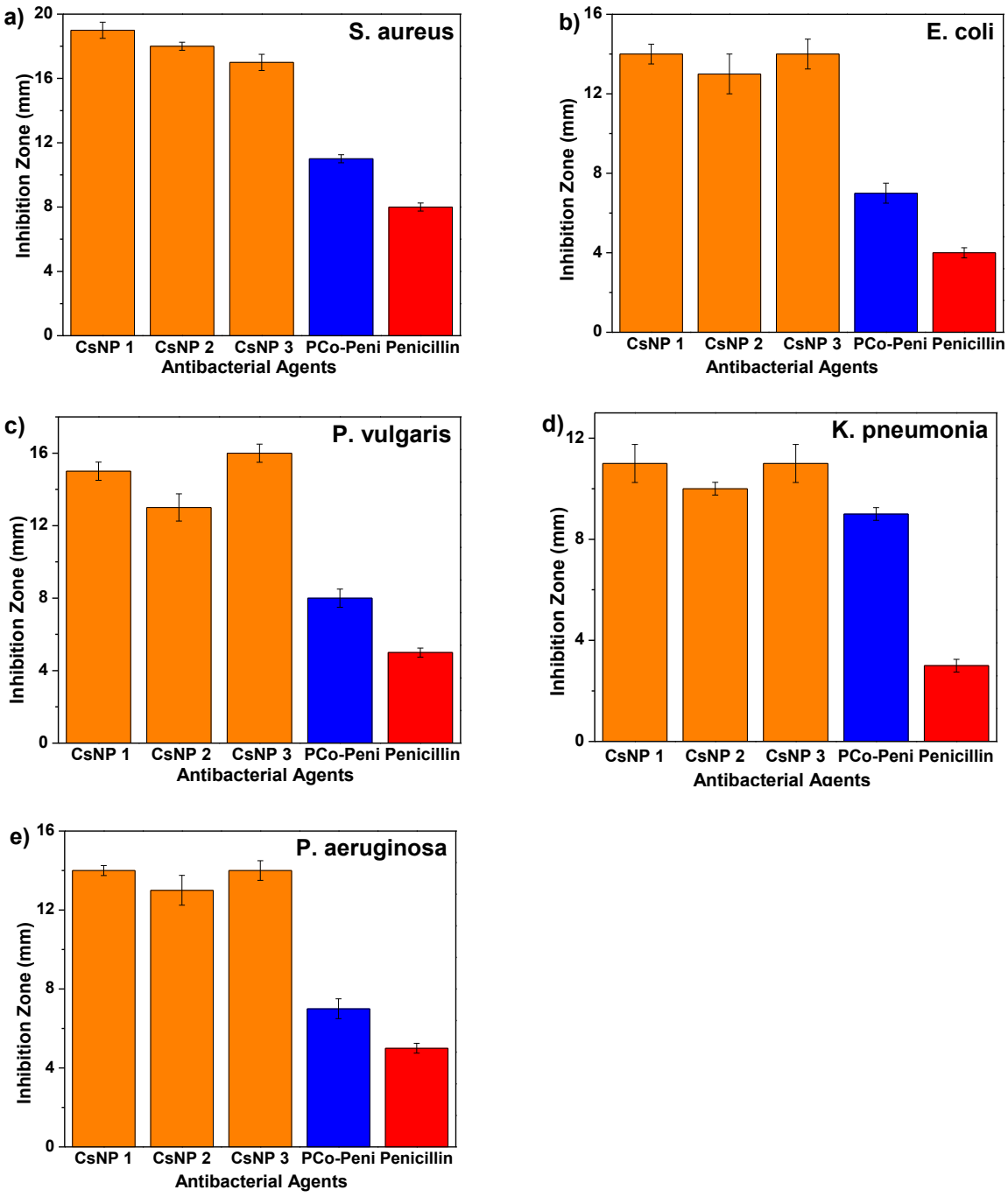

Figure 3.8 Inhibition zones of CsNP-Peni conjugates against various strains of bacteria at 6 μg penicillin-G/disk using disk-diffusion assays: a) *S. aureus*; b) *E. coli;* c) *P. vulgaris;* d) *K. pneumonia*; e) *P. aeruginosa*.

The CsNP conjugates have a greater charge density of cationic cobaltocenium on the surface, which provides an advantage for higher bactericidal efficacy when compared to the individual polymers. Even though the grafting densities of the nanoparticles were

different, the inhibition zones caused by the nanoparticle conjugates were similar. This could be attributed to the similar sizes of nanoparticle conjugates resulting in a similar zone of diffusion in the Agar gel. The diameters of nanoparticles were very close to each other; thus, we predict that similar zones of nanoparticle diffusion likely occurred in the agar gel leading to the observed similar antimicrobial activities.

Table 3.2 Minimum inhibitory concentrations (MICs) of different agents against five strains of bacteria.

Compounds	Minimum Inhibitory Concentration (MIC, µg/mL)				
	S. aureus	*E. coli*	*P. vulgaris*	*P. aeruginosa*	*K. pneumonia*
CsNP 1	3.03	5.57	5.42	5.57	10.92
CsNP 2	3.78	7.58	5.91	6.46	9.90
CsNP 3	2.73	4.85	5.20	5.57	10.10
Penicillin	13.48	17.06	17.50	19.41	26.66

Minimum inhibitory concentrations were calculated for each material/bacterial combination using established protocol and are given in Table 3.2.[51] The mean MIC of CsNPs against Gram-positive strain *S. aureus* was 3.18 $\pm$0.54 µg/mL, which was approximately four times lower than that of penicillin, 13.48 µg/mL. Similarly, for Gram-negative strains, the MIC values of CsNPs followed a similar trend and much lower than the penicillin alone. Compared with penicillin alone, nanoparticle-polymer conjugates produced significantly higher efficacies against both Gram-positive and Gram-negative strains.

The increased bactericidal effectiveness was further supported by qualitative observations using confocal scanning laser microscopy (CSLM) studies (Figure 3.9). LIVE/DEAD bacteria viability assays using CSLM indicated greater levels of cell death

and lower cell densities when bacterial cells were exposed to CsNP-Peni conjugates. Most of the cells exposed to penicillin alone were exhibited primarily green fluorescence indicating live cells, while cells incubated with CsNP-Peni bioconjugates displayed primarily red or yellow fluorescence, indicating cell death.

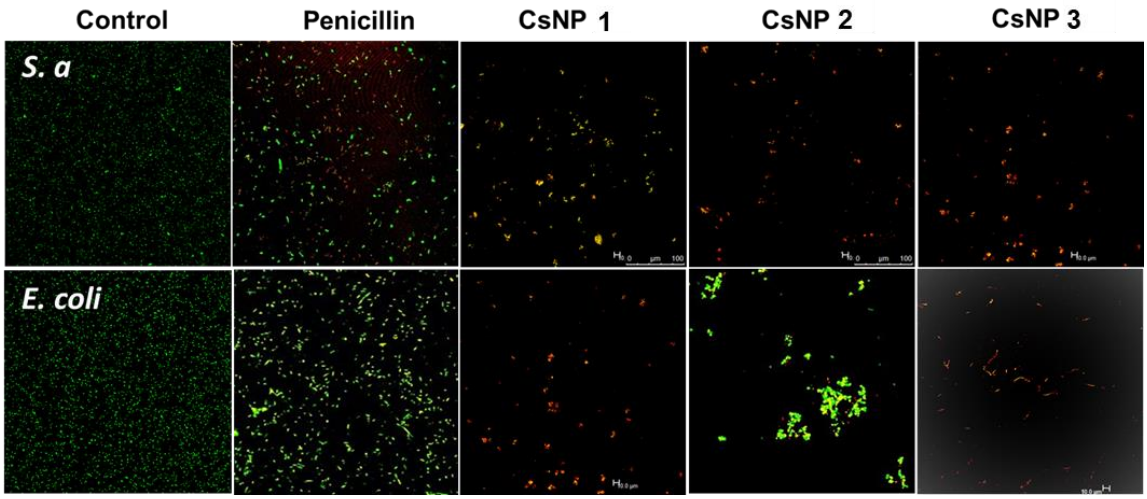

Figure 3.9 Confocal scanning laser microscopy images of control, penicillin and CsNP-penicillin conjugates with a concentration of penicillin 6 μg/mL (using BacLight live/dead stain, green indicates live cells, red indicates dead cells) against *E. coli* and *S. aureus.* The bacterial solution without CsNPs was used as the control.

Also, the SEM imaging was used to compare differences in morphology before- and after-treatment with CsNP-Peni conjugates (Figure 3.10). Control samples contained intact bacterial cells with smooth surfaces while the cells incubated with conjugates were significantly damaged with obvious disruptions in the original morphology. The collapsed cell envelopes of the incubated bacterial cells marked the physical damage of cell membranes.

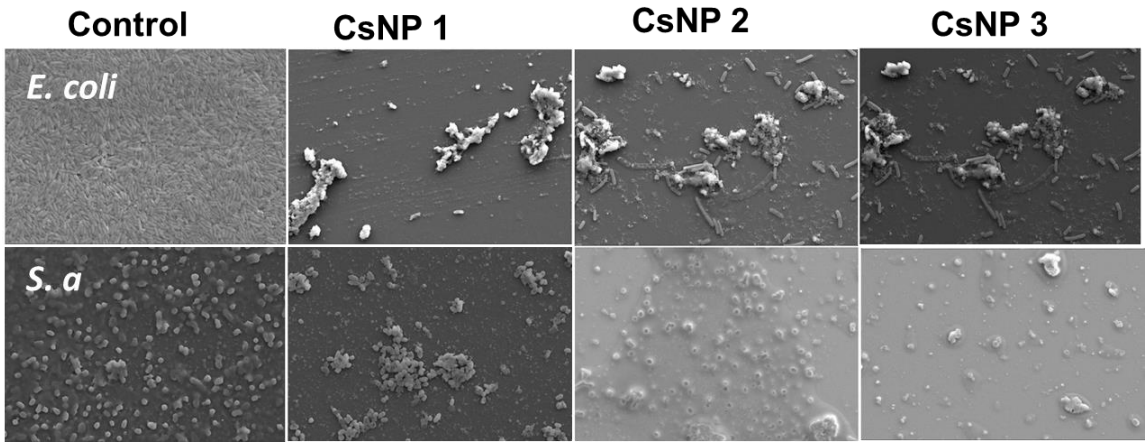

Figure 3.10 Scanning electron microscopy (SEM) images of control and CsNP-penicillin conjugates with a concentration of penicillin at 6 μg/mL against *E. coli* and *S. aureus*. Bacterial solutions without CsNPs were used as the control.

The nitrocefin assay, in conjunction with UV-Vis spectrophotometry, was used to observe the effects of CsNP on β-lactamase activity (Figure 3.4). The original yellow color of controls of a nitrocefin solution, changed to red within a few minutes after the addition of β-lactamase. The change in color was the result of hydrolysis of β-lactam ring of antibiotics, and can be observed by an absorption peak near 480 nm (Figure 3.4b).[63] When nitrocefin was complexed with CsNP, there was a minimal change in color implying the protection of β-lactam ring by the cobaltocenium moiety complex. When a higher concentration of CsNP was used, the color of the yellow solution remained unchanged. This was interpreted as the complete shutdown of β-lactamase activity against β-lactam antibiotics.

To evaluate the probability of the CsNP-penicillin conjugates to induce resistance in bacteria, drug resistance study was conducted for the most potent nanoparticle conjugate, CsNP 3 (lowest MIC) against both Gram-positive and Gram-negative bacteria. As shown in Figure 3.11, the OD_{600} values of the nanoparticle conjugates remain virtually constant

even after 15 consecutive passages against both *S. aureus* and *E. coli*, indicating that the bacteria did not develop resistance readily toward the nanoparticle conjugate.

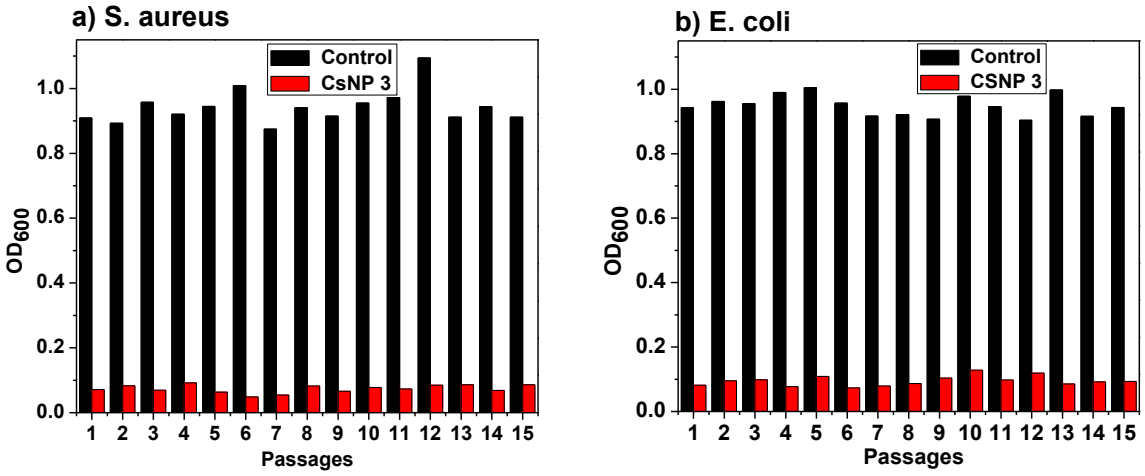

Figure 3.11 Drug resistance study of CsNP-penicillin conjugates against various bacteria.

The improved bactericidal efficiencies of CsNP-penicillin conjugates could be attributed to the enhanced local concentration of cobaltocenium-penicillin complex on the nanoparticle surface. Most of the antibacterial agents administered in the body to combat microbial infections diffuse to cell membranes once solubilized. This process could result in a lower concentration of antibacterial compounds a given bacterial cell receives, and thus could be less effective. In contrast, we increased the concentration of the cobaltocenium-penicillin conjugates on the surface, which supplied an enhanced dose to overwhelm the bacterial cell, resulting in effective lysis. In addition, the larger surface area of the nanoparticle could provide more active sites to contact the bacteria resulting in more bacterial death. In order to determine the toxicity of the CsNPs, we analyzed the cytotoxicity of CsNP 3 on red blood cells (RBCs) by evaluating whether they could lead to hemolysis of RBCs. We found that even at a concentration as high as 500 µg/mL, extremely low (< 5%) percentages of cells were lysed by CsNP 3 compared to the negative

control group as shown in Figure 3.5. This implies that the CsNPs do not cause significant toxicity and hence could be safe in the host.

3.5 Conclusions

In summary, we engineered the surfaces of silica nanoparticles with cobaltocenium polymers, having varied grafting densities using RAFT polymerization. These nanoparticles were then loaded with the β-lactam antibiotic penicillin-G, based on electrostatic interaction between cationic cobaltocenium moiety and anionic antibiotic. The resulting conjugates showed vastly improved bactericidal efficiencies against both Gram-positive and Gram-negative bacterial pathogen strain, and facilitated the revitalization of the β-lactam drug, penicillin. The nanoparticle-drug complex resisted hydrolysis by β-lactamase, the enzymatic mechanism used by many bacteria to resist β-lactam drugs. Not only did the complex rejuvenate bactericidal efficacy, but also provided an enhanced local dose of the penicillin and overwhelmed the bacterial cells, proving to be a more effective antimicrobial agent. This design has enabled us to achieve a promising new paradigm to improve the vitality of conventional antibiotics, with strong bactericidal effects and minimal cytotoxicity to host human cells.

3.6 References

1. van Duin, D.; Paterson, D. L., Multidrug-Resistant Bacteria in the Community: Trends and Lessons Learned. *Infectious Disease Clinics of North America* **2016,** 30, (2), 377-390.
2. Courtney, C. M.; Goodman, S. M.; McDaniel, J. A.; Madinger, N. E.; Chatterjee, A.; Nagpal, P., Photoexcited quantum dots for killing multidrug-resistant bacteria. *Nat. Mater* **2016,** 15, (5), 529-534.
3. García-Quintanilla, M.; Pulido, M. R.; Carretero-Ledesma, M.; McConnell, M. J., Vaccines for Antibiotic-Resistant Bacteria: Possibility or Pipe Dream? *Trends in Pharmacological Sciences* **2016,** 37, (2), 143-152.
4. Mizutani, M.; Palermo, E. F.; Thoma, L. M.; Satoh, K.; Kamigaito, M.; Kuroda, K., Design and Synthesis of Self-Degradable Antibacterial Polymers by Simultaneous Chain- and Step-Growth Radical Copolymerization. *Biomacromolecules* **2012,** 13, (5), 1554-1563.

5. Engler, A. C.; Wiradharma, N.; Ong, Z. Y.; Coady, D. J.; Hedrick, J. L.; Yang, Y.-Y., Emerging trends in macromolecular antimicrobials to fight multi-drug-resistant infections. *Nano Today* **2012,** 7, (3), 201-222.
6. Pu, Y.; Hou, Z.; Khin, M. M.; Zamudio-Vázquez, R.; Poon, K. L.; Duan, H.; Chan-Park, M. B., Synthesis and Antibacterial Study of Sulfobetaine/Quaternary Ammonium-Modified Star-Shaped Poly[2-(dimethylamino)ethyl methacrylate]-Based Copolymers with an Inorganic Core. *Biomacromolecules* **2017,** 18, (1), 44-55.
7. Li, P.; Poon, Y. F.; Li, W.; Zhu, H.-Y.; Yeap, S. H.; Cao, Y.; Qi, X.; Zhou, C.; Lamrani, M.; Beuerman, R. W.; Kang, E.-T.; Mu, Y.; Li, C. M.; Chang, M. W.; Jan Leong, S. S.; Chan-Park, M. B., A polycationic antimicrobial and biocompatible hydrogel with microbe membrane suctioning ability. *Nat. Mater.* **2011,** 10, (2), 149-156.
8. Tew, G. N.; Scott, R. W.; Klein, M. L.; DeGrado, W. F., De Novo Design of Antimicrobial Polymers, Foldamers, and Small Molecules: From Discovery to Practical Applications. *Acc. Chem. Res.* **2010,** 43, (1), 30-39.
9. Ganewatta, M. S.; Tang, C., Controlling macromolecular structures towards effective antimicrobial polymers. *Polymer* **2015,** 63, A1-A29.
10. Muñoz-Bonilla, A.; Fernández-García, M., Polymeric materials with antimicrobial activity. *Prog. Polym. Sci.* **2012,** 37, (2), 281-339.
11. Takahashi, H.; Caputo, G. A.; Vemparala, S.; Kuroda, K., Synthetic Random Copolymers as a Molecular Platform To Mimic Host-Defense Antimicrobial Peptides. *Bioconjugate Chem.* **2017,** 28, (5), 1340-1350.
12. Abd-El-Aziz, A. S.; Agatemor, C.; Etkin, N., Antimicrobial resistance challenged with metal-based antimicrobial macromolecules. *Biomaterials* **2017,** 118, (Supplement C), 27-50.
13. Yan, Y.; Zhang, J.; Ren, L.; Tang, C., Metal-containing and related polymers for biomedical applications. *Chem. Soc. Rev.* **2016,** 45, (19), 5232-5263.
14. Stark, W. J.; Stoessel, P. R.; Wohlleben, W.; Hafner, A., Industrial applications of nanoparticles. *Chem. Soc. Rev.* **2015,** 44, (16), 5793-5805.
15. Elsabahy, M.; Wooley, K. L., Design of polymeric nanoparticles for biomedical delivery applications. *Chem. Soc. Rev.* **2012,** 41, (7), 2545-2561.
16. Aruguete, D. M.; Kim, B.; Hochella, M. F.; Ma, Y.; Cheng, Y.; Hoegh, A.; Liu, J.; Pruden, A., Antimicrobial nanotechnology: its potential for the effective management of microbial drug resistance and implications for research needs in microbial nanotoxicology. *Environmental Science: Processes & Impacts* **2013,** 15, (1), 93-102.
17. Richter, A. P.; Brown, J. S.; Bharti, B.; Wang, A.; Gangwal, S.; Houck, K.; Cohen Hubal, E. A.; Paunov, V. N.; Stoyanov, S. D.; Velev, O. D., An environmentally benign antimicrobial nanoparticle based on a silver-infused lignin core. *Nat Nano* **2015,** 10, (9), 817-823.
18. Sharma, V. K.; Yngard, R. A.; Lin, Y., Silver nanoparticles: Green synthesis and their antimicrobial activities. *Advances in Colloid and Interface Science* **2009,** 145, (1–2), 83-96.
19. Rai, M.; Yadav, A.; Gade, A., Silver nanoparticles as a new generation of antimicrobials. *Biotechnology Advances* **2009,** 27, (1), 76-83.
20. Li, X.; Robinson, S. M.; Gupta, A.; Saha, K.; Jiang, Z.; Moyano, D. F.; Sahar, A.; Riley, M. A.; Rotello, V. M., Functional Gold Nanoparticles as Potent Antimicrobial Agents against Multi-Drug-Resistant Bacteria. *ACS Nano* **2014,** 8, (10), 10682-10686.

21. Zhao, Y.; Chen, Z.; Chen, Y.; Xu, J.; Li, J.; Jiang, X., Synergy of Non-antibiotic Drugs and Pyrimidinethiol on Gold Nanoparticles against Superbugs. *J. Am. Chem. Soc.* **2013,** 135, (35), 12940-12943.
22. Dykman, L.; Khlebtsov, N., Gold nanoparticles in biomedical applications: recent advances and perspectives. *Chem. Soc. Rev.* **2012,** 41, (6), 2256-2282.
23. Sirelkhatim, A.; Mahmud, S.; Seeni, A.; Kaus, N. H. M.; Ann, L. C.; Bakhori, S. K. M.; Hasan, H.; Mohamad, D., Review on Zinc Oxide Nanoparticles: Antibacterial Activity and Toxicity Mechanism. *Nano-Micro Letters* **2015,** 7, (3), 219-242.
24. Raghupathi, K. R.; Koodali, R. T.; Manna, A. C., Size-Dependent Bacterial Growth Inhibition and Mechanism of Antibacterial Activity of Zinc Oxide Nanoparticles. *Langmuir* **2011,** 27, (7), 4020-4028.
25. Shi, Y.; Wang, F.; He, J.; Yadav, S.; Wang, H., Titanium dioxide nanoparticles cause apoptosis in BEAS-2B cells through the caspase 8/t-Bid-independent mitochondrial pathway. *Toxicol Lett* **2010,** 196.
26. Chen, X.; Mao, S. S., Titanium Dioxide Nanomaterials: Synthesis, Properties, Modifications, and Applications. *Chem. Rev.* **2007,** 107, (7), 2891-2959.
27. Song, J.; Kong, H.; Jang, J., Enhanced antibacterial performance of cationic polymer modified silicananoparticles. *Chem. Comm.* **2009**, (36), 5418-5420.
28. Wang, L.; Chen, Y. P.; Miller, K. P.; Cash, B. M.; Jones, S.; Glenn, S.; Benicewicz, B. C.; Decho, A. W., Functionalised nanoparticles complexed with antibiotic efficiently kill MRSA and other bacteria. *Chem. Comm.* **2014,** 50, (81), 12030-12033.
29. Ren, G.; Hu, D.; Cheng, E. W. C.; Vargas-Reus, M. A.; Reip, P.; Allaker, R. P., Characterisation of copper oxide nanoparticles for antimicrobial applications. *International Journal of Antimicrobial Agents* **2009,** 33, (6), 587-590.
30. Stoimenov, P. K.; Klinger, R. L.; Marchin, G. L.; Klabunde, K. J., Metal Oxide Nanoparticles as Bactericidal Agents. *Langmuir* **2002,** 18, (17), 6679-6686.
31. Kang, S.; Pinault, M.; Pfefferle, L. D.; Elimelech, M., Single-Walled Carbon Nanotubes Exhibit Strong Antimicrobial Activity. *Langmuir* **2007,** 23, (17), 8670-8673.
32. Kang, S.; Herzberg, M.; Rodrigues, D. F.; Elimelech, M., Antibacterial Effects of Carbon Nanotubes: Size Does Matter! *Langmuir* **2008,** 24, (13), 6409-6413.
33. Chen, H.; Wang, B.; Gao, D.; Guan, M.; Zheng, L.; Ouyang, H.; Chai, Z.; Zhao, Y.; Feng, W., Broad-Spectrum Antibacterial Activity of Carbon Nanotubes to Human Gut Bacteria. *Small* **2013,** 9, (16), 2735-2746.
34. Tegos, G. P.; Demidova, T. N.; Arcila-Lopez, D.; Lee, H.; Wharton, T.; Gali, H.; Hamblin, M. R., Cationic Fullerenes Are Effective and Selective Antimicrobial Photosensitizers. *Chemistry & Biology* **2005,** 12, (10), 1127-1135.
35. Zou, X.; Zhang, L.; Wang, Z.; Luo, Y., Mechanisms of the Antimicrobial Activities of Graphene Materials. *J. Am. Chem. Soc.* **2016,** 138, (7), 2064-2077.
36. Bitar, A.; Ahmad, N. M.; Fessi, H.; Elaissari, A., Silica-based nanoparticles for biomedical applications. *Drug Discovery Today* **2012,** 17, (19–20), 1147-1154.
37. Tang, F.; Li, L.; Chen, D., Mesoporous Silica Nanoparticles: Synthesis, Biocompatibility and Drug Delivery. *Adv. Mater.* **2012,** 24, (12), 1504-1534.
38. Moritz, M.; Geszke-Moritz, M., The newest achievements in synthesis, immobilization and practical applications of antibacterial nanoparticles. *Chemical Engineering Journal* **2013,** 228, 596-613.

39. Kim, S. H.; Jeyakumar, M.; Katzenellenbogen, J. A., Dual-Mode Fluorophore-Doped Nickel Nitrilotriacetic Acid-Modified Silica Nanoparticles Combine Histidine-Tagged Protein Purification with Site-Specific Fluorophore Labeling. *J. Am. Chem. Soc.* **2007,** 129, (43), 13254-13264.
40. Bharali, D. J.; Klejbor, I.; Stachowiak, E. K.; Dutta, P.; Roy, I.; Kaur, N.; Bergey, E. J.; Prasad, P. N.; Stachowiak, M. K., Organically modified silica nanoparticles: A nonviral vector for in vivo gene delivery and expression in the brain. *Proc. Nat. Acad. Sci. U.S.A.* **2005,** 102, (32), 11539-11544.
41. Jun, L.; Andrea, L. L.; John, S. M.; Mamoru, Y.; Robert, J. L.; Xueliang, P.; Thomas, J. R., Nanoparticles as image enhancing agents for ultrasonography. *Physics in Medicine and Biology* **2006,** 51, (9), 2179.
42. Besinis, A.; De Peralta, T.; Handy, R. D., The antibacterial effects of silver, titanium dioxide and silica dioxide nanoparticles compared to the dental disinfectant chlorhexidine on Streptococcus mutans using a suite of bioassays. *Nanotoxicology* **2014,** 8, (1), 1-16.
43. Sun, T.; Zhang, Y. S.; Pang, B.; Hyun, D. C.; Yang, M.; Xia, Y., Engineered Nanoparticles for Drug Delivery in Cancer Therapy. *Angew. Chem. Int. Ed.* **2014,** 53, (46), 12320-12364.
44. Kowalczuk, A.; Trzcinska, R.; Trzebicka, B.; Müller, A. H. E.; Dworak, A.; Tsvetanov, C. B., Loading of polymer nanocarriers: Factors, mechanisms and applications. *Prog. Polym. Sci.* **2014,** 39, (1), 43-86.
45. Elsabahy, M.; Heo, G. S.; Lim, S.-M.; Sun, G.; Wooley, K. L., Polymeric Nanostructures for Imaging and Therapy. *Chem. Rev.* **2015,** 115, (19), 10967-11011.
46. Nederberg, F.; Zhang, Y.; Tan, J. P. K.; Xu, K.; Wang, H.; Yang, C.; Gao, S.; Guo, X. D.; Fukushima, K.; Li, L.; Hedrick, J. L.; Yang, Y.-Y., Biodegradable nanostructures with selective lysis of microbial membranes. *Nat. Chem.* **2011,** 3, (5), 409-414.
47. Zhang, J.; Chen, Y. P.; Miller, K. P.; Ganewatta, M. S.; Bam, M.; Yan, Y.; Nagarkatti, M.; Decho, A. W.; Tang, C., Antimicrobial Metallopolymers and Their Bioconjugates with Conventional Antibiotics against Multidrug-Resistant Bacteria. *J. Am. Chem. Soc* **2014,** 136, (13), 4873-4876.
48. Zhang, J.; Yan, J.; Pageni, P.; Yan, Y.; Wirth, A.; Chen, Y.-P.; Qiao, Y.; Wang, Q.; Decho, A. W.; Tang, C., Anion-Responsive Metallopolymer Hydrogels for Healthcare Applications. *Sci. Rep.* **2015,** 5, 11914.
49. Li, C.; Han, J.; Ryu, C. Y.; Benicewicz, B. C., A Versatile Method To Prepare RAFT Agent Anchored Substrates and the Preparation of PMMA Grafted Nanoparticles. *Macromolecules* **2006,** 39, (9), 3175-3183.
50. Zhang, J.; Yan, Y.; Chance, M. W.; Chen, J.; Hayat, J.; Ma, S.; Tang, C., Charged Metallopolymers as Universal Precursors for Versatile Cobalt Materials. *Angew. Chem. Int. Ed.* **2013,** 52, (50), 13387-13391.
51. Bauer, A.; Kirby, W.; Sherris, J. C.; Turck, M., Antibiotic susceptibility testing by a standardized single disk method. *American journal of clinical pathology* **1966,** 45, (4), 493.
52. Ren, L.; Hardy, C. G.; Tang, C., Synthesis and Solution Self-Assembly of Side-Chain Cobaltocenium-Containing Block Copolymers. *J. Am. Chem. Soc* **2010,** 132, (26), 8874-8875.

53. Zhang, J.; Ren, L.; Hardy, C. G.; Tang, C., Cobaltocenium-Containing Methacrylate Homopolymers, Block Copolymers, and Heterobimetallic Polymers via RAFT Polymerization. *Macromolecules* **2012,** 45, (17), 6857-6863.
54. Zhang, J.; Yan, Y.; Chen, J.; Chance, W. M.; Hayat, J.; Gai, Z.; Tang, C., Nanostructured Metal/Carbon Composites from Heterobimetallic Block Copolymers with Controlled Magnetic Properties. *Chem. Mater.* **2014,** 26, (10), 3185-3190.
55. Moad, G.; Rizzardo, E.; Thang, S. H., Radical addition–fragmentation chemistry in polymer synthesis. *Polymer* **2008,** 49, (5), 1079-1131.
56. Chiefari, J.; Chong, Y.; Ercole, F.; Krstina, J.; Jeffery, J.; Le, T. P.; Mayadunne, R. T.; Meijs, G. F.; Moad, C. L.; Moad, G., Living free-radical polymerization by reversible addition− fragmentation chain transfer: the RAFT process. *Macromolecules* **1998,** 31, (16), 5559-5562.
57. Boyer, C.; Bulmus, V.; Davis, T. P.; Ladmiral, V.; Liu, J.; Perrier, S., Bioapplications of RAFT polymerization. *Chem.Rev.* **2009,** 109, (11), 5402-5436.
58. Li, Y.; Benicewicz, B. C., Functionalization of silica nanoparticles via the combination of surface-initiated RAFT polymerization and click reactions. *Macromolecules* **2008,** 41, (21), 7986-7992.
59. Bao, C.; Tang, S.; Horton, J. M.; Jiang, X.; Tang, P.; Qiu, F.; Zhu, L.; Zhao, B., Effect of Overall Grafting Density on Microphase Separation of Mixed Homopolymer Brushes Synthesized from Y-Initiator-Functionalized Silica Particles. *Macromolecules* **2012,** 45, (19), 8027-8036.
60. Kumar, S. K.; Jouault, N.; Benicewicz, B.; Neely, T., Nanocomposites with polymer grafted nanoparticles. *Macromolecules* **2013,** 46, (9), 3199-3214.
61. Wiegand, I.; Hilpert, K.; Hancock, R. E. W., Agar and broth dilution methods to determine the minimal inhibitory concentration (MIC) of antimicrobial substances. *Nat. Protocols* **2008,** 3, (2), 163-175.
62. Pendleton, J. N.; Gorman, S. P.; Gilmore, B. F., Clinical relevance of the ESKAPE pathogens. *Expert Review of Anti-infective Therapy* **2013,** 11, (3), 297-308.
63. O'Callaghan, C. H.; Morris, A.; Kirby, S. M.; Shingler, A. H., Novel Method for Detection of β-Lactamases by Using a Chromogenic Cephalosporin Substrate. *Antimicrobial Agents and Chemotherapy* **1972,** 1, (4), 283-288.

CHAPTER 4

RECYCLABLE MAGNETIC NANOPARTICLES GRAFTED WITH ANTIMICROBIAL METALLOPOLYMER-ANTIBIOTIC BIOCONJUGATES[3]

[3] Pageni, P.; Yang P.; Bam M.; Zhu T.; Chen Y. P.; Decho A. W.; Nagarkatti M.; Tang, C. Recyclable Magnetic Nanoparticles Grafted with Antimicrobial Metallopolymer-Antibiotic Bioconjugates *Biomaterials*, **2018**, In press. Reprinted here with permission of publisher.

4.1 Abstract

Over-prescription and improper use of antibiotics has led to the emergence of bacterial resistance and now poses a major threat to public health. There has been significant interest in the development of alternative therapies and agents to combat antibiotic resistance. We report the preparation of recyclable magnetic iron oxide nanoparticles grafted with charged cobaltocenium-containing metallopolymers by surface-initiated reversible addition-fragmentation chain transfer (RAFT) polymerization. β-Lactam antibiotics were then conjugated with metallopolymers to enhance their vitality against both Gram-positive and Gram-negative bacteria. The enhanced antibacterial activity was a result of synergy of antimicrobial segments that facilitate the inhibition of hydrolysis of antibiotics and local enhancement of antibiotic concentration on a nanoparticle surface. These magnetic nanoparticles can be recycled numerous times without losing the initial antimicrobial potency. Studies suggested negligible toxicity of metallopolymer-grafted nanoparticles to red blood cells and minimal tendency to induce resistance in bacteria.

4.2 Introduction

The emergence of antibiotic resistance is not only a threat to global health but also to the economy. Antibiotic resistance infections result in increased mortality and excess costs in both clinical and community settings. According to a report by CDC, it is now predicted that global mortality by bacterial infection would reach 10 million annually by the year 2050 and cost an estimated $100 trillion dollars in lost economic output[1]. As a result of excessive use, traditional antibiotics exhibit a rapidly decreased efficacy. In some cases, infections become untreatable and more patients succumb from other conditions such as AIDS, whose etiology is complicated by antibiotic resistance infections[2]. This threatens

many of the most significant medical advances that have been made, and results in increasing therapeutic costs and extended hospitalization. The antibiotics have lost their efficacy gradually as a result of emergence and circulation of antibiotic resistance among bacteria. Inspired by antimicrobial peptides, synthetic polymers containing cationic groups like quaternary ammonium or sulfonium have been studied extensively and almost exclusively as a measure to fight back bacterial resistance due to the physical nature of their action of damage to the membranes[3-11]. However, the less selective mode of action of these polymers results in toxicity towards mammalian cells, and thus the quest persists for safer, more-effective antimicrobial agents.

Nanomaterials have been gaining much attention as antimicrobials that are complementary to antibiotics, and fill important gaps where antibiotics often fail[12]. The diversity of nanoparticles that are currently in use ranges from metal, metal oxides to organic forms. Nanoparticles can be engineered with high specificity to produce surfaces having different types of functional groups, charges and other properties. Magnetic nanoparticles have been an area of interest for researchers from a wide range of disciplines including catalysis[13, 14], data storage[15, 16], environmental remediation[17], magnetic resonance imaging[18] and biomedicines[19-22]. In particular, a wide variety of biomedical applications range from contrast agents for magnetic resonance imaging to the deterioration of cancer cells via hyperthermic treatment[23].

Specifically, iron oxide particles, with size ranges of nanometer scale, display superparamagnetic properties and could interact magnetically with each other when not properly stabilized. Due to their extremely large surface-to-volume ratio and the large surface energy, magnetic nanoparticles tend to aggregate. In addition, naked metallic

nanoparticles have a high chemical activity and are prone to oxidation in air resulting in loss of magnetism and dispersibility[24]. To circumvent these problems, it is essential to protect and stabilize the naked magnetic nanoparticles by using either ionic compounds or large molecules such as polymers or surfactants containing long hydrocarbon chains. Polymer grafting has become a popular technique for tuning the surface properties of nanoparticles[25-29]. Also, magnetic nanoparticles without polymer coatings often aggregate in water or tissue fluid, which may limit their applications. Grafting of polymers not only stabilizes the nanoparticles but also opens the door for further functionalization.

Antibiotics have been the major therapy to treat various kinds of bacterial infections for nearly a century. However, there is hardly any class of antibiotics that has escaped the resistance mechanism by bacteria. The time interval between the launch of a new antibiotic in clinical practice and the emergence of resistance has been variable and rapidly shortening over the past century[30]. The strategy of discovering and developing new antibiotics is necessary but may not address the concern of bacterial resistance for long. The approach to breathe life into traditional antibiotics and antimicrobial agents using new therapeutic approaches to treat infection-associated diseases seems fruitful and addresses the urgent need and provides economic incentives.

We postulated that linking antimicrobial agents to nanoparticles may represent a powerful, yet adaptable tool to more-efficiently limit antibiotic-resistant infections. We recently developed a class of charged cobaltocenium-containing metallopolymers with minimal toxicity and good antimicrobial efficacy[31-33]. These metallopolymers not only kill the bacteria but also protect β-lactam antibiotics from the detrimental hydrolysis of β-lactamase enzyme.

Scheme 4.1. Synthesis of cobaltocenium-containing silica nanoparticles by surface-initiated RAFT polymerization.

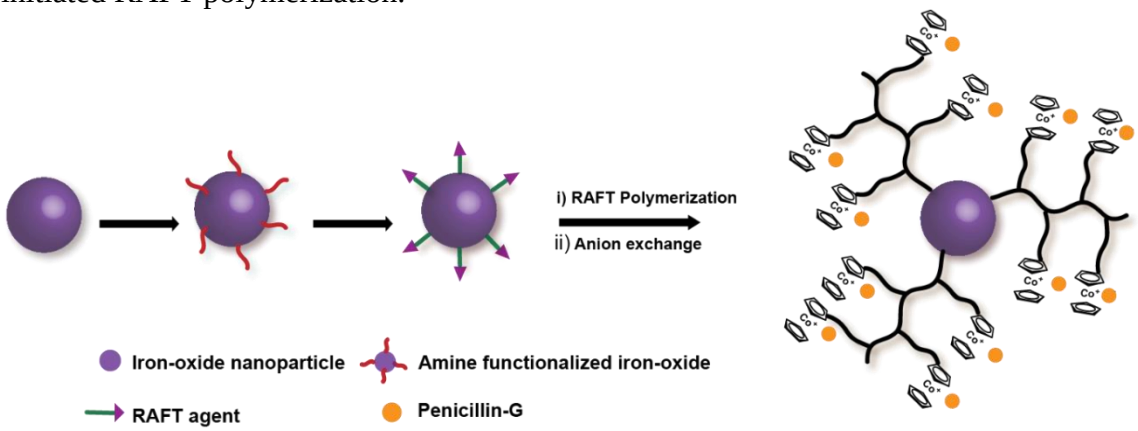

Herein we report new work on grafting cobaltocenium-containing polymers from iron oxide nanoparticles using surface-initiated reversible addition-fragmentation chain transfer (SI-RAFT) polymerization (Scheme 4.1). In doing so, the magnetic properties of nanoparticles compliment the antimicrobial features of cobaltocenium-containing polymers, and result in a new class of materials having highly-applicable characteristics such as magnetic antimicrobial nanoparticles that can impact therapies to tackle rampant bacterial infections. These nanoparticles were then conjugated with β-lactam antibiotics, such as penicillin, *via* ion-pairing between the cationic cobaltocenium moiety in the nanoparticles and the carboxylate anion of antibiotics. The newly-synthesized nanoparticle conjugates displayed significantly enhanced antimicrobial efficacy against both Gram-positive and Gram-negative strains. In addition, they can be recycled for at least 15 passages without losing the potency.

4.3 EXPERIMENTAL SECTION

Characterization

^{1}H (400 MHz), ^{13}C (100 MHz), and ^{19}F (376 MHz) NMR spectra were recorded on a Varian Mercury 400 NMR spectrometer with tetramethylsilane (TMS) as an internal

reference. Mass spectrometry was conducted on a Waters Micromass Q-TOF mass spectrometer, and the ionization source was positive ion electrospray. UV−vis was carried out on a Shimadzu UV-2450 spectrophotometer with a 10.00 mm quartz cuvette and monochromatic light of various wavelengths over a range of 190−900 nm. A Hitachi 8000 transmission electron microscope (TEM) was applied to take images at an operating voltage of 150 kV. TEM samples were prepared by dropping solution on carbon-supported copper grids and then dried before observation. Dynamic light scattering (DLS) was operated on a Nano-ZS instrument, model ZEN 3600 (Malvern Instruments). Field-Emission Scanning Electron Microscopy (FE-SEM, Zeiss UltraPlus) was used to take images of bacterial cells after incubating overnight with test drugs. The samples were coated with gold using Denton Dest II Sputter Coater for 45 s and then observed by SEM.

Materials and Methods

2-Cobaltoceniumamidoethyl methacrylate hexafluorophosphate ($CoAEMAPF_6$) was synthesized according to our earlier reports[52, 56]. 2-Aminoethyl methacrylate hydrochloride (90%), *N*-(3-dimethylaminopropyl)-*N′*-ethylcarbodiimide hydrochloride (EDC-HCl, 98%), 4-(dimethylamino) pyridine and tetrabutylammonium chloride (TBACl) were purchased from Aldrich and used as received. Water was from Thermo Scientific Nanopure with ion conductivity at 18.2 MΩ. The following bacterial strains were purchased from ATCC: *Staphylococcus aureus* (*S. aureus*, ATCC-33591), *Bacillus cereus* (*B. cereus*, ATCC 11778), *Escherichia coli* (*E. coli*, ATCC-11775), *Klebsiella pneumoniae* (*K. pneumoniae*, ATCC-35596), *Proteus vulgaris* (*P. vulgaris* ATCC 33420). Nitrocefin was purchased from TOKU-E and used as received. Sodium salt of penicillin-G was purchased from VWR and used as received. 4-Cyanopentanoic acid dithiobenzoate

(CPDB) was obtained from Strem Chemical Inc. Azobisisobutyronitrile (AIBN) was recrystallized from methanol before use. All other chemicals and reagents were from commercial sources and used as received.

Synthesis of iron oxide nanoparticles

The iron oxide nanoparticles were prepared by a co-precipitation method using a mixture of two salts ($FeCl_2$ and $FeCl_3$)[57]. Briefly, 0.01 mol $FeCl_2.4H_2O$ and 0.02 mol $FeCl_3.6H_2O$ were dissolved in 100 mL of deionized and deoxygenated water. Then, 0.08 mol of NaOH in 100 mL was added dropwise for 3 hours under nitrogen using a Soxhlet funnel while stirring. The precipitate was washed with water/ethanol repeatedly and dried in a desiccator for 24 hours. The RAFT agent was anchored in the nanoparticles following a reported procedure[44]. In short, Iron oxide nanoparticles (0.5 g) was dispersed in dry THF and 3-aminopropyldimethylethoxysilane (0.32 mL, 1 mmol) was added. The mixture was refluxed in an oil bath for 6 h under nitrogen protection. After cooling to room temperature, the reaction was precipitated in 250 mL hexanes. The particles were precipitated three times and each time they were easily recovered by centrifugation. For the next part, 0.2 g, (0.4 mmol) of activated 4-cyano-4-(phenylcarbonylthioylthio)pentanoate (CPDB) was added dropwise to the dispersed solution of iron oxide nanoparticles in THF at room temperature. The solution was stirred overnight and precipitated in hexanes. The CPDB-anchored nanoparticles were recovered by centrifugation and dried in vacuum. The particles were then dispersed in THF and stored for later use.

Synthesis of cobaltocenium-containing iron oxide nanoparticles

CoAEMAPF$_6$ (200 mg, 0.41 mmol), CPDB-coated iron oxide nanoparticles (245 mg, 1 mmol) and 0.4 mL dry dimethyformamide (DMF) were added to a 10 mL Schlenk tube. To ensure good dispersion of nanoparticles, the solution was sonicated for 5 minutes, and AIBN (0.2 mg, 1.23 µmol) was added. The resulting solution was degassed by purging nitrogen for 30 minutes and then placed in an oil bath of 90 °C until the desired conversion was met. The polymerization was quenched by opening to air and cooling with ice water. The reaction mixture was precipitated in cold dichloromethane three times and vacuum-dried. Ion-exchange of Cl^- was performed according to a previous report using tetrabutylammonium chloride salt (TBACl) [53]. A typical procedure was as follows:1 mL PF_6^- paired FeNP (30 mg/mL in acetonitrile) was slowly dropped into 5 mL TBACl solution (in acetonitrile) under vigorous stirring. After stirring for 5 minutes, the precipitated Cl^- paired FeNP was collected and washed by acetonitrile three times to remove PF_6^- anions and excess TBACl. The solid yellow FeNP-Cl was then vacuum-dried and collected.

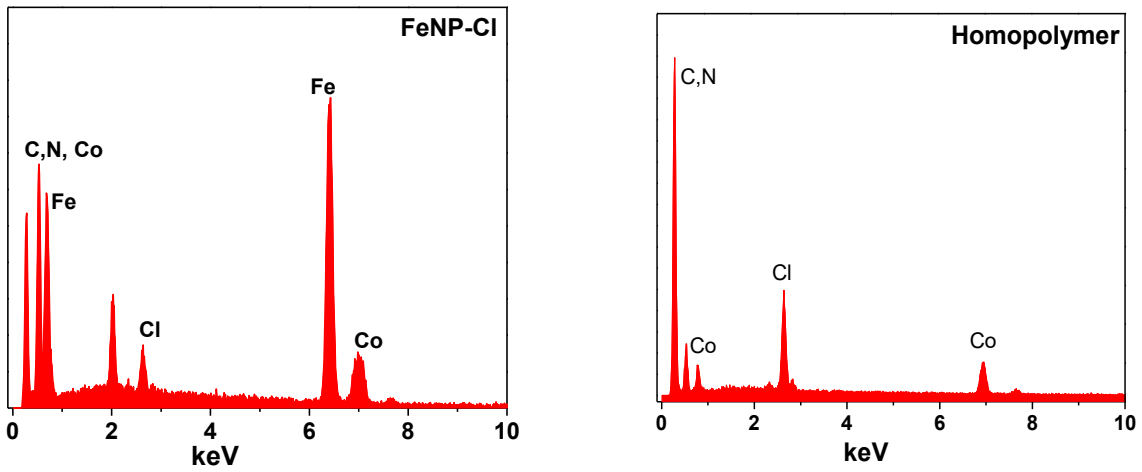

Figure 4.1 EDX elemental analysis of cobaltocenium-containing iron oxide nanoparticles and cobaltocenium-containing homopolymer.

Synthesis of FeNP-Penicillin bioconjugates

Cobaltocenium-containing iron oxide nanoparticles with Cl^- was initially dispersed in deionized water and solution of penicillin-G sodium salt was added slowly with molar ratios (penicillin salt to cobaltocenium moieties) in the range of 1.15 to 1.0. The solution was stirred for 2 h and then dialyzed against 3L deionized water for 9 hours. The solution in a dialysis bag was collected and freeze-dried. The FeNP-Pen conjugates were obtained as a yellow powder.

Growth of bacteria

The antibacterial activity of cobaltocenium-containing iron oxide nanoparticles was evaluated using standard disk-diffusion assay (ASTM: the Kirby Bauer diffusion test)[55]. Firstly, actively-growing cultures of each bacterial strain on Mannitol salt agar (MSA) were inoculated on Tryptic Soy Broth (TSB) agar plates. The bacterial growth culture (cell concentrations were 1.0×10^6 CFU/mL) 10 μL was diluted to 1 mL in TSB, and 100 μL of cell culture was spread on TSB agar plates to form a bacterial lawn covering the plate surface. Then a 6 mm filter disc was laid on the agar surface, to which the nanoparticle solution was added at a desired concentration. All plates were incubated overnight at 37^{o}C.

Bacterial morphology by FE-SEM.

Field-emission scanning electron microscopy (FE-SEM) was used to examine the morphology of bacterial cells after incubating with test drugs. In summary, 20 μL of bacterial cell solution was grown on one glass slide in a six-well plate containing 2 mL TSB medium at 37 ^{o}C overnight. Cell suspensions were diluted with OD_{600} = 1.0. After adding calculated amount of test drugs to the 1 mL cell stock solution, it was left to incubate overnight at 37 ^{o}C. A cell suspension without added chemicals was used as the control.

The samples were then fixed in cacodylate buffered with 2.5% glutaraldehyde solution (pH = 7.2) for 2–3 h at 4 ºC and post-fixed with 1% osmium tetroxide at 4 ºC for 1 h. Samples were dehydrated under critical point, then coated with gold using Denton Dest II Sputter Coater for 120s and observed by FE-SEM.

LIVE/DEAD bacterial viability assays

The five bacterial strains were inoculated and prepared by a similar procedure as mentioned above. 1 mL of active bacterial stock solution was introduced to 5 μg penicillin solutions. An untreated cell suspension was used as the control. Following overnight incubation at 37ºC, 1 μL LIVE/DEAD BacLight (Bacterial Viability Kit; Invitrogen Inc.) was added to the incubation solution. After incubation for 15 minutes, cells were imaged using a Leica TCS SP5 Confocal Scanning Laser Microscope with 63X oil-immersion lens. Stained cells were excited at 488 nm with a Krypton-Argon laser. Bacteria cells having intact membranes display green fluorescence (Emission = 515 nm) and bacteria with disrupted membranes fluoresce red (Emission = 635 nm).

Drug Resistance Study

50 μL aqueous solution of FeNP-penicillin conjugates with one-half the MIC concentration were added to 96-well plates. Then, 150 μL bacterial TSB solution (OD_{600} = 1.00) were added to the wells. The bacterial TSB solution without conjugates was used as the control. The assay plate was incubated at 37ºC until the bacteria were grown to an optical density of about 1.00 (OD_{600} = ~ 1.00) in control samples. All assays were carried out in duplicate in the same assay plate. The process was repeated every 20-22h for up to 15 passages.

Recycling of FeNP-Pen for antibacterial assays

5 µl bacterial suspensions were inoculated into 3 mL TSB solutions at 37 °C for incubation at 300 rpm overnight. Identical bacterial culture solutions were prepared in three different tubes. The first tube was used as the control without adding any test samples while the second tube was used to determine the activity of penicillin. 2 × MIC of nanoparticle conjugates was added to the third tube before incubation. Bacterial growth was measured at OD_{600}, and was compared with the control tube. The inhibition efficiency was calculated as follows: inhibition efficiency (%) = (Control OD_{600} - Sample OD_{600})/ Control OD_{600} × 100. The control OD_{600} was determined from the blank tube.

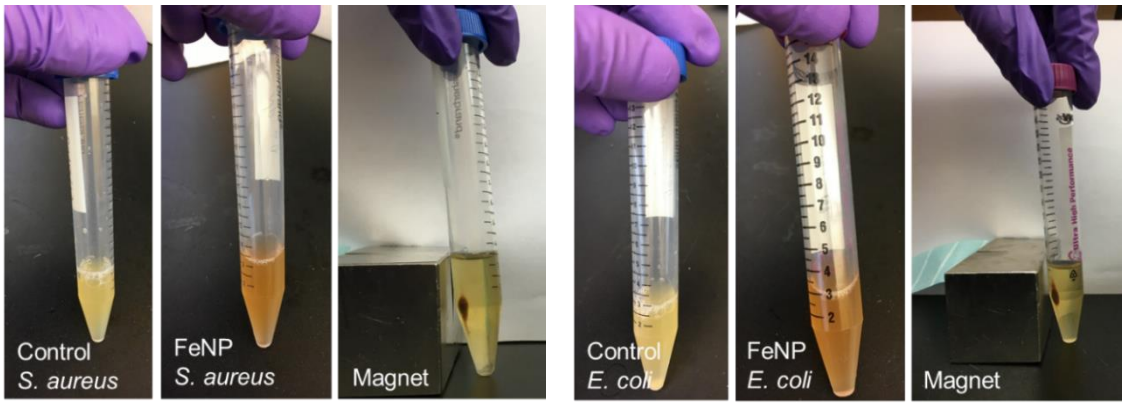

Figure 4.2 Images of cobaltocenium-containing iron oxide nanoparticles incubating and recycling against various bacteria

Each test was conducted in duplicate. After incubating overnight, the tube was placed adjacent to a magnet stand at room temperature for 10 min. The nanoparticles were attracted to the wall of the tube via magnetic force. After removing the supernatant from the tube, penicillin was added to complex with the nanoparticle. Any remaining penicillin was removed by washing with aqueous solution. The test was then repeated for total of 5 passages.

Time-kill Study

The kinetics of antibacterial activity of nanoparticle conjugate was investigated. In summary, various concentrations of the nanoparticle conjugate were incubated at a time interval of 1 h, 2 h, 4 h, 6 h, 8 h and 12 h. During each interval, 100 µL of the culture solution was taken and diluted to 10^6 times. The final diluted solution was spread on agar plates to incubate at 37°C overnight and the colonies were counted next day. The experiment was carried out in duplicate.

Hemolysis evaluation for cytotoxicity determination.

Blood was collected from mice in heparinized tubes and diluted by mixing 800 µL blood with 1000 µL PBS. Nanoparticle samples were prepared in PBS at concentrations 10, 50, 100 and 500 µg/mL and added 60 µL of the diluted blood samples to 3 mL of the nanoparticle conjugates, PBS or 0.1% Triton-X100 in PBS. The samples were incubated for 1 h at 37°C followed by centrifugation for 10 minutes at 1500 rpm. Supernatants were collected and OD was measured at 545 nm to calculate Hemolysis rate by using the formulae, HR=(AS-AN)/(AP-AN) where AS, AN and AP are OD values of the supernatants from test samples, negative control (PBS) and positive control (0.1% Triton-X100) respectively.

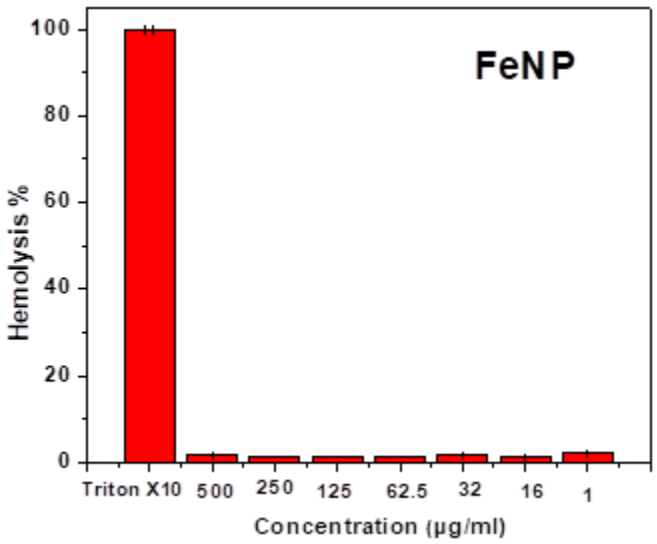

Figure 4.3 Hemolysis test results for FeNP nanoparticles.

4.4 Results and Discussion

Synthesis of Cobaltocenium-Containing Iron Oxide Nanoparticles

We introduced cationic cobaltocenium along with antibiotics onto iron oxide nanoparticles to form magnetic antimicrobial nanoparticles, as shown in Scheme 4.2. To be specific, cobaltocenium-containing polymers were grafted from iron oxide nanoparticles, which were then installed with penicillin via ionic complexation. Cobaltocenium, a cationic and high-oxidation state metallocene, has recently gathered a lot of attention for its various applications derived from its excellent chemical stability and superior binding ability to anions[34-42]. The pathway for the synthesis of magnetic nanoparticles consisted of the formation of iron oxide nanoparticles by coprecipitation of Fe^{2+} and Fe^{3+} salts in the presence of an alkaline solution followed by the immobilization of RAFT agent on to the nanoparticle surface. The commonly-used coprecipitation method was chosen because of its simplicity, low cost and high efficiency [43]. The surface of nanoparticles was further functionalized with 3-aminopropyldimethylethoxysilane

followed by an amidation reaction between its amino group and acid group of an RAFT agent, 4-cyanopentanoic acid dithiobenzoate (CPDB)[44]. The amount of RAFT agent anchored onto the modified iron oxide nanoparticles was quantitatively determined by comparing the absorption for CPDB from iron oxide nanoparticles to free CPDB. The grafting density was found to be 0.15 chain/nm^2 (16.5 μmol/g CPDB).

In conjunction with well-developed controlled radical polymerization techniques, especially RAFT, the "grafting from" strategy provides an efficient route to functionalize surface by controlling compositions and structures[45-49]. RAFT polymerization provides quantitative and precise control over the molecular weight[50, 51]. The next step was mediated by CPDB-coated iron oxide nanoparticles to carry out polymerization of a monomer, 2-cobaltocenium amidoethyl methacrylate hexaflurophosphate ($CoAEMAPF_6$), using AIBN as an initiator in dry DMF at 90 °C, as shown in Scheme 4.2. $CoAEMAPF_6$ was synthesized using a previously established procedure[52]. Cobaltocenium-containing polyelectrolytes with hydrophobic anions can be easily switched to hydrophilic ones using tetra-butylammonium salts via a facile phase-transfer ion-exchange method[53]. In this case, the nanoparticles with PF_6^- anions were subjected to ion exchange, which resulted in hydrophilic chloride-paired nanoparticles. The newly formed nanoparticles had good aqueous solubility, which opened the door for use in biomedicines. The nanoparticles were further conjugated with anionic penicillin-G (i.e. penicillin, hereafter) via electrostatic interaction between the cationic cobaltocenium moiety and anionic penicillin by mixing them together. Any unbound penicillin was removed by dialysis.

Scheme 4.2. Modification of iron oxide nanoparticles using cobaltocenium-containing polymer by RAFT.

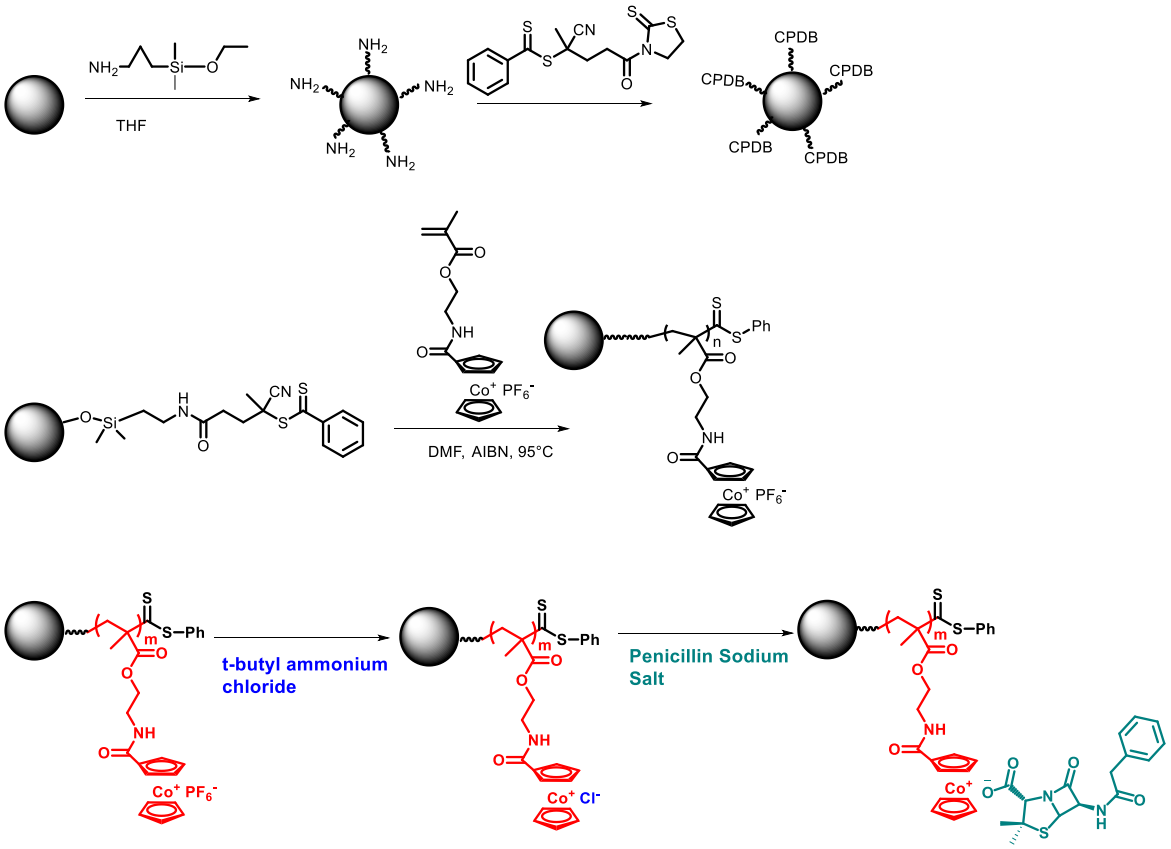

The mean diameter of cobaltocenium-containing nanoparticles was ~ 25 nm as measured by dynamic light scattering and was consistent with measurements obtained by TEM, as shown in Figure 4.3 a. After loading penicillin to the nanoparticle by electrostatic interaction, the diameter rose up to 33 nm as seen in DLS. The nanoparticle was also characterized by FTIR and EDX elemental analysis to confirm major chemical bonds and elements in the nanoparticles, respectively (Figure 4.1).

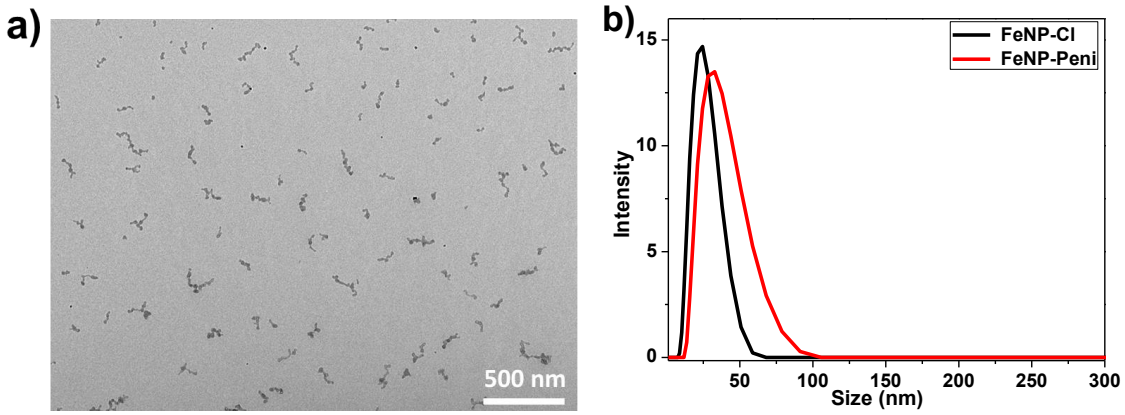

Figure 4.4 a) TEM image of FeNP-Cl nanoparticles; and b) Dynamic Light Scattering (DLS) measurements showing sizes of nanoparticles.

Thermogravimetric analysis (TGA) was implemented to determine the accurate weight loss of nanoparticles after loss of attached organic compounds. The TGA of iron oxide nanoparticles with RAFT agent and cleaved polymer chains was compared with that of cobaltocenium-containing iron oxide nanoparticles alone. Based on the TGA measurement, the total weight percentage of cobaltocenium in the iron oxide nanoparticle (FeNP) was 56 wt%. It was found that cationic cobaltocenium moiety complexed with carboxylate anions of penicillin at a 1:1 pairing. This allowed us to calculate the final weight percentage of penicillin in the nanoparticles to be around 30 wt%.

Antimicrobial Activity of Cobaltocenium-Containing Iron Oxide Nanoparticles

The nanoparticles were tested for their antimicrobial activity against two different Gram-positive, *Staphylococcus aureus* (ATCC 33591) and *Bacillus cereus* (ATCC 11778), and three different Gram-negative bacteria, *Escherichia coli* (ATCC 11775), *Proteus vulgaris (*ATCC 33420) and *Klebsiella pneumonia* (ATCC 35596), by the conventional agar disk-diffusion assay following a protocol of Kirby Bauer diffusion test[54]. Initially, concentrations of penicillin ranging from 4 µg to 10 µg were tested. The optimal antibacterial activity was obtained with 7 µg penicillin and was used for all subsequent

disk diffusion assays. The development of a clear zone around the disk represents an inhibition zone, which indicates the ability of the test samples to kill the bacteria. To better compare the antimicrobial efficacy, four different samples were prepared for disk diffusion assays: homopolymer-penicillin conjugate (PCo-Pen), penicillin, FeNP-penicillin conjugate (FeNP-Pen) and FeNP without penicillin (FeNP-Cl). For *S. aureus,* the diameter of the inhibition zone caused by penicillin alone was 8 mm while the homopolymer conjugate resulted in a larger diameter of 11 mm, as shown in Figure 4.5. When the FeNP-penicillin conjugate was used, the inhibition zone was significantly enhanced and diameters increased to a mean of 18 mm. FeNP nanoparticles lacking penicillin had much smaller zones of inhibition owing to their much reduced antibacterial activity. When the assay was extended to another Gram-positive bacterium, *B. cereus*, a similar trend was observed, however, higher antimicrobial activities for all samples were observed. The zones of inhibition of penicillin and FeNP-penicillin conjugates increased to 10 mm and 20 mm, respectively, when compared to *S. aureus*. For further investigation, disk diffusion assays were carried out against several BSL2-level Gram-negative pathogen strains using the above-mentioned protocol: *Escherichia coli, Proteus vulgaris* and *Klebsiella pneumonia.* As shown in Figure 4.5, penicillin alone showed minimal antibacterial activity when compared to homopolymer-penicillin conjugates and FeNP-penicillin conjugates. For example, inhibition zones caused by penicillin were just 4 mm against *K. pneumonia,* while inhibition zones created by FeNP-penicillin conjugate were three times higher (12 mm). Inhibition zones caused by homopolymer conjugate (PCo-Pen) were larger than those of penicillin alone, but remained smaller than the FeNP-penicillin conjugates.

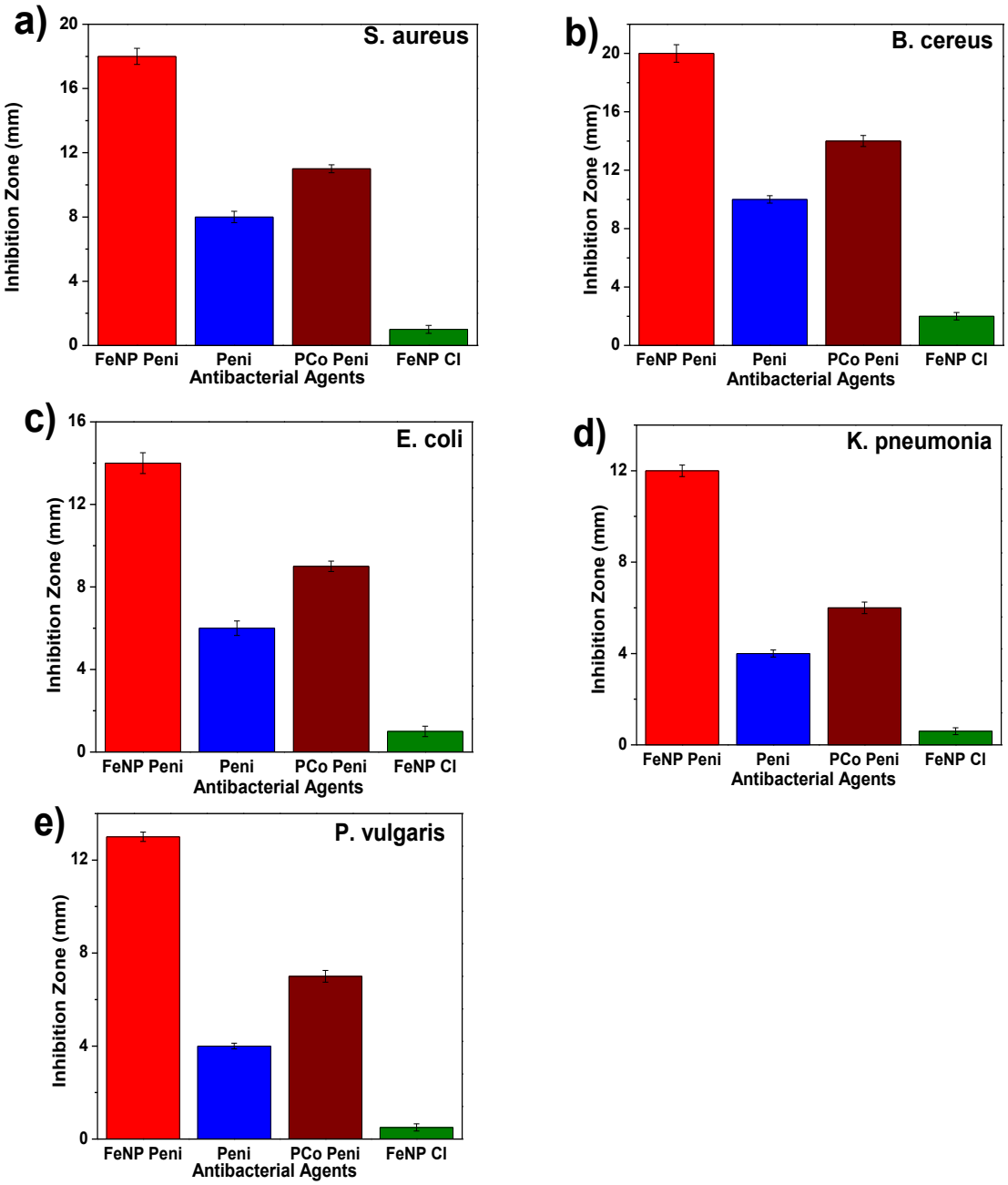

Figure 4.5**.** Inhibition zones of different agents against various strains of bacteria at an equivalent of 7 μg penicillin-G/disk using disk-diffusion assays: a) *S. aureus*; b) *B. cereus* C) *E. coli;* d) *K. pneumoniae*; e) *P. vulgaris.*

The cationic moiety of cobaltocenium displayed good antimicrobial activity at a higher concentration, but the concentration of cobaltocenium in the FeNP-Cl was probably not high enough to result in determinable antimicrobial activity. Compared to penicillin alone, all FeNP-conjugates exhibited much stronger antimicrobial activities for both Gram-

positive and Gram-negative strains.For penicillin and each of the FeNP-penicillin conjugates, minimum inhibitory concentrations (MIC) were calculated using the established protocol, and are given in Table 4.1[55]. The MIC values are based on the effective concentration of penicillin in the nanoparticle-penicillin conjugate. The mean MIC of FeNP-penicillin conjugates against Gram-positive strains, *S. aureus* was 3.4±0.4 µg/mL and *B. cereus* was 2.7 ±0.5 µg/mL, which was approximately four times lower than that of penicillin alone, 13.48 µg/mL and 10.92 µg/mL respectively, for these pathogens.

Table 4.1 Minimum inhibitory concentrations (MICs) of different agents against five strains of bacteria.

Entry	Minimum Inhibitory Concentration (MIC µg/mL)				
	S. aureus	*B. cereus*	*E. coli*	*P. vulgaris*	*K. pneumonia*
FeCo-Pen	3.4	2.7	5.6	6.5	7.6
Penicillin	13.5	10.9	22.3	17.5	26.7

As expected, the MIC values for three different Gram-negative strains were significantly higher. They followed a similar trend to the Gram-positive strains, and have much lower MIC values than those observed for penicillin alone. Compared with penicillin, nanoparticle-polymer conjugates produced significantly higher efficacies against both Gram-positive and Gram-negative strains**.** The additional outer polysaccharide layer (i.e. capsule) present in the Gram-negative bacteria might act as an extra layer of shielding for the test samples to penetrate, resulting in the observed smaller inhibition zones and higher MIC values.

The increased bactericidal activity and inhibition effect of FeNP-penicillin conjugates on various Gram-positive and Gram-negative strains was further confirmed by confocal laser scanning microscopy (CLSM) and scanning electron microscopy (SEM).

LIVE/DEAD stained bacteria viability assays using CSLM indicated greater levels of cell death and lower cell densities when bacterial cells were exposed to FeNP-Pen conjugates, as shown in Figure 4.6. Cells incubated with FeNP-Pen conjugates displayed primarily red or yellow fluorescence, indicative of cell death, as determined by rupture of cell membranes.

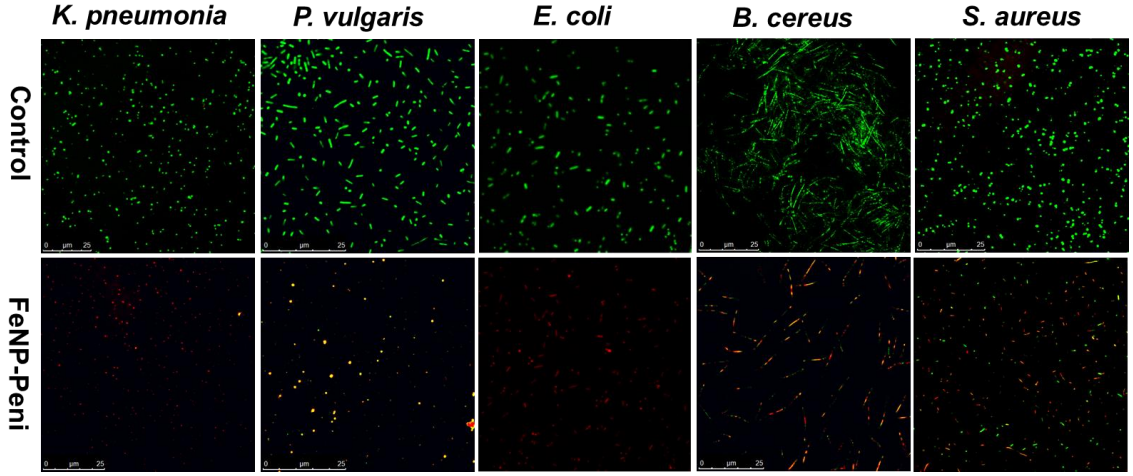

Figure 4.6. Confocal scanning laser microscopy (CSLM) images of controls and FeNP-penicillin conjugates exposed to a concentration equivalent of penicillin 7 μg/mL. Cells *S. aureus, B. cereus, E. coli, K. pneumonia* and *P. vulgaris* were stained using BacLight Live/Dead stain, where green indicates live cells, and red indicates dead cells). The bacterial solution without FeNP was used as the control.

Also, the SEM imaging was used to compare differences in morphology before- and after-treatment with FeNP-Pen conjugates as in Figure 4.7. Control samples consisted of intact bacterial cells with smooth surfaces while the cells incubated with nanoparticle conjugates displayed collapsed cell envelopes with obvious disruptions in the original morphology. We postulate that the high antibacterial efficacy resulted from the stable attachment of polymers to the nanoparticle surface, which in turn delivered increased densities of antibacterial species to the target bacterial cells. The bacterial cell wall is the primary target of β-lactam antibiotics such as penicillin, and bacteria usually resist these

antibiotics by secreting beta-lactamase enzymes, which cause the hydrolysis of the lactam ring and nullify the efficacy of antibiotic molecules.

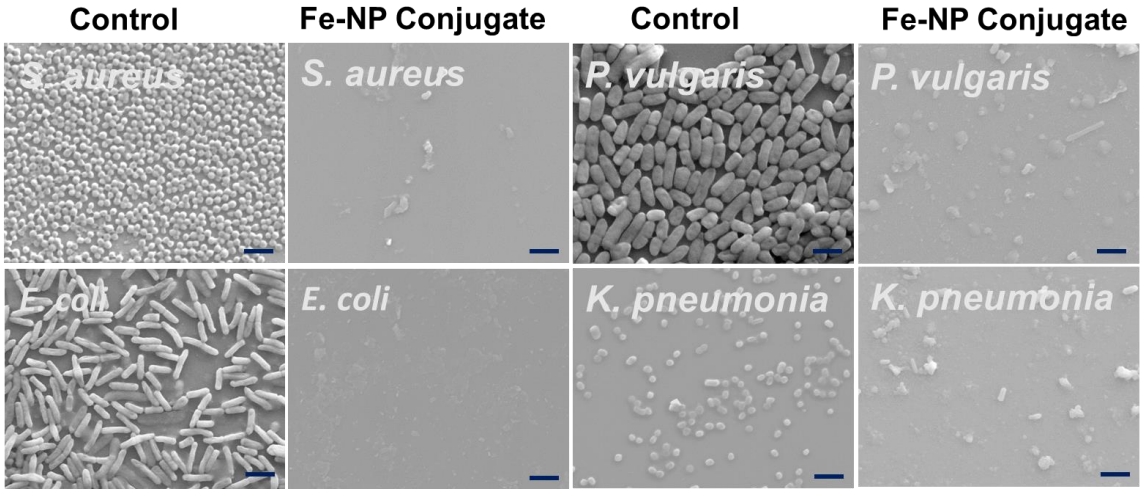

Figure 4.7 Scanning electron microscopy (SEM) images of control and FeNP-penicillin conjugates with a concentration of penicillin at 7 µg/mL against various Gram-positive and Gram-negative bacteria. Bacterial solutions without FeNP were used as the control. All scale bars are 2.0 µm.

The synergistic introduction of two antimicrobial segments, cobaltocenium and penicillin, acts through different mechanisms against the pathogenic bacteria. Thus, the possibility of circumventing both mechanisms by bacteria, in addition to the local concentration effect provided by nanoparticles, is reduced. When antibiotics are administered in a solution form, the concentration of antibiotic reaching the pathogenic cell is much reduced as the resulting scenario is much different as they tend to form a homogenous dispersion of molecules spread over the tissues.

One of the advantages using iron oxide nanoparticles is that the FeNP-penicillin conjugates can be easily extracted and recycled owing to the fast response to an applied magnetic field as shown in Scheme 4.3 and Figure 4.2 This not only saves the cost and time but also eliminates the possibility of nano-pollution in the biological environment. The dynamic shake flask method was used to evaluate the recyclability and antibacterial

efficacy of FeNP nanoparticle conjugates. The nanoparticle conjugates were shaken in a bacterial suspension at 37°C for 4 hours, and OD_{600} was measured.

Scheme 4.3 Schematic illustration of recycling cobaltocenium-containing magnetic nanoparticles for antibacterial application.

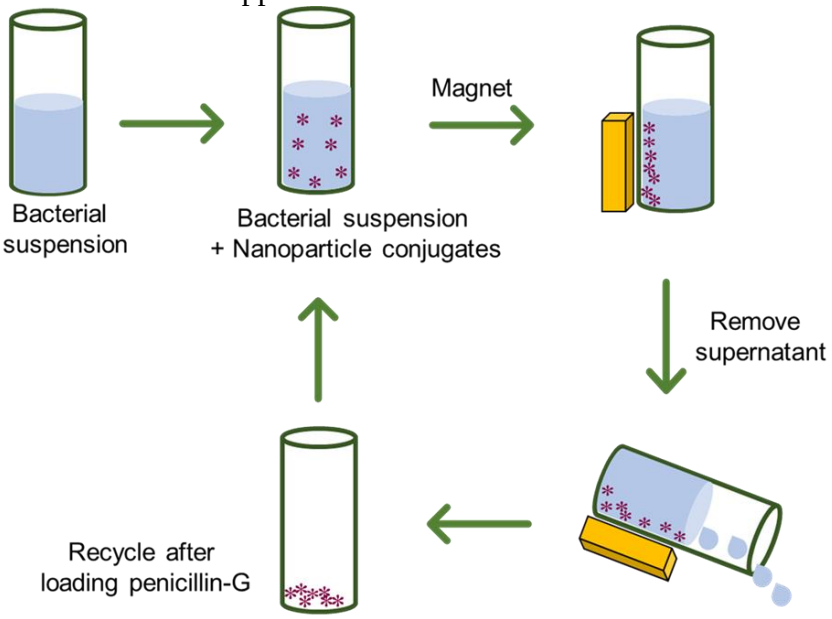

The nanoparticle conjugates were readily collected at the side of the tube using a magnet and the supernatant was removed. To confirm the equimolar pairing of cobaltocenium moiety with anionic penicillin for the next cycle, a fresh batch of penicillin was added. The nanoparticles were washed multiple times with aqueous solution to remove any excess penicillin. Thus, obtained conjugates were re-dispersed in the bacterial solution and the procedure, mentioned earlier, was repeated. The enhanced inhibition efficiency of nanoparticle conjugates using the recycled nanoparticles against both Gram-positive and Gram-negative bacteria was retained even after five cycles as shown in Figure 4.8.

Cobaltocenium-containing iron oxide nanoparticles have dual mode of action: cationic cobaltocenium can disrupt cell membranes and the antibiotics target cell walls. We conducted a dose-dependent time-kill study to investigate how rapid the nanoparticle conjugates can kill bacteria using a colony formation assay. After incubating overnight

with the nanoparticle conjugates, the solution was diluted and placed on an agar plate. The number of colony-forming units (CFU) was counted at various time up to 12 hours at the multiple of MIC concentration and expressed as $CFUmL^{-1}$.

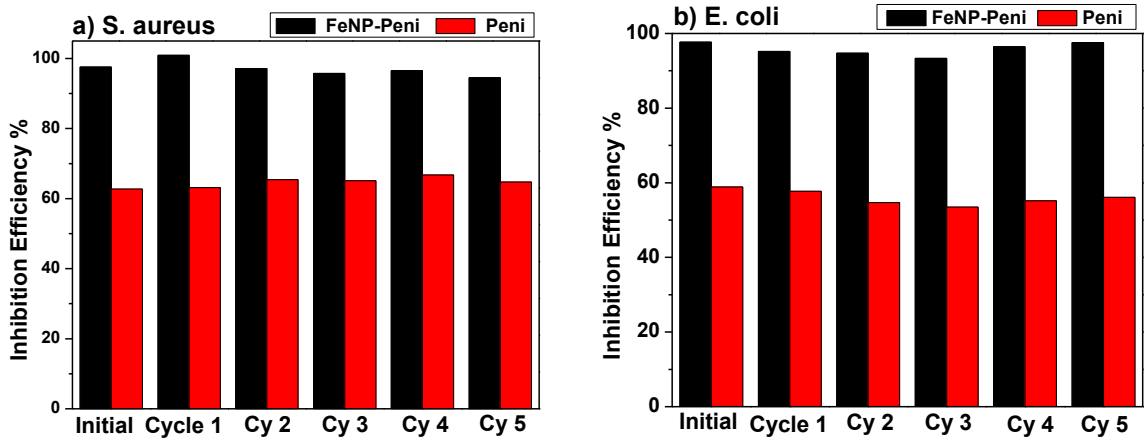

Figure 4.8 Inhibition activities of recyclable magnetic cobaltocenium-containing FeNP conjugates against Gram-positive (*S. aureus*) and Gram-negative bacteria (*E. coli*).

As shown in Figure 4.9**,** nanoparticle conjugates started to act instantaneously, which can be seen by the significant reduction in bacteria concentration. With the concentration of just four times above the MIC, all bacteria (*S. aureus*) were completely killed in just 4 hours. When the concentration was increased to eight times of MIC, it took approximately one hour to kill all bacteria.

One of the main concerns on antimicrobial agents is that over time the bacteria evolve as a part of their adaptive response, and develop resistance, which cause an array of diseases ranging from minor infections to persistent and life-threatening infections. To evaluate the probability of that FeNP-penicillin conjugates might elicit resistance in bacteria, a resistance-selection study was conducted against both Gram-positive and Gram-negative bacteria using OD_{600} measurements. Cultures were subsampled and transferred 15 times to new media containing their respective antibiotic conjugates at MIC concentration.

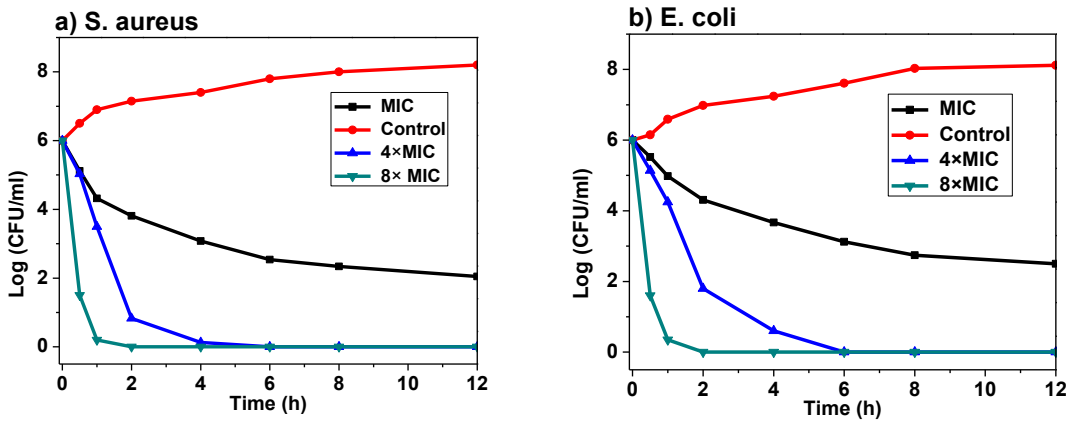

Figure 4.9 Time-kill curves of FeNP-conjugates against *S. aureus* and *E. coli*. Bactericidal activities were monitored for first 12 hours. The concentrations used were MIC, 4×MIC, and 8×MIC, respectively.

As shown in Figure 4.10, the OD_{600} values of the nanoparticle conjugates remained virtually constant even after 15 consecutive passages, indicating the nanoparticle conjugates did not induce drug resistance against both *S. aureus* and *E. coli*. In addition, the MIC values for *S. aureus* after 15 passages did not show any significant spikes ruling out any possibilities of resistance development. The cobaltocenium-moiety has the capability to directly contact the bacterial cell wall causing disruption, which makes antibiotic resistance mechanism irrelevant for the conjugate system.

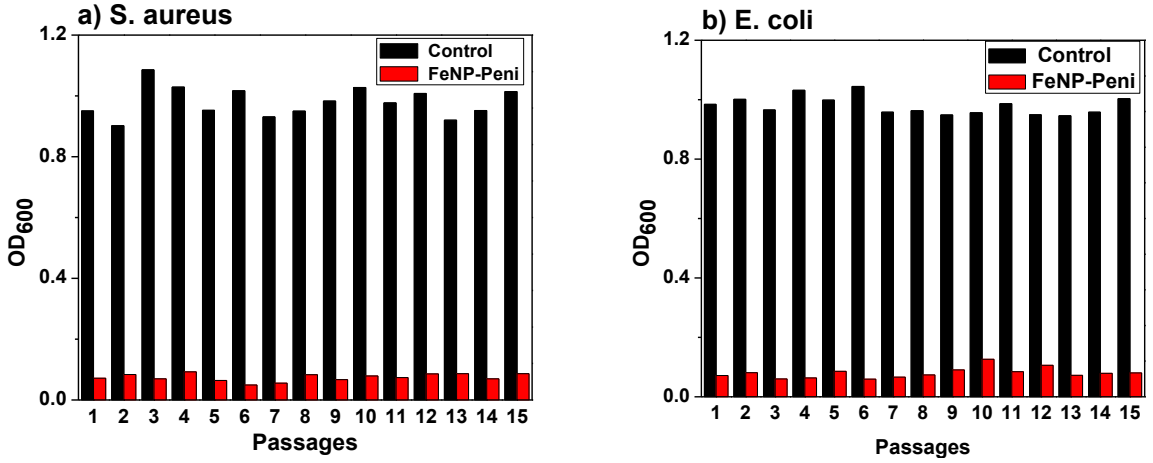

Figure 4.10 Drug resistance study of FeNP-penicillin conjugates against *S. aureus* and *E. coli*.

A typical bacterial cell is known to be in the micrometer range but the outer cell membranes consist of pores that are in the nanometer range. Thus, it enables the FeNP conjugates with diameters in the range of 30 nm to pass through the membrane to enter the cell causing the lysis of bacterial cells. As shown in Figure 4.11**,** the control bacterial cells are intact and have smooth surfaces. After treating with FeNP conjugates, outer cells membranes appeared to be disrupted with the entry of particles inside the cell and the bacterial cells seemed to have clumped together. This confers the particles can penetrate inside and cause lysis of bacterial cells.

Hemolysis is the lysis of red blood cells (RBC) and is commonly characterized as a side effect of cationic polymers. Therefore, a hemolytic assay was conducted to evaluate whether FeNP particles could lead to hemolysis of RBCs. We found that even at a concentration as high as 500 µg/mL, extremely low percentages of cells (< 5%) were lysed by FeNP compared to the negative control group, as shown in Figure 4.3. This implies that the FeNP has negligible or no toxicity towards host cells.

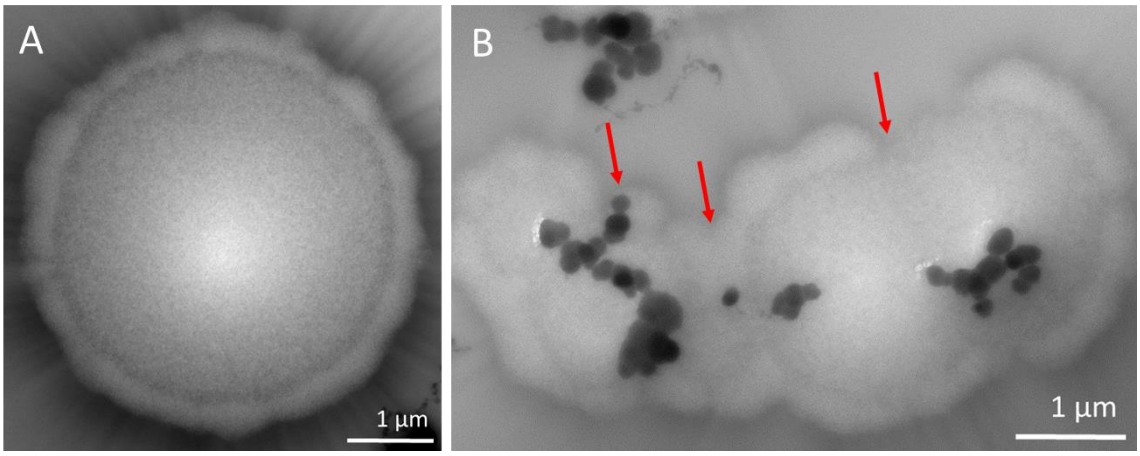

Figure 4.11 TEM images of *S. aureus* after incubating with (A) Control; and (B) FeNP-conjugates, with the concentration of penicillin at 7 µg/mL.

4.5 Conclusions

In summary, we designed and synthesized highly efficient charged metallopolymer-grafted magnetic nanoparticles via surface-initiated RAFT polymerization. β-Lactam antibiotic penicillin-G was loaded onto the magnetic nanoparticles, based on electrostatic interaction between cationic cobaltocenium moiety and anionic antibiotic molecule. The resulting nanoparticle conjugates showed good bactericidal efficiencies against both Gram-positive and Gram-negative pathogenic strains, which facilitated the revitalization of the penicillin. These nanoparticles displayed a response to external magnetic fields and were easily recycled after antibacterial tests. The recycled nanoparticle conjugates retained aqueous dispersibility and high antibacterial efficacy. In addition, the nanoparticle conjugates killed bacteria rapidly, and the susceptibility of both Gram-positive and Gram-negative strains to the nanoparticle conjugates remains almost unchanged even after 15 passages. The conjugates improved the bactericidal efficacy not only by rejuvenating antibiotics but also by providing an enhanced local concentration effect on the bacterial cells.

4.6 References

[1] Antibiotics Resistance Threats in the United States. https://www.cdc.gov/drugresistance/threat-report-2013/pdf/ar-threats-2013-508.pdf: Center for Disease Control; 2013.

[2] Levy SB, Marshall B. Antibacterial resistance worldwide: causes, challenges and responses. Nat Med. 2004;10:S122.

[3] Ilker MF, Nüsslein K, Tew GN, Coughlin EB. Tuning the Hemolytic and Antibacterial Activities of Amphiphilic Polynorbornene Derivatives. J Am Chem Soc. 2004;126:15870-5.

[4] Kenawy E-R, Worley SD, Broughton R. The Chemistry and Applications of Antimicrobial Polymers: A State-of-the-Art Review. Biomacromolecules. 2007;8:1359-84.

[5] Sambhy V, Peterson BR, Sen A. Antibacterial and Hemolytic Activities of Pyridinium Polymers as a Function of the Spatial Relationship between the Positive Charge and the Pendant Alkyl Tail. Angew Chem Int Ed. 2008;47:1250-4.

[6] Tew GN, Liu D, Chen B, Doerksen RJ, Kaplan J, Carroll PJ, et al. *De novo* design of biomimetic antimicrobial polymers. Proc Natl Acad Sci USA. 2002;99:5110-4.

[7] Engler AC, Wiradharma N, Ong ZY, Coady DJ, Hedrick JL, Yang Y-Y. Emerging trends in macromolecular antimicrobials to fight multi-drug-resistant infections. Nano Today. 2012;7:201-22.

[8] Takahashi H, Caputo GA, Vemparala S, Kuroda K. Synthetic Random Copolymers as a Molecular Platform To Mimic Host-Defense Antimicrobial Peptides. Bioconj Chem. 2017;28:1340-50.

[9] Mizutani M, Palermo EF, Thoma LM, Satoh K, Kamigaito M, Kuroda K. Design and Synthesis of Self-Degradable Antibacterial Polymers by Simultaneous Chain- and Step-Growth Radical Copolymerization. Biomacromolecules. 2012;13:1554-63.

[10] Ganewatta MS, Tang C. Controlling macromolecular structures towards effective antimicrobial polymers. Polymer. 2015;63:A1-A29.

[11] Sang P, Shi Y, Teng P, Cao A, Xu H, Li Q, et al. Antimicrobial AApeptides. Curr Top Med Chem. 2017;17:1266-79.

[12] Pelgrift RY, Friedman AJ. Nanotechnology as a therapeutic tool to combat microbial resistance. Adv Drug Del Rev. 2013;65:1803-15.

[13] Guo S, Zhang S, Sun S. Tuning Nanoparticle Catalysis for the Oxygen Reduction Reaction. Angew Chem Int Ed. 2013;52:8526-44.

[14] Govan J, Gun'ko Y. Recent Advances in the Application of Magnetic Nanoparticles as a Support for Homogeneous Catalysts. Nanomaterials. 2014;4:222.

[15] Wu L, Mendoza-Garcia A, Li Q, Sun S. Organic Phase Syntheses of Magnetic Nanoparticles and Their Applications. Chem Rev. 2016;116:10473-512.

[16] Weller D, Mosendz O, Parker G, Pisana S, Santos TS. L10 FePtX–Y media for heat-assisted magnetic recording. physica status solidi (a). 2013;210:1245-60.

[17] Takafuji M, Ide S, Ihara H, Xu Z. Preparation of Poly(1-vinylimidazole)-Grafted Magnetic Nanoparticles and Their Application for Removal of Metal Ions. Chem Mater. 2004;16:1977-83.

[18] Li Z, Wei L, Gao MY, Lei H. One-Pot Reaction to Synthesize Biocompatible Magnetite Nanoparticles. Adv Mater. 2005;17:1001-5.

[19] Ulbrich K, Holá K, Šubr V, Bakandritsos A, Tuček J, Zbořil R. Targeted Drug Delivery with Polymers and Magnetic Nanoparticles: Covalent and Noncovalent Approaches, Release Control, and Clinical Studies. Chem Rev. 2016;116:5338-431.

[20] Gupta AK, Gupta M. Synthesis and surface engineering of iron oxide nanoparticles for biomedical applications. Biomaterials. 2005;26:3995-4021.

[21] Dong H, Huang J, Koepsel RR, Ye P, Russell AJ, Matyjaszewski K. Recyclable Antibacterial Magnetic Nanoparticles Grafted with Quaternized Poly(2-(dimethylamino)ethyl methacrylate) Brushes. Biomacromolecules. 2011;12:1305-11.

[22] Wang L, Cole M, Li J, Zheng Y, Chen YP, Miller KP, et al. Polymer grafted recyclable magnetic nanoparticles. Polym Chem. 2015;6:248-55.

[23] Xu C, Sun S. Monodisperse magnetic nanoparticles for biomedical applications. Polym Int. 2007;56:821-6.

[24] Lu A-H, Salabas EL, Schüth F. Magnetic Nanoparticles: Synthesis, Protection, Functionalization, and Application. Angew Chem Int Ed. 2007;46:1222-44.

[25] Balazs AC, Emrick T, Russell TP. Nanoparticle Polymer Composites: Where Two Small Worlds Meet. Science. 2006;314:1107-10.

[26] Kohut A, Ranjan S, Voronov A, Peukert W, Tokarev V, Bednarska O, et al. Design of a New Invertible Polymer Coating on a Solid Surface and Its Effect on Dispersion Colloidal Stability. Langmuir. 2006;22:6498-506.

[27] Hill LJ, Pinna N, Char K, Pyun J. Colloidal polymers from inorganic nanoparticle monomers. Prog Polym Sci. 2015;40:85-120.

[28] Kango S, Kalia S, Celli A, Njuguna J, Habibi Y, Kumar R. Surface modification of inorganic nanoparticles for development of organic–inorganic nanocomposites—A review. Prog Polym Sci. 2013;38:1232-61.

[29] von Werne T, Patten TE. Atom Transfer Radical Polymerization from Nanoparticles: A Tool for the Preparation of Well-Defined Hybrid Nanostructures and for Understanding the Chemistry of Controlled/“Living” Radical Polymerizations from Surfaces. J Am Chem Soc. 2001;123:7497-505.

[30] D'Costa VM, King CE, Kalan L, Morar M, Sung WWL, Schwarz C, et al. Antibiotic resistance is ancient. Nature. 2011;477:457.

[31] Zhang J, Chen YP, Miller KP, Ganewatta MS, Bam M, Yan Y, et al. Antimicrobial Metallopolymers and Their Bioconjugates with Conventional Antibiotics against Multidrug-Resistant Bacteria. J Am Chem Soc. 2014;136:4873-6.

[32] Yang P, Bam M, Pageni P, Zhu T, Chen YP, Nagarkatti M, et al. Trio Act of Boronolectin with Antibiotic-Metal Complexed Macromolecules toward Broad-Spectrum Antimicrobial Efficacy. ACS Infectious Diseases. 2017;3:845-53.

[33] Pageni P, Yang P, Chen YP, Huang Y, Bam M, Zhu T, et al. Charged Metallopolymer-Grafted Silica Nanoparticles for Antimicrobial Applications. Biomacromolecules. 2018;19:417-25.

[34] Ren L, Hardy CG, Tang C. Synthesis and Solution Self-Assembly of Side-Chain Cobaltocenium-Containing Block Copolymers. J Am Chem Soc. 2010;132:8874-5.

[35] Yang P, Pageni P, Kabir MP, Zhu T, Tang C. Metallocene-Containing Homopolymers and Heterobimetallic Block Copolymers via Photoinduced RAFT Polymerization. ACS Macro Lett. 2016;5:1293-300.

[36] Yan Y, Pageni P, Kabir MP, Tang C. Metallocenium Chemistry and Its Emerging Impact on Synthetic Macromolecular Chemistry. Synlett. 2016;27:984-1005.

[37] Yan Y, Zhang J, Wilbon P, Qiao Y, Tang C. Ring-Opening Metathesis Polymerization of 18-e Cobalt(I)-Containing Norbornene and Application as Heterogeneous Macromolecular Catalyst in Atom Transfer Radical Polymerization. Macromol Rapid Commun. 2014;35:1840-5.

[38] Zhang J, Yan Y, Chen J, Chance WM, Hayat J, Gai Z, et al. Nanostructured Metal/Carbon Composites from Heterobimetallic Block Copolymers with Controlled Magnetic Properties. Chem Mater. 2014;26:3185-90.

[39] Zhu T, Xu S, Rahman A, Dogdibegovic E, Yang P, Pageni P, et al. Cationic Metallo-Polyelectrolytes for Robust Alkaline Anion-Exchange Membranes. Angew Chem Int Ed. 2018:DOI: 10.1002/anie.201712387.

[40] Rapakousiou A, Wang Y, Belin C, Pinaud N, Ruiz J, Astruc D. 'Click' Synthesis and Redox Properties of Triazolyl Cobalticinium Dendrimers. Inorg Chem. 2013;52:6685-93.

[41] Mayer UFJ, Gilroy JB, O'Hare D, Manners I. Ring-Opening Polymerization of 19-Electron [2]Cobaltocenophanes: A Route to High-Molecular-Weight, Water-Soluble Polycobaltocenium Polyelectrolytes. J Am Chem Soc. 2009;131:10382-3.

[42] Yan Y, Zhang J, Ren L, Tang C. Metal-containing and related polymers for biomedical applications. Chem Soc Rev. 2016;45:5232-63.

[43] Petcharoen K, Sirivat A. Synthesis and characterization of magnetite nanoparticles via the chemical co-precipitation method. Materials Science and Engineering: B. 2012;177:421-7.

[44] Li C, Han J, Ryu CY, Benicewicz BC. A Versatile Method To Prepare RAFT Agent Anchored Substrates and the Preparation of PMMA Grafted Nanoparticles. Macromolecules. 2006;39:3175-83.

[45] Hill MR, Carmean RN, Sumerlin BS. Expanding the Scope of RAFT Polymerization: Recent Advances and New Horizons. Macromolecules. 2015;48:5459-69.

[46] Roy D, Guthrie JT, Perrier S. Graft Polymerization: Grafting Poly(styrene) from Cellulose via Reversible Addition−Fragmentation Chain Transfer (RAFT) Polymerization. Macromolecules. 2005;38:10363-72.

[47] Lin E-W, Maynard HD. Grafting from Small Interfering Ribonucleic Acid (siRNA) as an Alternative Synthesis Route to siRNA–Polymer Conjugates. Macromolecules. 2015;48:5640-7.

[48] Cobo I, Li M, Sumerlin BS, Perrier S. Smart hybrid materials by conjugation of responsive polymers to biomacromolecules. Nat Mater. 2014;14:143.

[49] Kumar SK, Jouault N, Benicewicz B, Neely T. Nanocomposites with Polymer Grafted Nanoparticles. Macromolecules. 2013;46:3199-214.

[50] Boyer C, Bulmus V, Davis TP, Ladmiral V, Liu J, Perrier S. Bioapplications of RAFT Polymerization. Chem Rev. 2009;109:5402-36.

[51] Moad G, Chong YK, Postma A, Rizzardo E, Thang SH. Advances in RAFT polymerization: the synthesis of polymers with defined end-groups. Polymer. 2005;46:8458-68.

[52] Pageni P, Kabir MP, Yang P, Tang C. Binding of Cobaltocenium-Containing Polyelectrolytes with Anionic Probes. Journal of Inorganic and Organometallic Polymers and Materials. 2017;27:1100-9.

[53] Zhang J, Yan Y, Chance MW, Chen J, Hayat J, Ma S, et al. Charged Metallopolymers as Universal Precursors for Versatile Cobalt Materials. Angew Chem Int Ed. 2013;52:13387-91.

[54] Bauer AW, Kirby WM, Sherris JC, Turck M. Antibiotic susceptibility testing by a standardized single disk method. Am J Clin Pathol. 1966;45:493-6.

[55] Wiegand I, Hilpert K, Hancock REW. Agar and broth dilution methods to determine the minimal inhibitory concentration (MIC) of antimicrobial substances. Nat Protoc. 2008;3:163.

[56] Zhang J, Yan J, Pageni P, Yan Y, Wirth A, Chen Y-P, et al. Anion-Responsive Metallopolymer Hydrogels for Healthcare Applications. Sci Rep. 2015;5:11914.

[57] Mascolo M, Pei Y, Ring T. Room Temperature Co-Precipitation Synthesis of Magnetite Nanoparticles in a Large pH Window with Different Bases. Materials. 2013;6:5549.

CHAPTER 5

GOLD NANOPARTICLES WITH COBALTOCENIUM-ANTIBIOTIC CONJUGATES TOWARD BROAD SPECTRUM ANTIMICROBIAL EFFICACY

5.1 Abstract

Bacterial infections have evolved into one of the most urgent global health threats. Designing potent antimicrobial agents that can combat drug-resistant bacteria is essential for treating bacterial infections. In this report, we developed a strategy to graft metallopolymer-antibiotic bioconjugates on gold nanoparticles as an antibacterial agent to fight against different bacterial strains. Thus, these nanoparticle conjugates combined various components in one system to display enhanced bactericidal efficacy, in which small sized nanoparticles provide high surface area for bacteria to contact, cationic metal polymer frameworks interact with negatively charged cell membranes, and β-lactam antibiotics are revitalized with improved vitality to attack bacteria via evading the detrimental enzyme-catalyzed hydrolysis. These macromolecular systems exhibited high efficacy in combating pathogenic bacteria, especially Gram-negative strains, due to synergistic effects of multi components on interactions with bacterial cells.

5.2 Introduction

Bacterial infections are one of the most dangerous health crises the word is facing. The consequences includes increased healthcare cost, destruction of local tissues, patient disability, morbidity, and even death.[1-3] According to a study on antimicrobial resistance in 2014,[4] bacterial infections currently cause at least 50,000 deaths annually across the US and Europe, with significantly higher numbers in other areas. If more-effective strategies are not taken to prevent and treat bacterial infections, it has been predicted that by 2050 infections could claim 10 million lives with costs approaching $100 trillion (USD) dollars worldwide.[4] However, commonly-used antibiotics, such as penicillin and methicillin, have diminished antimicrobial efficacies and/or are ineffective against numerous multidrug-

resistant (MDR) bacterial pathogens because of overuse of these drugs for so many years.[5, 6] Therefore, restoring the vitality of conventional antibiotics or designing other potent antimicrobial agents that combat drug-resistant bacteria is essential for treating bacterial infections.[7, 8]

In recent years, cationic compounds and polymers,[9-11] such as quaternary ammonium,[12-14] phosphonium compounds,[15] and peptides[16, 17] have garnered a great deal of attention as antimicrobial agents because of their ability to adsorb onto the negatively-charged bacterial cell surfaces and to insert their hydrophobic groups into membranes to combat bacteria. But many of these antimicrobial agents are notoriously toxic towards mammalian cells due to physical damage of cell morphology, thus limiting their roles in clinical settings.[10] Recently, we reported a class of non-cytotoxic antimicrobial cationic metallopolymers,[18, 19] which could form bioconjugates with conventional β-lactam antibiotics, such as penicillin, amoxicillin and cefazolin, via unique ion-pairs between cationic metallocenium moieties and carboxylate anions. The bioconjugates efficiently protected β-lactam antibiotics from hydrolysis by a β-lactamase enzyme in bacteria and lysed different strains of methicillin-resistant *Staphylococcus aureus* (MRSA).

Compared with antibiotic molecules or polymers, nanoparticles (NPs) provide versatile platforms for therapeutic applications based on their physical properties.[20-23] For example, the size range of NPs is commensurate with biomolecular and bacterial cellular systems, providing additional interactions to small molecular antibiotics.[24-27] The high surface to volume ratio allows incorporation of abundant functional ligands, enabling multivalency on NP surface to enhance interactions to target bacteria.[28-31] The inherent features of gold nanoparticles (Au NPs) provides advantages of small size, large surface area,

straightforward surface modification by thiols and amines, not being the substrate of bacterial efflux pumps, and the safety approval by U.S. FDA , which allow Au NPs to be useful as antibacterial agents.[32-39]

Herein, we developed a strategy to fight against different strains of Gram-positive and Gram-negative bacteria by presenting metallopolymer-antibiotic bioconjugates on gold nanoparticles as an antibacterial agent to further enhance the activity of conventional β-lactam antibiotics. A variety of characterization techniques, including transmission electron microscopy (TEM), dynamic light scattering (DLS), thermal gravimetric analysis (TGA), Zeta-potential analysis, UV-visible spectra, and ^{1}H NMR, spectra were performed systematically to determine the formation of Au@PCo NPs (cobaltocenium polymers coating on Au NPs). After bio-conjugating with β-lactam antibiotic penicillin-G, the Au@PCo-Peni NPs showed enhanced antibacterial efficacy on both Gram-positive and Gram-negative bacteria, compared with homopolymer-penicillin conjugates and penicillin-G alone. Confocal laser scanning microscopy (CLSM), scanning electron microscopy (SEM) and TEM indicated that Au@PCo-Peni NPs can penetrate bacteria membranes and destroy their permeability, causing the bacterial death.

5.3 Experimental Section

Characterization

^{1}H (400 MHz), ^{1}NMR spectra were recorded on a Varian Mercury 400 NMR spectrometer with tetramethylsilane (TMS) as an internal reference. Mass spectrometry was conducted on a Waters Micromass Q-TOF mass spectrometer, and the ionization source was positive ion electrospray. Dynamic light scattering (DLS) and Zeta-potential were operated on a Nano-ZS instrument, model ZEN 3600 (Malvern Instruments). UV−vis

was carried out on a Shimadzu UV-2450 spectrophotometer with a 10.00 mm quartz cuvette and monochromatic light of various wavelengths over a range of 190−900 nm. Field-Emission Scanning Electron Microscopy (FE-SEM, Zeiss UltraPlus) was used to take images of bacterial cells after incubating overnight with test drugs. The samples were firstly coated with gold using Denton Dest II Sputter Coater for 45 s and then observed by SEM. A Hitachi 8000 transmission electron microscope (TEM) was applied to take images at an operating voltage of 150 kV. TEM samples were prepared by dropping solution on carbon-supported copper grids and then dried before observation.

Materials and Methods

2-Cobaltoceniumamidoethyl methacrylate hexafluorophosphate ($CoAEMAPF_6$) was synthesized according to our earlier report.[40] 2-Aminoethyl methacrylate hydrochloride (90%), *N*-(3-dimethylaminopropyl)-*N′*-ethylcarbodiimide hydrochloride (EDC-HCl, 98%), 4-(dimethylamino) pyridine and tetrabutylammonium chloride (TBACl) were purchased from Aldrich and used as received. Tetrakis(hydroxymethyl)phosphonim chloride (referred to hereafter as THPC) was an 80% aqueous solution (practical grade) from Fluka, chloroauric acid (hydrogen tetrachloroaurate(III)) was from Johnson Matthey, assayed at 49.42 %. Water was from Thermo Scientific Nanopure with ion conductivity at 18.2 MΩ. The following bacterial strains were purchased from ATCC: *Staphylococcus aureus* (*S. aureus*, ATCC-33591), *Escherichia coli* (*E. coli*, ATCC-11775), *Klebsiella pneumoniae* (*K. pneumoniae*, ATCC-35596), and *Pseudomonas aeruginosa* (*P. aeruginosa*, ATCC-10145). Nitrocefin was purchased from TOKU-E and used as received. Sodium salt of penicillin-G was purchased from VWR and used as received. 2-Cyano-2-propyl benzodithioate (CPB) was obtained from Strem Chemical Inc. CPDB immobilized

silica nanoparticles were synthesized according to the literature. Azobisisobutyronitrile (AIBN) was recrystallized from methanol before use. All other chemicals were from commercial sources and used as received.

Synthesis of poly(cobaltocenium (PCo) homopolymers.

Cobaltocenium monomer, 2-cobaltoceniumamidoethyl methacrylate hexafluorophosphate ($CoAEMAPF_6$), was synthesized according to a reported method. PCo homopolymers were synthesized via RAFT polymerization:[40, 45] $CoAEMAPF_6$ (490 mg, 1.0 mmol), and CPB (3.5 mg, 0.01 mmol) and AIBN (0.5mg, 0.003mmol) were dissolved in a 1.0 mL DMF solution in a 10 mL Schlenk flask and then degassed by purging N_2 for 30 min. The mixture was then heated at 90 ^oC for 1-2 h. After reaction, the mixture was precipitated in cold dichloromethane for three times and vacuum-dried. Finally, the PCo homopolymers became soluble in water through a facile phase-transfer ion-exchange from PF_6^- to Cl^- using TBACl according to a previous report. A typical procedure was as follows:1 mL PF_6^- paired PCo homopolymers (30 mg/mL in acetonitrile) was slowly dropped into 5 mL TBACl solution (in acetonitrile) under vigorous stirring. After stirring for 5 minutes, the precipitated Cl^- paired PCo homopolymers was collected and washed by acetonitrile three times to remove any remaining PF_6^- anions and excess TBACl. The solid copolymer was then vacuum-dried and collected.

Synthesis of Au@PCo Nanoparticles.

Gold nanoparticles were synthesized according to a reported method.[44] In a 100-mL round-bottomed flask , while stirring, with 45.5 mL of water and then, in order, portions of aqueous solutions of sodium hydroxide (0.2 M, 1.5 mL), the reducing agent THPC (1 mL of a solution of 1.2 mL of 80% aqueous solution diluted to 100 mL with water), and

the metal salt chloroauric acid (2 mL of dark-aged stock solution, 25 mM) results in the formation of orange-brown hydrosols of gold nanoparticles. The Au@PCo nanoparticles were prepared as following[43]: the PCo polymer (50 mg) was added to above gold NPs solution. Then, 1M $NaBH_4$ (2 mL) was added dropwise and the mixture was stirred at room temperature for 48h. The mixture was centrifuged for 1h at 13,000 rpm. After centrifuge and rinsing with water 3 times, the Au@PCo nanoparticles were obtained.

Synthesis of Au@PCo-Peni Nanoparticles.

Au@PCo NPs (15 mg) and antibiotic penicillin-G sodium salt (10 mg) were dissolved in deionized water (1 mL) with molar ratios (penicillin salt to cobaltocenium moieties) between of 1.1 to 1. The solution was stirred for 12 h and then dialyzed against 3L deionized water for 12 h. The solution in a dialysis bag was collected and freeze-dried. The Au@PCo-Peni nanoparticles was obtained.

Evaluation of antimicrobial effects.

The following bacterial strains were purchased from ATCC: *Staphylococcus aureus* (*S. aureus*, ATCC-33591), *Escherichia coli* (*E. coli*, ATCC-11775), *Klebsiella pneumoniae* (*K. pneumoniae*, ATCC-35596), *Proteus vulgaris* (*P. vulgaris*, ATCC-33420). For these bacteria, a single colony was inoculated in 30 mL Tryptic Soy broth (TSB) at 37 °C for 24 h, shaking at 190 rpm/min. All bacteria were grown to an optical density of about l.00 (OD_{600} = 1.00) for further use.

To conduct the agar disk-diffusion assays, actively-growing cultures of each bacterial strain on Mannitol salt agar (MSA) were inoculated on TSB agar plates. The bacterial growth culture (cell concentrations were 1.0×10^6 CFU/mL) 10 μL was diluted to 1 mL in TSB, and 100 μL of that was spread on TSB agar plates to form a bacterial lawn

covering the plate surface. Then 6 mm (diameter) filter discs were added to the plate surface. Penicillin-G, Au@PCo NPs or Au@PCo-Peni bioconjugates at different amounts in 30 μL water was added to disks, and the plates were incubated at 28°C for 18 h. The development of a clear zone around the disk was indicative of the ability of agents to kill bacteria.

The minimum inhibitory concentrations (MIC) of PCo copolymers and PCo homopolymers were determined. 50 μL aqueous solution of PCo copolymers or PCo homopolymers with different concentrations were added to 96-well plates. Then, 150 μL bacterial TSB solution (OD_{600} = 1.00) was added to the wells. The bacterial TSB solution without polymers was used as the control. The assay plate was incubated at 37°C for 12 hours. Bacterial growth was detected at OD_{600} and was compared to controls of bacterial TSB solution without polymers. All assays were carried out in duplicate in the same assay plate. Inhibitory percentages were calculated by following equation.

$$\text{Inhibition\%} = \frac{OD_{600}(t) - OD_{600}(0)}{OD_{600}(t)_c - OD_{600}(0)_c}$$

Here, OD_{600} (0) indicates the initial OD_{600} value, and OD_{600} (t) is the OD_{600} value for bacteria after incubation with polymers for t hours. $OD_{600}(0)_c$ is the initial OD_{600} value and $OD_{600}(t)_c$ is the OD_{600} value for control samples after incubation for t hours.

LIVE/DEAD bacterial viability assays.

The six bacteria strains were inoculated and prepared by a similar procedure used for inhibitory concentration determination studies. 1 mL of active bacterial stock of bacteria strains was introduced to 18.5 μg Au@PCo-Peni NPs (penicillin-G weight: 5μg). An untreated cell suspension was used as the control. Following 18 h incubation at 37 °C,

1 μL LIVE/DEAD BacLight (Bacterial Viability Kit; Invitrogen Inc.) was added to the incubation solution. After incubation for 15 minutes, cells were imaged using a Leica TCS SP5 CLSM with 63X oil immersion lens. When excited at 488 nm with Argon and Helium/Neon lasers, bacteria with intact membranes display green fluorescence (Emission = 500 nm) and bacteria with disrupted membranes fluoresce red (Emission= 635 nm).

Bacterial morphology assays.

The morphologies of different bacteria after incubation Au@PCo-Peni NPs were examined by FE-SEM with a similar procedure. In general, 10 μL of bacteria cell solution was grown on one glass slide in 12-well plate containing 1 mL TSB medium at 37 ^{o}C overnight. Cell suspensions were diluted to OD_{600} = 1.0. 18.5 μg Au@PCo-Peni bioconjugates (penicillin-G weight: 5μg) was added to the 1 mL cell stock solution, respectively and incubated at 37 ^{o}C overnight. A cell suspension without any chemicals was used as the control. The samples were then fixed in cacodylate buffered with 2.5% glutaraldehyde solution (pH = 7.2) for 2–3 h at 4 ^{o}C and post-fixed with 1% osmium tetraoxide at 4 ^{o}C for 1 h. The samples were dried under critical point, then coated with gold using Denton Dest II Sputter Coater for 120 s and observed by FE-SEM. An untreated cell suspension was used as the control.

5.4 RESULTS AND DISCUSSION

The cationic cobaltocenium polymer (PCo) was first synthesized via reversible-addition fragmentation chain transfer (RAFT) polymerization[40, 41] using 2-cobaltocenium amidoethyl methacrylate hexafluorophosphate ($CoAEMAPF_6$) as a monomer, 2-Cyano-2-propyl benzodithioate (CPB) as a chain transfer agent (CTA) (**Scheme 1**). The PCo polymer became hydrophilic and highly soluble in water after facile phase-transfer ion-

exchange from PF_6^- to Cl^- using tetrabutylammonium chloride (TBACl) as an ion-exchange reagent.[42] Then, the dithioester end groups of RAFT agent in PCo polymer were reduced to thiol groups by $NaBH_4$ in aqueous media at ambient temperature. The thiol end-capped PCo could be coated on Au-NPs to form Au@PCo nanoparticles by a "grafting-to" approach.[43] Finally, a bioconjugate between cationic PCo and anionic β-lactam antibiotics such as penicillin-G could circumvent major enzymatic hydrolysis via β-lactamase(s) and thus resume the effectiveness of antibiotics on attacking bacteria.

Scheme 5.1 a) Synthesis of cationic thiol end-capped cobaltocenium polymers by RAFT polymerization and dithioester reduction. b) Synthesis of antimicrobial Au@PCo-Peni nanoparticles by a "grafting-to" approach and a bioconjugation between cationic PCo and anionic β-lactam antibiotic Penicillin-G.

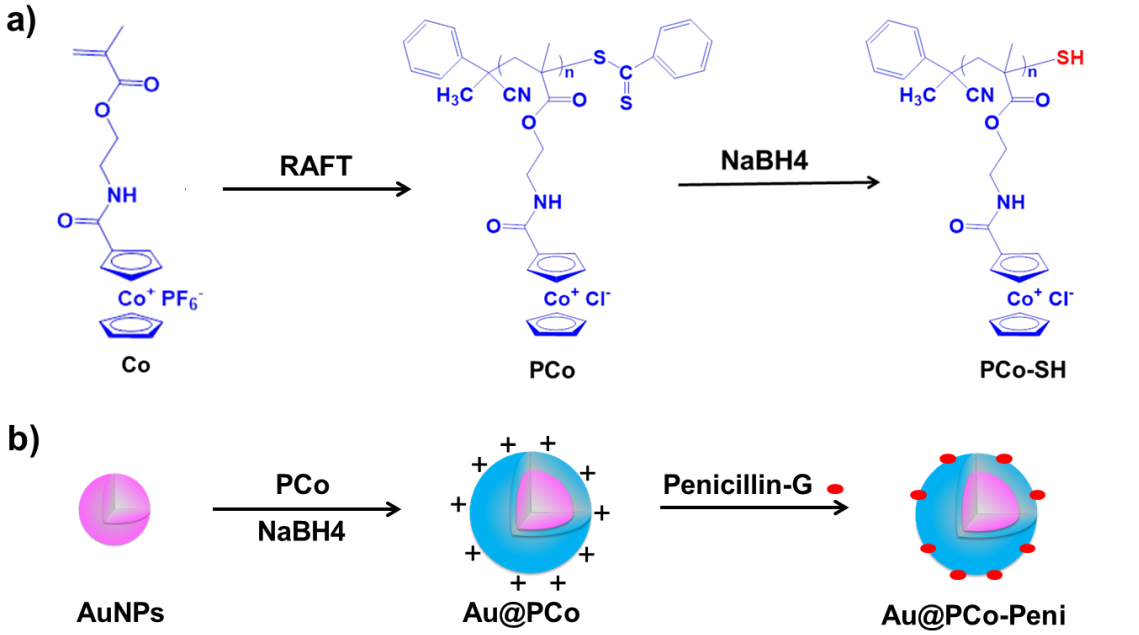

Compared with ^1H NMR spectrum of $CoAEMAPF_6$ monomer, the vinyl proton signals from methacrylate double bond at ~6.10 and ~5.70 ppm disappeared in PCo polymers. Meanwhile, the three peaks at ~6.25 to ~5.80 ppm corresponding to the cyclopentadienyl (Cp) rings of the cobaltocenium unit remained, indicating the successful polymerization of cobaltocenium monomers. The final molecular weight of PCo could be

determined by tracking the NMR conversion during the polymerization process. Three cobaltocenium polymers with different molecular weight, respectively, 6,000 g/mol (noted as PCo-6K), 15,000 g/mol (PCo-15K), 30,000 g/mol (PCo-30K), were finally synthesized.

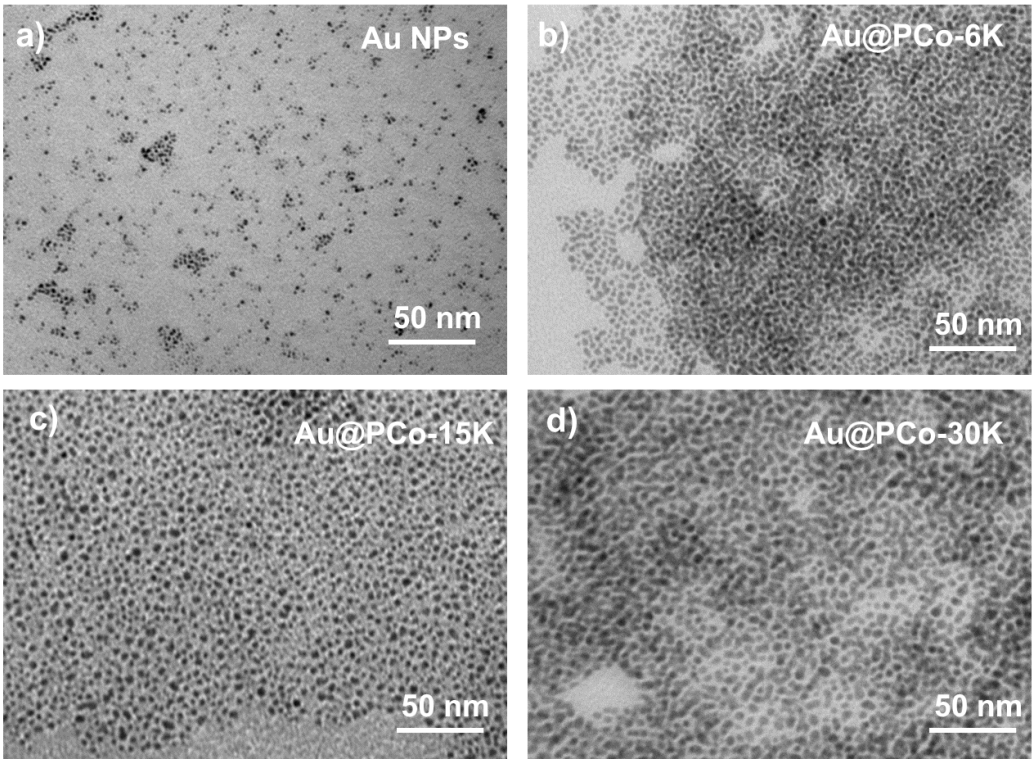

Figure 5.1 TEM images of a) Au NPs, b) Au@PCo-6K, c) Au@PCo-15K, and d) Au@PCo-30K.

Au NPs were prepared using chloroauric acid as the precursor, tetrakis(hydroxymethyl)phosphonium chloride (THPC) as the reducing agent, which could produce ultrafine gold particles.[44] TEM and DLS showed the diameter of Au NPs was about 2-3 nm (Figure 5.1a). After coating PCo polymers with different molecular weights, we got three sets of Au@PCo NPs (referred to as Au@PCo-6K, Au@PCo-15K and Au@PCo-30K). TEM images indicated all Au@PCo NPs had good dispersions (Figure 5.1b-d). As expected, the size of Au@PCo NPs increased to ~4 nm (Au@PCo-6K), 6 nm (Au@PCo-15K) and 9 nm (Au@PCo-30K), respectively, with the increase of molecular

weight of PCo polymers. DLS analysis further confirmed the increased sizes of Au@PCo NPs under different polymer molecular weight as shown in Figure 5.2a.

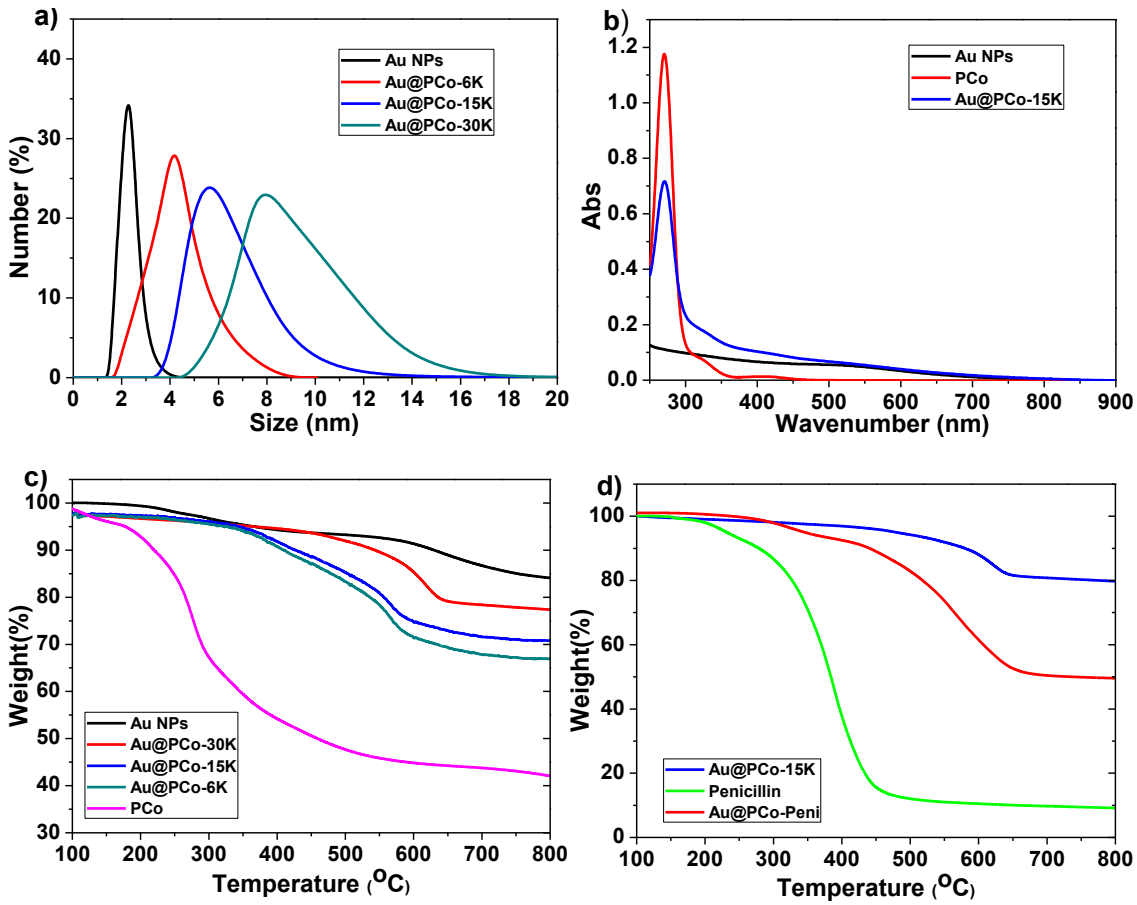

Figure 5.2 a) Size distribution of different gold nanoparticles analyzed by DLS. b) UV-vis absorption spectra of various samples c) TGA data of Au NPs, PCo homopolymers and Au@PCo NPs with different cobaltocenium polymer molecular weights. d) TGA data of Au@PCo-15K NPs, penicillin-G and Au@PCo-Peni.

The successful surface functionalization of gold nanoparticles with cationic cobaltocenium ligands was also analyzed by Zeta-potential analysis, UV-Vis and NMR. Compared to the negative zeta potential of Au NPs at -26 eV, the mean positive potential of all Au@PCo NPs increased to about +40 eV. The UV-visible absorption of Au NPs only had a broad shoulder under the ultraviolet region, while the spectrum of Au@PCo NPs showed an obvious absorption peak of cobaltocenium polymer at 280 nm (Figure 5.2b).

We first evaluated antimicrobial activities of Au NPs, PCo and Au@PCo NPs against Gram-positive bacteria *S. aureus* and Gram-negative bacteria *K. pneumonia* using disk-diffusion assays. The ability of the compound to kill the bacteria was represented by the development of a clear zone around the disk, also known as the inhibition zone. As expected, Au NPs alone could not inhibit the proliferation of *S. aureus* and *K. pneumonia* even at high concentrations. Compared with PCo-15K homopolymers, the Au@PCo-15K NPs showed significantly enhanced activities against both *S. aureus* and *K. pneumonia* at different concentrations. However, there was more significant molecular weight-dependent response on bacterial proliferation for PCo homopolymers than that for the Au@PCo NPs. For example, the PCo-15K homopolymers displayed the biggest inhibition zone against both *S. aureus* and *K. pneumonia* (Figure 5.3a) compared with PCo-6K and PCo-30K homopolymers. While the Au@PCo-15K NPs also exhibited the highest antimicrobial activity, the difference of activities among these three Au@PCo NPs was very small, especially for Gram-negative bacteria *K. pneumonia.* In order to further enhance the antimicrobial activity of Au@PCo NPs, we then studied bioconjugates of Au@PCo NPs with a β-lactam antibiotic, for which we chose penicillin-G. We simply mixed penicillin-G with Au@PCo-15K NPs to form a bioconjugate (labeled as Au@PCo-Peni) via ionic complexation between cationic cobaltocenium and anionic antibiotic. TGA data (Figure 5.2) suggested that the weight percentage of penicillin-G in the Au@PCo-Peni NPs was about 27%, with a molar ratio of cobaltocenium to penicillin-G at ~ 1:0.8. Disk-diffusion assays were first used to evaluate antimicrobial activities of Au@PCo-Peni bioconjugates against four strains of bacteria including Gram-positive bacteria (*S. aureus*) and Gram-negative bacteria (*E. coli*, *K. pneumoniae* and *P. aeruginosa*). To better compare

bactericidal efficiency, we prepared a bioconjugate only containing polycobaltocenium (15,000 g/mol) and penicillin-G as a control. Initially, various amounts of penicillin-G ranging from 5 μg to 15 μg was tested. As shown in Figure 5.3a, when the amount of penicillin-G was 5 μg, penicillin-G alone exhibited minimal antimicrobial efficacy against *S. aureus*. In contrast, PCo-Peni and Au@PCo-Peni bioconjugates displayed clear zones of inhibition, which increased to 11 mm and 14.5 mm, respectively. By increasing the amount of penicillin-G to 10 μg, the inhibition zones of penicillin-G, PCo-Peni, and Au@PCo-Peni appreciably increased to 9.5 mm, 15 mm and 19 mm, respectively. At the highest amount of penicillin-G (15 μg), Au@PCo-Peni still showed the biggest inhibition zone (21 mm), compared with penicillin-G (15 mm) and PCo-Peni (20 mm). For Gram-negative bacteria, penicillin-G showed much lower antimicrobial activity as compared to Gram-positive bacteria. Even by increasing the amount of penicillin-G to 10 μg, penicillin-G alone showed minimal antibacterial activity against all three Gram-negative bacteria (Figure 5.3a ii-iv). This is because Gram-negative bacteria possessed double membranes with a variety of additional resistance mechanisms to evade antibiotics. Using nanoparticles as antimicrobial agents could increase the permeability of bacterial membranes and enhance antimicrobial activity against Gram-negative bacteria. As shown in Figure 2a, Au@PCo-Peni NPs exhibited the strongest antimicrobial activities against all three Gram-negative at different amount of penicillin-G.

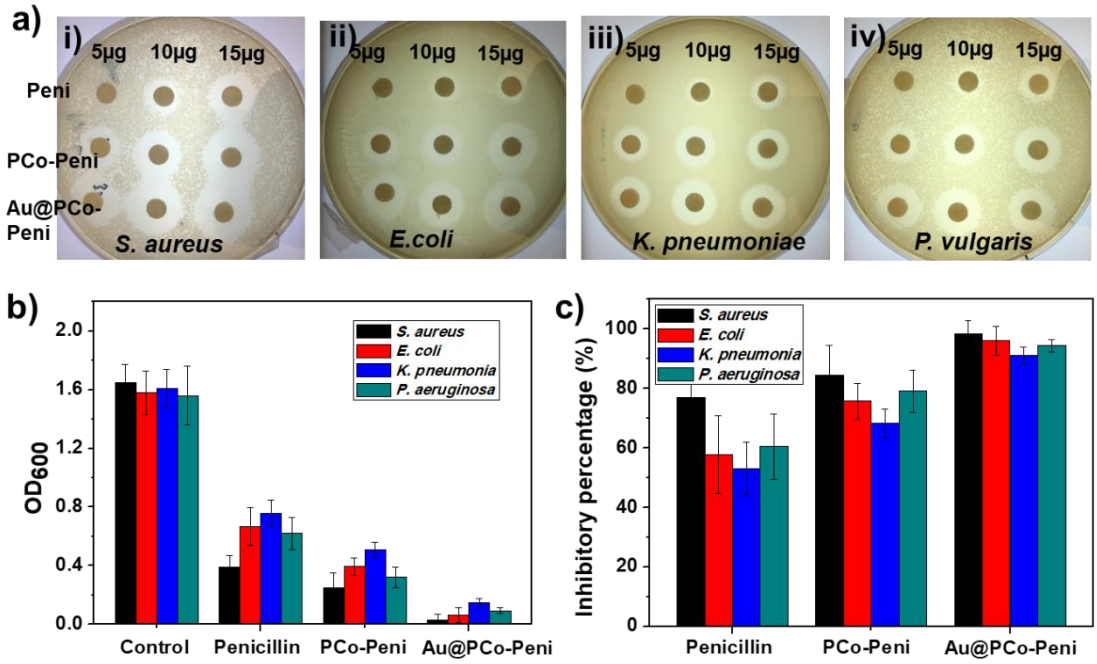

Figure 5.3 a) Disk-diffusion assays against (i) S.aureus (i)*E. coli*, (i) *K. pneumonia*, and (iv) *P. vulgaris* of penicillin-G, PCo-Peni and Au@PCo -Peni NPs. b) OD_{600} values and c) inhibitory percentage of four bacteria incubated with penicillin-G, PCo-Peni and Au@PCo-Peni NPs, respectively. The bacterial TSB solution without antimicrobial agents was used as the control.

To better quantify the inhibition efficacy of Au@PCo-Peni NPs, bacteria were incubated with different antimicrobial agents in TBS solution for 8 h. Then, bacterial growth was detected with OD_{600} (Figure 5.3b) and inhibitory percentages (Figure 5.3c) were calculated, compared to controls of bacterial TSB solution without agents. As for *S. aureus*, the OD_{600} value of Au@PCo-Peni NPs was only 0.03, which was approximately 55 times lower than that of the control (1.65), 13 times lower than penicillin-G (0.39), and 8 times lower than PCo-Peni (0.25), respectively (Figure 5.2b). The inhibitory efficiency of Au@PCo-Peni against *S. aureus* increased to 98.5% from 84.5% (PCo-Peni) and 76.8% (the control) as shown in Figure 5.2c. The similar antibacterial trends and inhibitory efficiency were also found for other Gram-negative bacteria, which was consistent with the results from the disk-diffusion assays.

Table 5.1 The Minimum Inhibitory Concentrations of different antimicrobial agents against Gram-positive and Gram-negative strains.

Compounds	Minimum Inhibitory Concentration (μg/mL)			
	S. aureus	*E. coli*	*K. pneumonia*	*P. vulgaris*
Penicillin-G	15.8	20.4	23.2	22.6
PCo-Peni	6.4	8.3	8.9	7.8
Au@ PCo-Peni	2.6	4.5	5.4	4.9

The Minimum Inhibitory Concentrations (MICs) of penicillin-G, PCo-Peni and Au@PCo-Peni against different Gram-negative strains are given in Table 5.1. It should be mentioned that the MIC values are based on the effective concentration of penicillin in the polymer-penicillin conjugates. The MICs of Au@PCo-Peni NPs against *S. aureus* was 2.6 $\mu g/mL^{-1}$. These values are significantly lower than those of PCo-Peni (6.4 $\mu g/mL^{-1}$) and penicillin-G (15.8 $\mu g/mL^{-1}$). Similarly, as for three Gram-negative strains, MIC values of Au@PCo-Peni conjugate are almost 2~3 times less than PCo-Peni and 4~5 times less than penicillin-G alone.

The inhibition effects by Au@PCo-Peni NPs on the four bacterial strains were further confirmed by Confocal Laser Scanning Microscopy (CLSM) and Scanning Electron Microscopy (SEM). Results of LIVE/DEAD bacterial viability assays using CLSM suggested almost all bacteria incubated with Au@PCo-Peni NPs were killed, with CLSM micrographs displaying obvious red or yellow fluorescence from dead bacteria as in Figure 5.4a. From FESEM images in Figure 5.4b, we can observe that the Au@PCo-Peni NPs damaged bacterial membranes, made bacteria shrink and effectively killed them, while the

untreated bacteria (control groups) exhibited a typical spherical or rod morphology with a smooth surface.

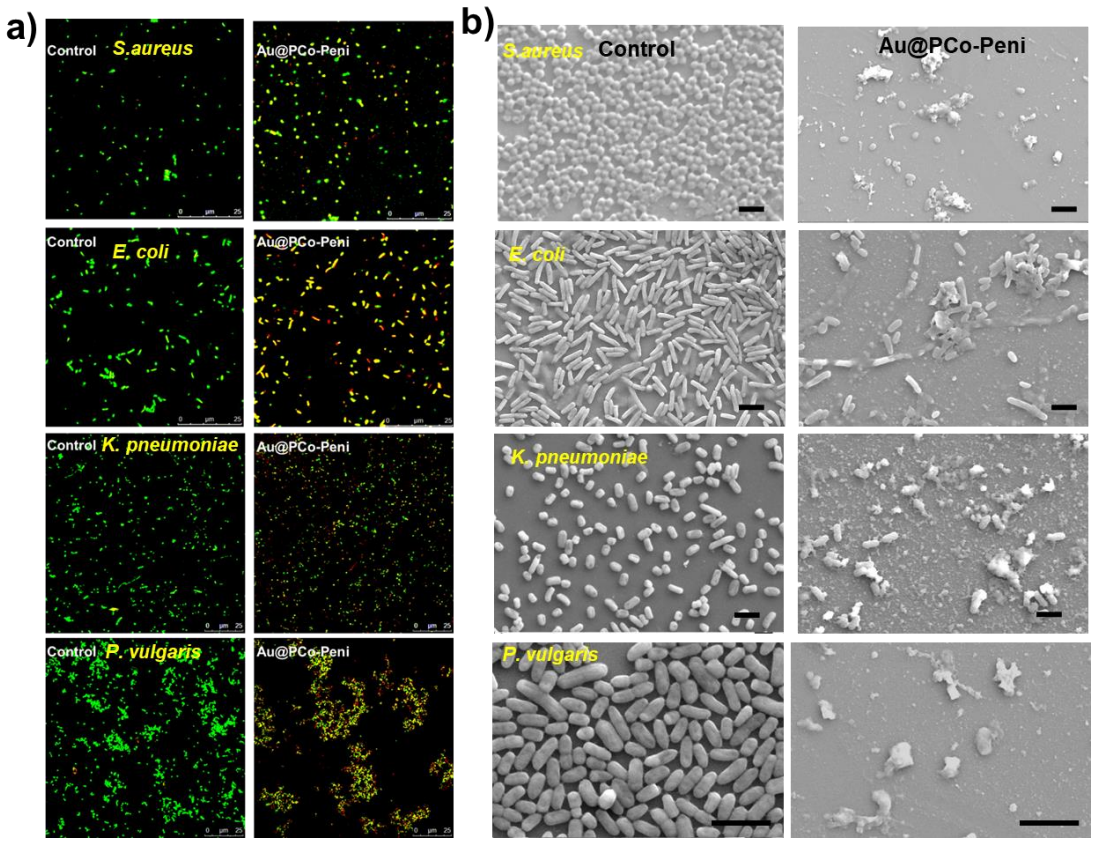

Figure 5.4 a) CLSM and b) SEM images of the control and Au@PCo-Peni NPs (18.5 μg/mL, with the concentration of penicillin-G at 5 μg/mL) against various strains of bacteria. CLSM using BacLight live/dead stain, green indicates live cells, red indicates dead cells. Bacteria concentration was 1.0×10^6 CFU/mL. All scale bars in SEM images are 2 μm.

TEM showed Au@PCo-Peni NPs aggregated around bacterial membranes and then penetrated bacteria, making the outer bacterial membranes disrupted, while the control bacterial cells kept intact and smooth surfaces (Figure 5.5). All these studies suggested the Au@PCo-Peni NPs have excellent antimicrobial efficiency against broad-spectrum bacteria.

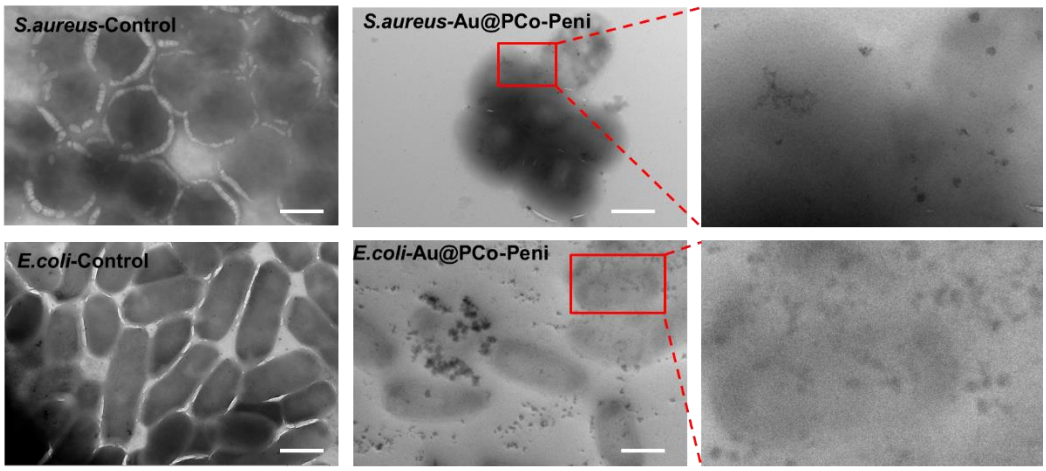

Figure 5.5. TEM images of the control and Au@PCo-Peni NPs (18.5 μg/mL, with the concentration of penicillin-G at 5 μg/mL) against *S.aureus* and *E.coli*. Bacteria concentration were 1.0×10^6 CFU/mL. All scale bars are 1 μm.

The high bactericidal efficacy of Au@PCo-Peni NPs resulted from three synergistic effects: i) the cationic cobaltocenium motif can interact with the negatively-charged bacterial membrane enabling Au@PCo-Peni NPs to attach on the surface of bacteria more closely; ii) the small sizes of nanoparticle provided larger bacterial contact area of Au@PCo-Peni NPs to enhance their permeability into membranes and penetrate more easily; iii) once NP conjugates enter bacterial cells, the cobaltocenium motif would release penicilin-G and bind to β-lactamase, which can block the electrostatic chelation between penicillin-G and amino acid residue of β-lactamase preventing hydrolysis of penicillin-G. Finally, we analyzed the toxicity of Au@PCo NPs on red blood cells (RBCs) by evaluating whether they could lead to hemolysis of RBCs. We found that even at a concentration as high as 500 μg/mL, the lysis of RBCs was extremely low (< 10%) compared to the negative control group (Figure 5.6), suggesting low cytotoxicity to mammalian cells.

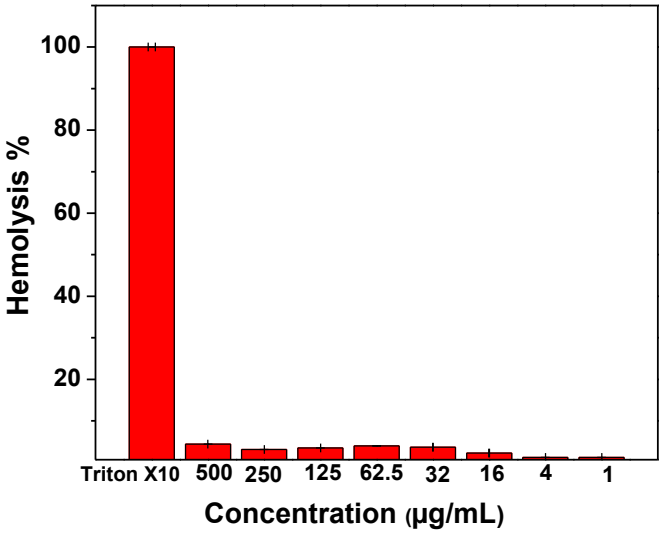

Figure 5.6 Hemolysis test results for Au@PCo nanoparticles.

5.5 Conclusions

In summary, we have developed a strategy to present metallopolymer-antibiotic bioconjugates on gold nanoparticles as an antibacterial agent to fight against different strains of Gram-positive and Gram-negative bacteria. The thiol end-capped cobaltocenium polymers could be easily coated on Au nanoparticles to form Au@PCo NPs by a "grafting-to" approach. After bio-conjugating with an anionic β-lactam antibiotic penicillin-G, the formed cationic Au@PCo-Peni NPs with a small size and a large contact area can attach to the membranes of bacteria more closely, improve the vitality of penicillin-G and kill bacteria more effectively. We hope these multifunctional metallopolymer-based nanoparticles could be further explored in combating clinic infections by the pathogens resistant to conventional antibiotics.

5.6 References

(1) Hancock, R. E.; Nijnik, A.; Philpott, D. J. Modulating immunity as a therapy for bacterial infections. *Nat. Rev. Microbiol.* **2012**, *10*, 243.

(2) Bierne, H.; Hamon, M.; Cossart, P. Epigenetics and bacterial infections. *Cold Spring Harb. Perspect. Med.* **2012**, *2*, a010272.

(3) Fernebro, J. Fighting bacterial infections—future treatment options. *Drug Resistance Updates* **2011**, *14*, 125-139.

(4) Curtis, J.; Yang, S.; Patkar, N.; Chen, L.; Singh, J.; Cannon, G.; Mikuls, T.; Delzell, E.; Saag, K.; Safford, M. Risk of hospitalized bacterial infections associated with biologic treatment among US veterans with rheumatoid arthritis. *Arthritis Care Res.* **2014**, *66*, 990-997.

(5) Alanis, A. J. Resistance to Antibiotics: Are We in the Post-Antibiotic Era? *Arch. Med. Res.* **2005**, *36*, 697-705.

(6) Zhang, Q.-Q.; Ying, G.-G.; Pan, C.-G.; Liu, Y.-S.; Zhao, J.-L. Comprehensive evaluation of antibiotics emission and fate in the river basins of China: source analysis, multimedia modeling, and linkage to bacterial resistance. *Environ. Sci. Technol.* **2015**, *49*, 6772-6782.

(7) Sterling, S. A.; Miller, W. R.; Pryor, J.; Puskarich, M. A.; Jones, A. E. The impact of timing of antibiotics on outcomes in severe sepsis and septic shock: a systematic review and meta-analysis. *Crit. Care Med.* **2015**, *43*, 1907.

(8) Cox, L. M.; Blaser, M. J. Antibiotics in early life and obesity. *Nat. Rev. Endocrinol.* **2015**, *11*, 182.

(9) Yang, Y.; Cai, Z.; Huang, Z.; Tang, X.; Zhang, X. Antimicrobial cationic polymers: From structural design to functional control. *Polym. J.* **2018**, *50*, 33.

(10) Engler, A. C.; Wiradharma, N.; Ong, Z. Y.; Coady, D. J.; Hedrick, J. L.; Yang, Y.-Y. Emerging trends in macromolecular antimicrobials to fight multi-drug-resistant infections. *Nano Today* **2012**, *7*, 201-222.

(11) Ganewatta, M. S.; Tang, C. Controlling macromolecular structures towards effective antimicrobial polymers. *Polymer* **2015**, *63*, A1-A29.

(12) Jiao, Y.; Niu, L.-n.; Ma, S.; Li, J.; Tay, F. R.; Chen, J.-h. Quaternary ammonium-based biomedical materials: State-of-the-art, toxicological aspects and antimicrobial resistance. *Prog. Polym. Sci.* **2017**, *71*, 53-90.

(13) Asri, L. A.; Crismaru, M.; Roest, S.; Chen, Y.; Ivashenko, O.; Rudolf, P.; Tiller, J. C.; van der Mei, H. C.; Loontjens, T. J.; Busscher, H. J. A Shape-Adaptive, Antibacterial-Coating of Immobilized Quaternary-Ammonium Compounds Tethered on Hyperbranched Polyurea and its Mechanism of Action. *Adv. Funct. Mater.* **2014**, *24*, 346-355.

(14) Geng, Z.; Finn, M. Thiabicyclononane-Based Antimicrobial Polycations. *J. Am. Chem. Soc.* **2017**, *139*, 15401-15406.

(15) Hisey, B.; Ragogna, P. J.; Gillies, E. R. Phosphonium-functionalized polymer micelles with intrinsic antibacterial activity. *Biomacromolecules* **2017**, *18*, 914-923.

(16) Fjell, C. D.; Hiss, J. A.; Hancock, R. E.; Schneider, G. Designing antimicrobial peptides: form follows function. *Nat. Rev. Drug Discov.* **2012**, *11*, 37.

(17) Narayana, J. L.; Chen, J.-Y. Antimicrobial peptides: possible anti-infective agents. *Peptides* **2015**, *72*, 88-94.

(18) Zhang, J.; Chen, Y. P.; Miller, K. P.; Ganewatta, M. S.; Bam, M.; Yan, Y.; Nagarkatti, M.; Decho, A. W.; Tang, C. Antimicrobial metallopolymers and their bioconjugates with conventional antibiotics against multidrug-resistant bacteria. *J. Am. Chem. Soc.* **2014**, *136*, 4873-4876.

(19) Yang, P.; Bam, M.; Pageni, P.; Zhu, T.; Chen, Y. P.; Nagarkatti, M.; Decho, A. W.; Tang, C. Trio Act of Boronolectin with Antibiotic-Metal Complexed Macromolecules toward Broad-Spectrum Antimicrobial Efficacy. *ACS Infect. Dis.***2017**, *3*, 845-853.

(20) Peng, B.; Zhang, X.; Aarts, D. G.; Dullens, R. P. Superparamagnetic nickel colloidal nanocrystal clusters with antibacterial activity and bacteria binding ability. *Nature nanotechnology* **2018**, 1.

(21) Li, F.; Lu, J.; Kong, X.; Hyeon, T.; Ling, D. Dynamic nanoparticle assemblies for biomedical applications. *Adv. Mater.* **2017**.

(22) Lucky, S. S.; Soo, K. C.; Zhang, Y. Nanoparticles in photodynamic therapy. *Chem. Rev.* **2015**, *115*, 1990-2042.

(23) Zhang, L.; Pornpattananangkul, D.; Hu, C.-M.; Huang, C.-M. Development of nanoparticles for antimicrobial drug delivery. *Curr. Med. Chem.* **2010**, *17*, 585-594.

(24) Hajipour, M. J.; Fromm, K. M.; Ashkarran, A. A.; de Aberasturi, D. J.; de Larramendi, I. R.; Rojo, T.; Serpooshan, V.; Parak, W. J.; Mahmoudi, M. Antibacterial properties of nanoparticles. *Trends Biotechnol.* **2012**, *30*, 499-511.

(25) Qi, G. B.; Zhang, D.; Liu, F. H.; Qiao, Z. Y.; Wang, H. An "On-Site Transformation" Strategy for Treatment of Bacterial Infection. *Adv. Mater.* **2017**, *29*.

(26) Radovic-Moreno, A. F.; Lu, T. K.; Puscasu, V. A.; Yoon, C. J.; Langer, R.; Farokhzad, O. C. Surface charge-switching polymeric nanoparticles for bacterial cell wall-targeted delivery of antibiotics. *ACS Nano* **2012**, *6*, 4279-4287.

(27) Lam, S. J.; O'Brien-Simpson, N. M.; Pantarat, N.; Sulistio, A.; Wong, E. H.; Chen, Y.-Y.; Lenzo, J. C.; Holden, J. A.; Blencowe, A.; Reynolds, E. C. Combating multidrug-resistant Gram-negative bacteria with structurally nanoengineered antimicrobial peptide polymers. *Nat. Microbiol.* **2016**, *1*, 16162.

(28) Roy, I.; Shetty, D.; Hota, R.; Baek, K.; Kim, J.; Kim, C.; Kappert, S.; Kim, K. A Multifunctional Subphthalocyanine Nanosphere for Targeting, Labeling, and Killing of Antibiotic-Resistant Bacteria. *Angew. Chem.* **2015**, *127*, 15367-15370.

(29) Song, H.; Ahmad Nor, Y.; Yu, M.; Yang, Y.; Zhang, J.; Zhang, H.; Xu, C.; Mitter, N.; Yu, C. Silica nanopollens enhance adhesion for long-term bacterial inhibition. *J. Am. Chem. Soc.* **2016**, *138*, 6455-6462.

(30) Chen, J.; Andler, S. M.; Goddard, J. M.; Nugen, S. R.; Rotello, V. M. Integrating recognition elements with nanomaterials for bacteria sensing. *Chem. Soc. Rev.* **2017**, *46*, 1272-1283.

(31) Nguyen, T.-K.; Selvanayagam, R.; Ho, K. K.; Chen, R.; Kutty, S. K.; Rice, S. A.; Kumar, N.; Barraud, N.; Duong, H. T.; Boyer, C. Co-delivery of nitric oxide and antibiotic using polymeric nanoparticles. *Chem. Sci.* **2016**, *7*, 1016-1027.

(32) Pissuwan, D.; Niidome, T.; Cortie, M. B. The forthcoming applications of gold nanoparticles in drug and gene delivery systems. *J. Control. Release* **2011**, *149*, 65-71.

(33) Chen, W. Y.; Chang, H. Y.; Lu, J. K.; Huang, Y. C.; Harroun, S. G.; Tseng, Y. T.; Li, Y. J.; Huang, C. C.; Chang, H. T. Self-Assembly of Antimicrobial Peptides on Gold Nanodots: Against Multidrug-Resistant Bacteria and Wound-Healing Application. *Adv. Funct. Mater.* **2015**, *25*, 7189-7199.

(34) Zhou, Y.; Kong, Y.; Kundu, S.; Cirillo, J. D.; Liang, H. Antibacterial activities of gold and silver nanoparticles against Escherichia coli and bacillus Calmette-Guérin. *J. Nanobiotechnology* **2012**, *10*, 19.

(35) Abadeer, N. S.; Murphy, C. J. Recent progress in cancer thermal therapy using gold nanoparticles. *J. Phys. Chem. C* **2016**, *120*, 4691-4716.

(36) Feng, Z. V.; Gunsolus, I. L.; Qiu, T. A.; Hurley, K. R.; Nyberg, L. H.; Frew, H.; Johnson, K. P.; Vartanian, A. M.; Jacob, L. M.; Lohse, S. E. Impacts of gold nanoparticle charge and ligand type on surface binding and toxicity to Gram-negative and Gram-positive bacteria. *Chem. Sci.* **2015**, *6*, 5186-5196.

(37) Tao, Y.; Ju, E.; Ren, J.; Qu, X. Bifunctionalized mesoporous silica-supported gold nanoparticles: intrinsic oxidase and peroxidase catalytic activities for antibacterial applications. *Adv. Mater.* **2015**, *27*, 1097-1104.

(38) Zhao, Y.; Tian, Y.; Cui, Y.; Liu, W.; Ma, W.; Jiang, X. Small molecule-capped gold nanoparticles as potent antibacterial agents that target gram-negative bacteria. *J. Am. Chem. Soc.* **2010**, *132*, 12349-12356.

(39) Bindhu, M.; Umadevi, M. Antibacterial activities of green synthesized gold nanoparticles. *Mater. Lett.* **2014**, *120*, 122-125.

(40) Zhang, J.; Ren, L.; Hardy, C. G.; Tang, C. Cobaltocenium-containing methacrylate homopolymers, block copolymers, and heterobimetallic polymers via RAFT polymerization. *Macromolecules* **2012**, *45*, 6857-6863.

(41) Yang, P.; Pageni, P.; Kabir, M. P.; Zhu, T.; Tang, C. Metallocene-Containing Homopolymers and Heterobimetallic Block Copolymers via Photoinduced RAFT Polymerization. *ACS Macro Lett.* **2016**, *5*, 1293-1300.

(42) Zhang, J.; Yan, Y.; Chance, M. W.; Chen, J.; Hayat, J.; Ma, S.; Tang, C. Charged Metallopolymers as Universal Precursors for Versatile Cobalt Materials. *Angew. Chem. Int. Ed.* **2013**, *52*, 13387-13391.

(43) Lowe, A. B.; Sumerlin, B. S.; Donovan, M. S.; McCormick, C. L. Facile preparation of transition metal nanoparticles stabilized by well-defined (co) polymers synthesized via aqueous reversible addition-fragmentation chain transfer polymerization. *J. Am. Chem. Soc.* **2002**, *124*, 11562-11563.

(44) Duff, D. G.; Baiker, A.; Edwards, P. P. A new hydrosol of gold clusters. 1. Formation and particle size variation. *Langmuir* **1993**, *9*, 2301-2309.

(45) Roy, D.; Cambre, J. N.; Sumerlin, B. S. Sugar-responsive block copolymers by direct RAFT polymerization of unprotected boronic acid monomers. *Chem. Commun.* **2008**, 2477-2479.

CHAPTER 6

SUMMARY AND OUTLOOK

6.1 Dissertation Summary

A unique combination of organic and inorganic components in one macromolecular system offers exciting science for many areas, including medicinal chemistry, energy-related science, and advanced catalytic chemistry. Thus, a full benefit could be achieved by simultaneously incorporating the mechanical and processing properties of polymeric frameworks and the electronic, catalytic, magnetic and radioactive properties of metal building blocks. The study of electrostatic charge on the relative affinity and comparison of the relative binding strength of a cobaltocenium-containing polyelectrolyte was carried out initially. It was demonstrated that low cytotoxic cationic cobaltocenium metallopolymers have antimicrobial efficacy against various bacterial strains including multidrug resistant bacteria by disarming activities of β-lactamase. We devised new strategy of developing novel materials using nontraditional therapy combining nanoparticles, antibiotics, and metal-containing macromolecules in nullifying multiple strains of bacteria with high antimicrobial efficacy. Silica and iron oxide nanoparticles grafted with charged cobaltocenium-containing metallopolymers were synthesized by surface-initiated reversible addition-fragmentation chain transfer (RAFT) polymerization using “grafting-from” strategy. These nanoparticles were characterized in detail. Both the nanoparticle conjugates displayed enhanced antimicrobial activity and did not induce bacterial resistance and were safe to use in animals with little to non-toxicity. Iron oxide nanoparticles displayed magnetic property so that it could be recycled without losing its effectiveness for multiple cycles. “Grafting-to” technique was utilized to make cobaltocenium-containing gold nanoparticles. The thiol end-capped cobaltocenium polymers was obtained after reducing the polymer with RAFT agent end groups and coated

on gold nanoparticles to form cobaltocenium-containing gold nanoparticles. The improved bactericidal efficiencies of all these nanoparticle conjugates could be attributed to the joint act of multiple components in the nanoparticle system. A cationic metal-containing macromolecular framework binds to the outer membrane via electrostatic interactions and nanoparticle surface provides enhanced local concentration of cobaltocenium-penicillin complex A bioconjugate between metal-containing macromolecules and conventional β-lactam antibiotics could circumvent major enzymatic hydrolysis and thus resume the effectiveness of antibiotics attacking peptidoglycan which is critical for cell wall synthesis. Together, these multiple killing components provide multifaceted and versatile means for penetrating cellular barriers to fight bacterial resistance.

6.2 Future Work

Metallopolymers incorporates metal centers and macromolecules leading to materials that merge the electronic, magnetic and catalytic properties of metal with the mechanical and processing capability of polymeric frameworks. However, the development of efficient and scalable synthetic methodologies to make metallocenium derivatives is still challenging. So, metallocenium chemistry should be developed in several directions before it gains wide spread applications to prepare various functional materials. Although this dissertation demonstrated a promising way to make novel metallocenium-containing antimicrobial materials, further investigations are required to explore the synthesis of other materials. It could provide a new pathway for designing multifunctional macromolecular scaffolds to regenerate vitality of conventional antibiotics to kill multidrug resistant bacteria and address potential bacterial resistance. Future research should expand to drug-resistant strains including *in vivo* studies to establish the

relevance of these conjugates as drugs. Further structural modifications and tailoring will be necessary to make the metallopolymer conjugates more effective against drug-resistant Gram-negative pathogens, which possess double membranes with a variety of additional resistance mechanisms to evade antibiotics. Also, the polymer backbone should be switched from methacrylate to biodegradable backbone so the polymeric contents will be eliminated from the biological system following their action. Microbial biofilms are the source of a majority of infections so the field of metallopolymers should move forward with more focus on antibiofilm research. Particularly, future research can target the microbial communication system (quorum sensing) to control their biofilm formation. Quorum sensing plays an active role in regulating the microbial biofilm so the incorporation of strategies that inhibit microbial quorum sensing can provide a major boost to address the issue of biofilm. One of the ways can be by conjugating or incorporating various quorum sensing inhibitors with metallopolymers.

Considering the unique properties of cationic cobaltocenium moieties, another direction to explore would be to make novel stimuli responsive block cobaltocenium-containing block copolymers to carry out behavior and morphology studies. Metallocene-containing polyelectrolytes are inherently redox responsive and thus the introduction of another stimuli-response will yield multi-responsive polymers. The combination of functional metallocenium with other biomacromolecules such as DNA can result in a colloidally stable polyplex which provides the opportunity for gene delivery. Another direction worth to explore will be to make poly(ionic liquids) using metallocenium monomers which could have applications in multitude of fields such as thermoresponsive materials, porous polymers, energy harvest and biomedicine.

APPENDIX A – PERMISSION TO REPRINT

SPRINGER NATURE LICENSE
TERMS AND CONDITIONS

May 21, 2018

This Agreement between USC -- Parasmani Pageni ("You") and Springer Nature ("Springer Nature") consists of your license details and the terms and conditions provided by Springer Nature and Copyright Clearance Center.

License Number	4353690930017
License date	May 21, 2018
Licensed Content Publisher	Springer Nature
Licensed Content Publication	Journal of Inorganic and Organometallic Polymers and Materials
Licensed Content Title	Binding of Cobaltocenium-Containing Polyelectrolytes with Anionic Probes
Licensed Content Author	Parasmani Pageni, Mohammad Pabel Kabir, Peng Yang et al
Licensed Content Date	Jan 1, 2017
Licensed Content Volume	27
Licensed Content Issue	4
Type of Use	Thesis/Dissertation
Requestor type	non-commercial (non-profit)
Format	print and electronic
Portion	full article/chapter
Will you be translating?	no
Circulation/distribution	<501
Author of this Springer Nature content	yes
Title	CATIONIC METALLOCENE-CONTAINING MATERIALS FOR ANTIMICROBIAL APPLICATIONS

Figure A.1. Copyright release for Chapter 2.

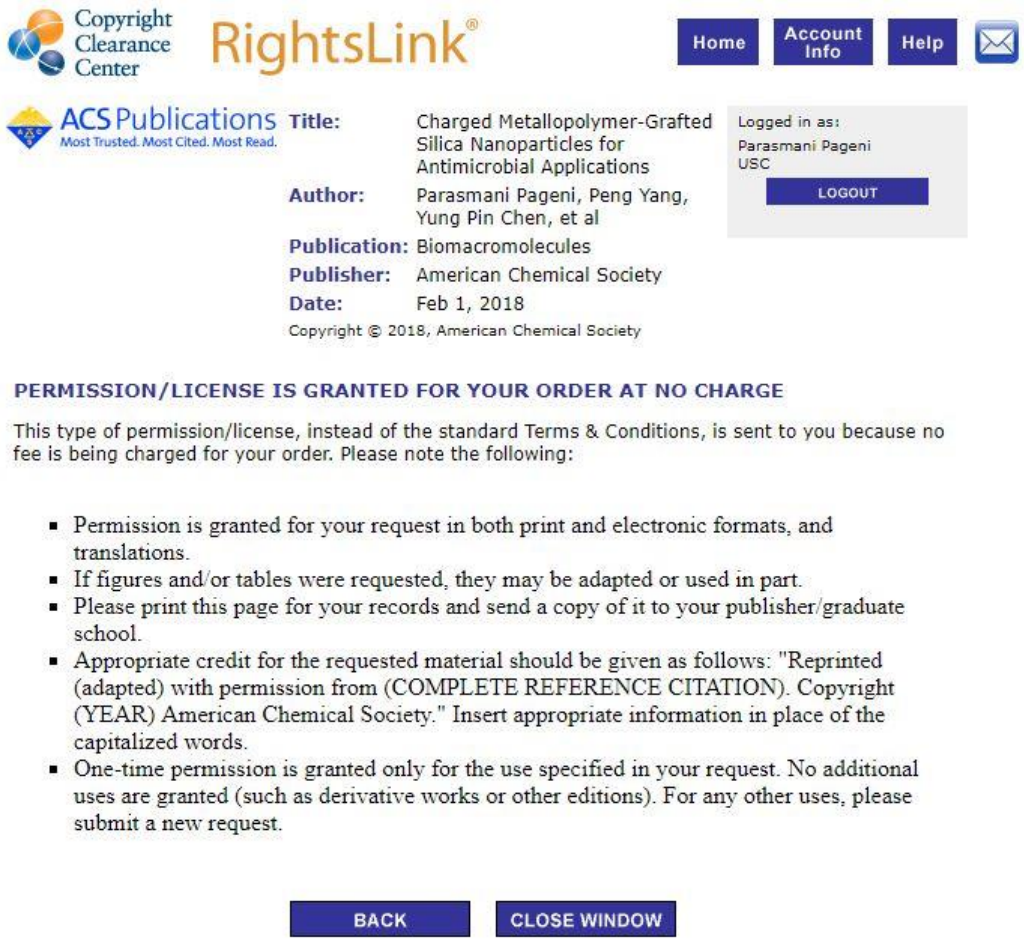

Figure A.2. Copyright release for Chapter 3.

Figure A.3. Copyright release for Chapter 4.